(12)

REPORT NO. ADCR-80-1

DEMONSTRATION OF A METHOD FOR DETERMINING CRITICAL STORE CONFIGURATIONS FOR WING-STORE FLUTTER

by

(10) Richard R. Chipman and Edward J. Laurie

(11) May 1980

(9) Final Report for Contract (15) N00019-79-C-0062

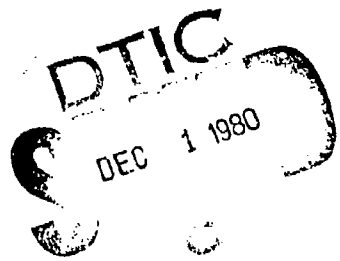

Prepared by

GRUMMAN AEROSPACE CORPORATION
Bethpage, New York 11714

for

NAVAL AIR SYSTEMS COMMAND
Washington, D.C.

ACKNOWLEDGEMENTS

This final report was prepared for the Naval Air Systems Command, Washington, DC, under contract N00019-79-C-0062. Funding was provided via NAIR-320B, initially staffed by Dr Allan Somoroff and subsequently by Dr. Daniel Mulville. The technical monitor of this contract was Mr. George Maggos, NAIR-530214.

The authors wish to acknowledge the contributions of Dr. Joel Markowitz and Mr. Jerome Kohn of Grumman Aerospace Corporation, and Ms. Kathleen Demetri and Dr. John Malone, formerly of Grumman, for their technical assistance. Ms. Demetri programmed the constrained search algorithm of the pilot External Stores Program (ESP) developed under the contract. Drs. Markowitz and Malone assisted in reprogramming various portions of a previously developed Flutter and Strength Optimization Program (FASTOP) for use in ESP. Mr. Kohn determined the inertial properties of the store inventory for the demonstration problem and set up the search constraints.

Additionally, Mr. Keith Wilkinson is to be credited for suggesting the original concept of applying optimization techniques to the prediction of store flutter. Also, Messrs. Emmanuel Pasyanos and Elmer Bauer are thanked for providing math models used in the A-6 demonstration. Finally, we wish to acknowledge the advice, technical contributions, and critiques of Mr. John Smedfjeld and Mr. Charles Squires.

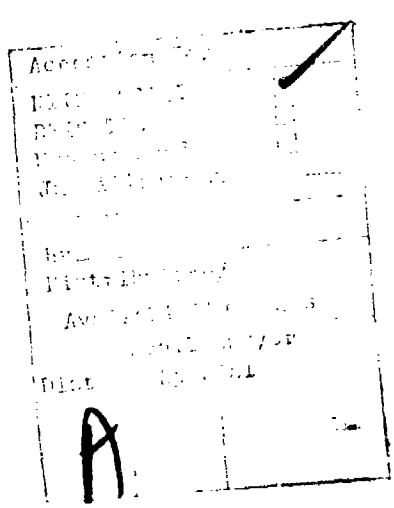

CONTENTS

CONTENTS (Cont)

ILLUSTRATIONS

ILLUSTRATION (Cont)

ILLUSTRATIONS (Cont)

TABLES

1 - SUMMARY

A gradient-directed numerical search technique is presented for determining those configurations of multiple external stores that are most flutter-critical for a given aircraft. The search is performed in a design space defined by the store properties at each specified store location. Constraints on the space are imposed by the extent of the aircraft store inventory. From expressions for the derivatives of flutter speed with respect to the store properties, gradient directions in the space are computed to guide the search. The search technique used is called Rank One Correction and belongs to the class of quadratically convergent search algorithms. To implement the method, a pilot computer program having the acronym ESP (External Stores Program) was written.

To demonstrate the technique on a realistic problem, the A-6E aircraft and its extensive store inventory were analyzed. Searches of the inventory singled out two potentially critical configurations that gave flutter speeds well within the flight envelope for low assumed values of structural damping. Comparisons with the results of previous A-6 studies (which did not identify these configurations as critical) were made and possible explanations for the apparent anomaly were explored. It was concluded that, if these configurations had been uncovered during aircraft design, they would have been flagged for flight flutter test. Their omission is evidence of the extreme difficulty and poor reliability of current practice.

The new method offers an efficient alternative to current practices for determining potentially flutter-critical store combinations from the many thousands (or even millions) of store loadings that can occur on modern attack aircraft. Also, the use of the new, automated approach significantly reduces the heavy reliance on engineering judgement that is characteristic of contemporary methods, thereby minimizing the danger of 'missing' critical configurations.

2 - INTRODUCTION

The increasingly large inventory of wing-mounted external stores carried by current attack aircraft necessitates the development of safer and more efficient methods for predicting critical configurations for wing-store flutter. The methods must be safer in the sense of minimizing the risk of "missing" flutter-critical configurations from the many thousands of store configurations that must often be considered, and they must be more efficient in terms of reducing both computer usage and/or wind-tunnel test time and the effective calendar time required to formulate design requirements.

Under a feasibility study sponsored by the Naval Air Systems Command (N00019-76-C-0160), a new method - that of applying design search techniques to automatically determine critical store configurations for wing-store flutter - was explored (Ref. 1). The study was conducted for a simple wing with two store stations. Store mass and pitch/yaw moment of inertia at each station were taken as the design variables of the problem, and a search was conducted over the space defined by an arbitary range in each of these parameters. With the exception of certain regions associated with discontinuities in the flutter speed, the basic gradient-directed search algorithm developed for the study successfully located local minimum (critical configurations) in reasonably few iterations. In the regions of discontinuities, modifications were introduced into the basic algorithm that met with initial success.

Subsequent work has led to faster convergence in locating minima (Ref. 2). This improvement was accomplished by using a more sophisticated search algorithm, Rank One Correction, which also increased reliability (absence of search failure).

In the present study, the method has been further developed and demonstrated on a representative aircraft (A-6E) and its store inventory. Store center-of-gravity location and pylon flexibility have been added to the analysis to supplement store mass and moments of inertia as search parameters, and the search algorithm has been modified to account for nonconstant (linear) constraints on the search parameters. With these added capabilities, the method is able to handle multiple- and triple-ejection racks (MERs and TERs), as well as single-store racks, and to more accurately model the extent of the store inventory.

Section 3 of this report discusses the theory behind the method; schemes for both unconstrained and constrained searches are described. In Section 4, the analytical formulae for the derivatives of flutter speed with respect to the various store parameters are derived. The pilot computer code ESP (External Stores Program) written to implement the method is described in Section 5. Section 6 discusses the A-6 dynamics and aerodynamics math models used for the demonstration. Section 7 is devoted to enumerating the A-6 store inventory and constructing the constraints for the search. Section 8 discusses the strategy used in initiating the searches and presents the results. Conclusions and recommendations are given in Section 9.

3 - THEORY

3.1 PROBLEM FORMULATION

The determination of critical store-flutter configurations may be viewed as an optimization problem in which the combination of permissible store parameters that results in a minimum flutter speed for the aircraft under consideration is to be found. The store properties are considered the "design variables" of the problem, on which the aircraft store inventory imposes certain limits or "constraints". Flutter speed is chosen as the "objective or cost function" which is to be minimized. By treating the "design space" of permissible store properties prescribed within the specified constraints as a continuum rather than as an assemblage of many discrete points, numerical search techniques can be applied to determine the critical combination of stores that minimizes the objective function, i.e., results in the lowest flutter speed (see Fig. 3-1).

The problem is characterized by a fixed set of store carriage locations at which each of the store parameters may vary. The parameters may be store mass, moments of inertia and center-of-gravity location, and pylon stiffness.

The objective is to determine the critical combination of N store parameters, denoted by $\vec{x}$, which results in the minimum flutter speed, denoted by the function $f^0(\vec{x})$, subject to a set of m* linear constraints on the store parameters, denoted by $f^j(\vec{x}) \leq 0$ for $1 \leq j \leq m^*$. Since the constraints are linear, they can be written as

$$f^j(\vec{x}) = \vec{g}^j \cdot \vec{x} - b^j \leq 0,$$

$$[G]^T \vec{x} - \vec{b} \leq 0, \qquad (3\text{-}1)$$

where

$\vec{g}^j$ is the unit normal vector to the jth constraint plane

b^j is the distance from the origin to the jth constraint plane.

3.2 UNCONSTRAINED SEARCH

The function f^0 can be expanded by a Taylor series about any given point $\vec{x}_k$ as follows:

$$f^0(\vec{x}) \approx f^0(\vec{x}_k) + (\vec{x} - \vec{x}_k) \cdot \vec{g}_k^0 + \frac{1}{2} (\vec{x} - \vec{x}_k) \cdot [H_k] (\vec{x} - \vec{x}_k), \qquad (3\text{-}2)$$

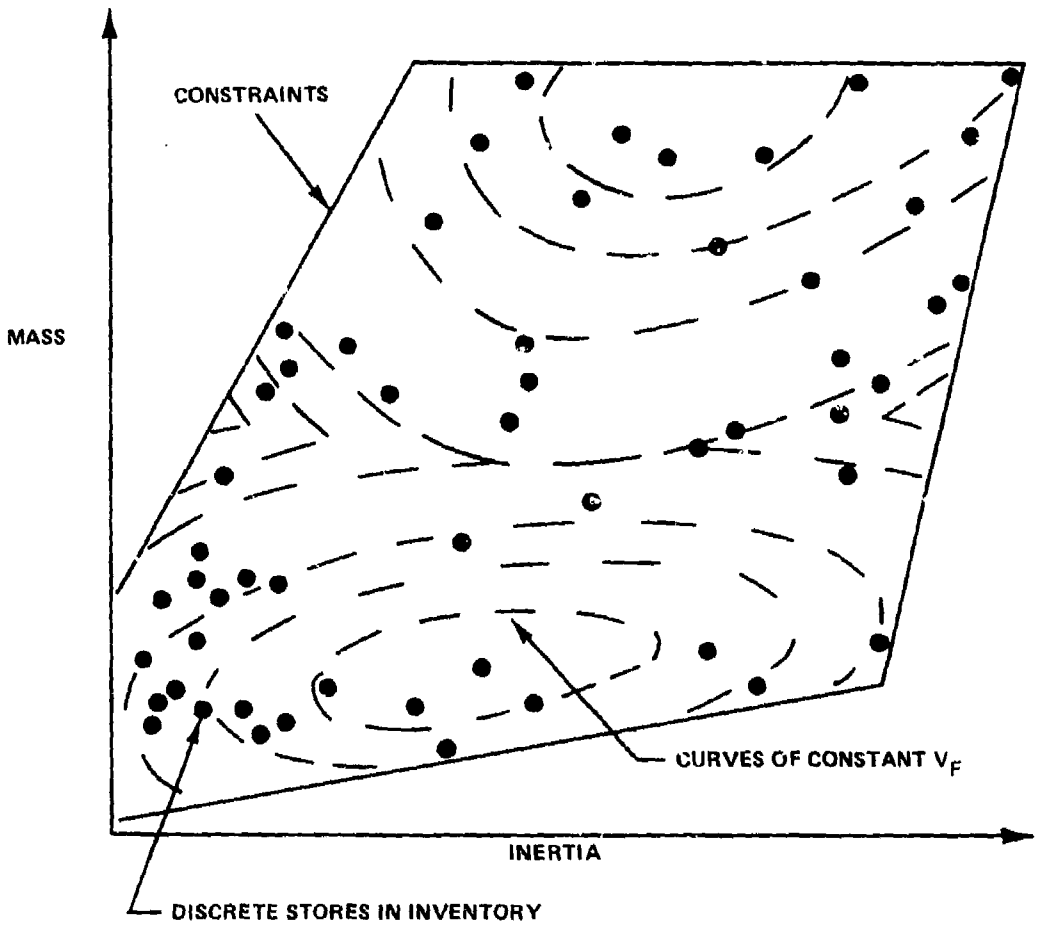

- STORE PROPERTIES BECOME 'DESIGN VARIABLES'
- FLUTTER SPEED IS 'COST OR OBJECTIVE FUNCTION'
- LIMITS ON STORE PROPERTIES IN INVENTORY ARE 'CONSTRAINTS'
- 'SPACE' OF PREMISSIBLE COMBINATIONS OF STORE PROPERTIES IS TREATED AS CONTINUOUS
- THIS SPACE IS SEARCHED FOR THE COMBINATION OF PARAMETERS THAT RESULTS IN A MINIMUM OF OBJECTIVE FUNCTION; I.E. THE STORES THAT CAUSE THE LOWEST FLUTTER SPEED

RBD-1469-001(T)

Fig. 3-1 Basic Approach for Determining Critical Stores

where

$\vec{g}_k^o$ is the local gradient (vector of first partial derivatives of f^o, flutter speed, with respect to the design variables)

$[H_k]$ is the local Hessian (matrix of second partial derivatives of f^o).

Differentiating the above expression yields

$$\vec{g}^o(\vec{x}) = \vec{g}_k^o + [H_k](\vec{x} - \vec{x}_k),$$

$$(\vec{x} - \vec{x}_k) = [H_k]^{-1}(\vec{g}^o(\vec{x}) - \vec{g}_k^o). \tag{3-3}$$

If we are sufficiently close to the minimum, denoted by $\vec{x}^*$, (3-3) becomes

$$(\vec{x}^* - \vec{x}_k) = -[H_k]^{-1}\vec{g}_k^o. \tag{3-4}$$

This equation suggests the following strategy for determining an unconstrained minimum: Starting with any feasible combination of store parameters, denoted by $\vec{x}_o$, a succession of steps is made toward the minimum. Each step takes the form

$$\Delta\vec{x}_k = \alpha_k \vec{d}_k,$$

$$\vec{x}_{k+1} = \vec{x}_k + \Delta\vec{x}_k, \quad k = 0, 1, \ldots \tag{3-5}$$

where

$\vec{x}$ is a combination of store parameters

$\Delta\vec{x}$ is a step in the search

$\vec{d}$ is the direction of the step

α is the step size.

The direction is given by

$$\vec{d}_k = -[S_k]\vec{g}_k^o \quad , \tag{3-6}$$

where $[S_k]$ is the current estimate of the inverse of the local Hessian matrix.

In the absence of any detailed information, $[S_k]$ could be taken to be the identity matrix. With this choice, the search direction becomes the local negative gradient, i.e.,

$$\vec{d}_k = -\vec{g}_k^o.$$

The resulting algorithm, called steepest descent, is known to have poor convergence characteristics (locating a minimum may require an excessive number of steps); consequently, in the present work, a more effective scheme (Rank One Correction, Ref. 3) is used. In this scheme, by continually updating the estimate [S] as the search progresses, the inverse Hessian is built up without explicitly calculating it. Thereby, as shown in Fig. 3-2, the direction of search departs from the local gradient and homes in on the minimum. The method of obtaining the update is derived in the following discussion.

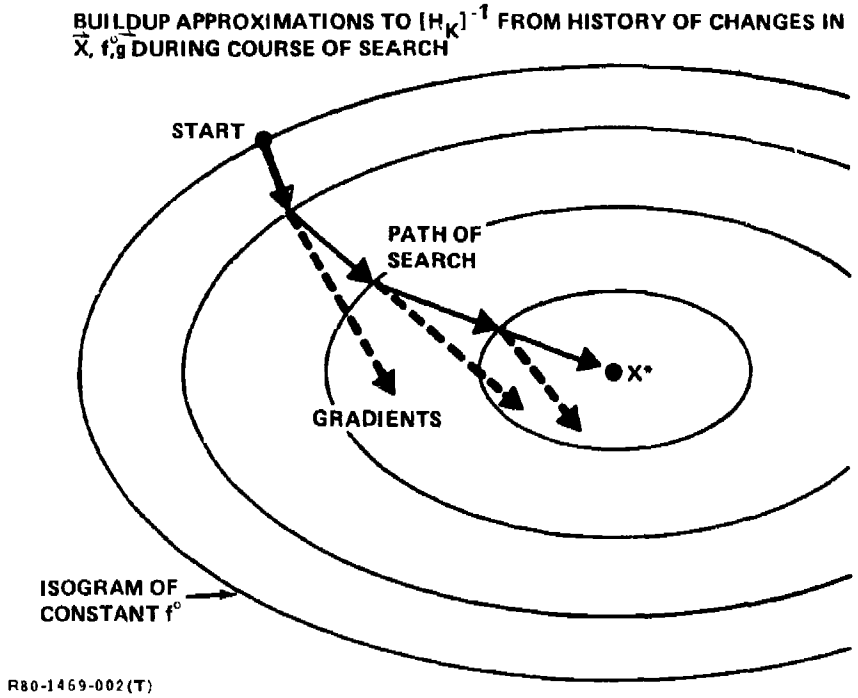

Fig. 3-2 Typical Rank-One-Corrector Search Pattern

Writing (3-4) for two successive points near the minimum, one has

$$\vec{x}^* - \vec{x}_k = -[H_k]^{-1}\vec{g}^\circ_k \cong -[H]^{-1}\vec{g}^\circ_k$$

$$\vec{x}^* - \vec{x}_{k-1} = -[H_{k-1}]^{-1}\vec{g}^\circ_{k-1} \cong -[H]^{-1}\vec{g}^\circ_{k-1}.$$

Subtraction of the first equation from the second yields

$$\Delta\vec{x}_{k-1} = [H]^{-1}\,\Delta\vec{g}^\circ_{k-1}.$$

Substituting (3-5) and $[S_k]$, one obtains

$$\alpha_{k-1}\vec{d}_{k-1} = [S_k]\ \Delta\vec{g}^{\circ}_{k-1}$$

We shall require that the estimate $[S_k]$ satisfy this equation for each step up to this point in the search, i.e.,

$$\alpha_j\vec{d}_j = [S_k]\ \Delta\vec{g}^{\circ}_j \quad \text{for } 1 \leq j \leq (k-1). \tag{3-7}$$

Since [H] is symmetric, [S] must be also; hence, one can write

$$[S_k] = [S_{k-1}] + [\vec{Z}_k(\vec{Z}_k)^T], \tag{3-8}$$

where, since $\vec{Z}_k$ is a vector, the update maxtrix is of rank one. Enforcing (3-7) for $j = k-1$, one obtains

$$(\alpha\vec{d})_{k-1} = [S_k]\ \Delta\vec{g}^{\circ}_{k-1},$$

or, upon substitution of (3-8),

$$(\alpha\vec{d})_{k-1} = [S_{k-1}]\ \Delta\vec{g}^{\circ}_{k-1} + [\vec{Z}_k(\vec{Z}_k)^T]\ \Delta\vec{g}^{\circ}_{k-1}. \tag{3-9}$$

Some algebraic manipulation is now performed:

$$(\alpha\vec{d})_{k-1} - [S_{k-1}]\ \Delta\vec{g}^{\circ}_{k-1} = [\vec{Z}_k(\vec{Z}_k)^T]\ \Delta\vec{g}^{\circ}_{k-1}$$

$$[(\alpha\vec{d})_{k-1} - [S_{k-1}]\ \Delta\vec{g}^{\circ}_{k-1}]^T = (\Delta\vec{g}^{\circ}_{k-1})^T\vec{Z}_k(\vec{Z}_k)^T$$

$$[(\alpha\vec{d})_{k-1} - [S_{k-1}]\ \Delta\vec{g}^{\circ}_{k-1}][(\alpha\vec{d})_{k-1} - [S_{k-1}]\ \Delta\vec{g}^{\circ}_{k-1}]^T = \vec{Z}_k(\vec{Z}_k^T\Delta\vec{g}^{\circ}_{k-1})^2 Z_k^T$$
$$= (\vec{Z}_k^T\Delta\vec{g}^{\circ}_{k-1})^2\vec{Z}_k\vec{Z}_k^T.$$

(3-10)

Now (3-9) is premultiplied by $\Delta\vec{g}^{\circ T}_{k-1}$ to yield

$$(\Delta\vec{g}^{\circ}_{k-1})^T(\alpha\vec{d})_{k-1} = (\Delta\vec{g}^{\circ}_{k-1})^T[S_{k-1}]\ \Delta\vec{g}^{\circ}_{k-1} + (\Delta\vec{g}^{\circ}_{k-1})^T\vec{Z}_k Z_k^T\Delta\vec{g}^{\circ}_{k-1}$$
$$= (\Delta\vec{g}^{\circ}_{k-1})^T[S_{k-1}]\ \Delta\vec{g}^{\circ}_{k-1} + (\vec{Z}_k^T\Delta\vec{g}^{\circ}_{k-1})^2.$$

Thus

$$(\vec{Z}^T \triangle \vec{g}^\circ_{k-1})^2 = (\triangle \vec{g}^\circ_{k-1})^T \; [(\alpha\vec{d})_{k-1} - [S_{k-1}] \; \triangle \vec{g}^\circ_{k-1}] .$$

Substituting this expression into (3-10) yields (after some manipulation) the expression for the correction:

$$\vec{Z}_k \vec{Z}_k^T = \frac{[(\alpha\vec{d})_{k-1} - [S_{k-1}] \triangle \vec{g}^\circ_{k-1}] \; [(\alpha\vec{d})_{k-1} - [S_{k-1}] \triangle \vec{g}^\circ_{k-1}]^T}{(\triangle \vec{g}^\circ_{k-1})^T \; [(\alpha\vec{d})_{k-1} - [S_{k-1}] \; \triangle \vec{g}^\circ_{k-1}]} \qquad (3\text{-}11)$$

Using (3-8) and (3-11), we have the following expression for the updated estimate of the inverse Hessian in terms of previously computed values:

$$[S_k] = [S_{k-1}] + \frac{1}{c} [\vec{y}\,\vec{y}^T] ,$$

where

$$\vec{y} = (\alpha\vec{d})_{k-1} - [S_{k-1}] \; \triangle \vec{g}^\circ_{k-1}$$

$$c = (\triangle \vec{g}^\circ_{k-1})^T y \qquad (3\text{-}12)$$

The search is initiated by choosing $[S_o]$ as the identity matrix [I].

It is shown in Ref. 3 that the algorithm defined by (3-5), (3-6), and (3-12) will converge for a quadratic function in only N steps, where N is the number of variables. This rapid rate of convergence is desirable since the cost of each function evaluation (determination of flutter speed) is high.

3.3 CONSTRAINED SEARCH

The constrained-search algorithm of Ref 4 is a generalization of the Gradient-Projection technique of Ref. 5. In this case, the direction given by (3-6) is used in place of a negative-gradient direction. The strategy that will be discussed is illustrated in Fig. 3-3.

Assume that the search has reached a point, $\vec{x}_k$, on a constraint and that the computed move $\alpha_k \vec{d}_k$ would violate the constraint by moving out of the feasible space to the unconstrained minimum, $\hat{\vec{x}}$. A feasible move is determined by projecting $\alpha_k \vec{d}_k$ back onto the constraint to a point $\vec{x}^*$, which is the constrained minimum. The problem

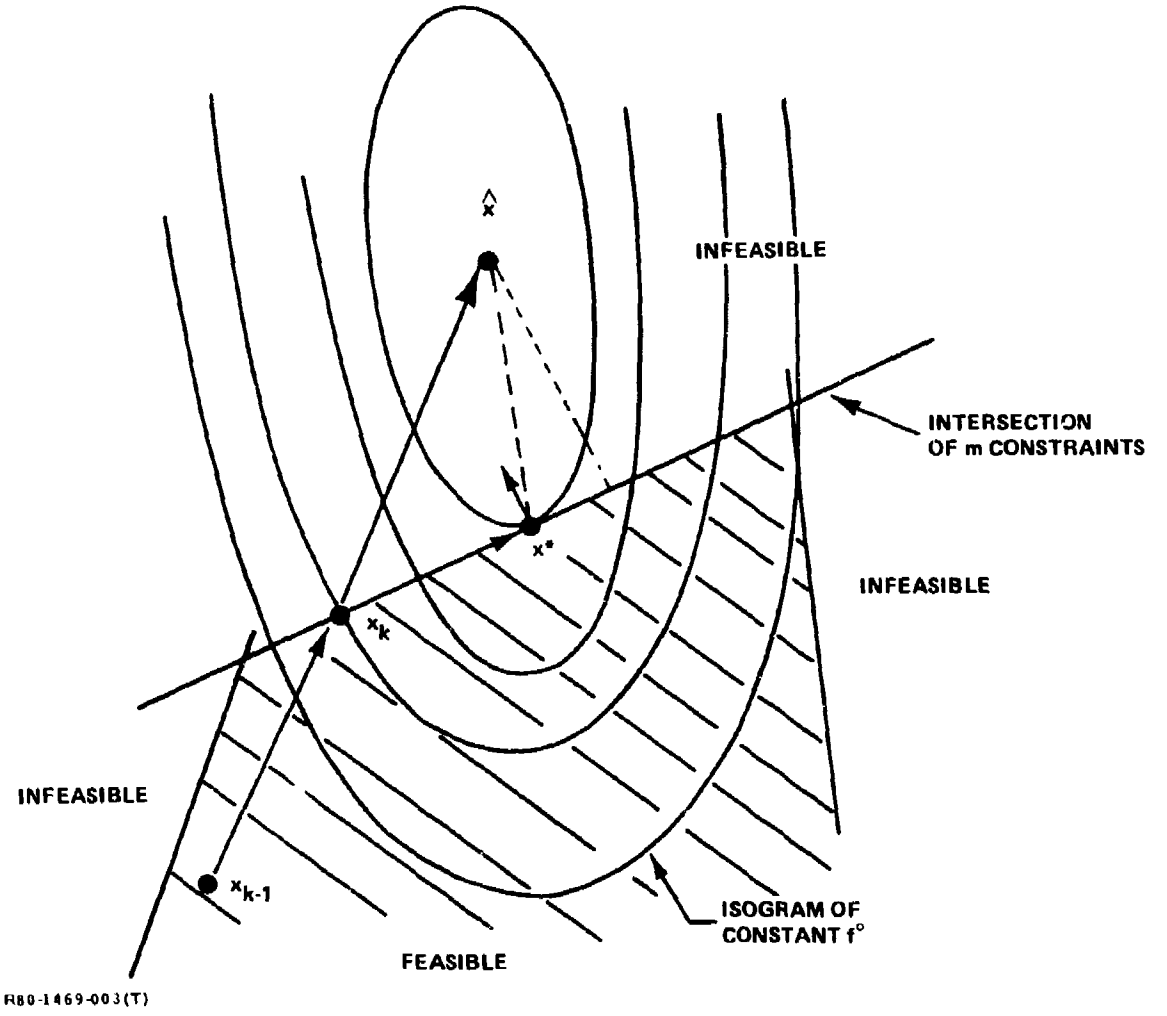

Fig. 3-3 Projection at Constraints

is harder (if not impossible) to visualize in higher-dimensional space, but the procedure can be stated as the projection of the unconstrained move back onto the facet of the space formed by the intersection of the active constraints. Since the constraints themselves are linear, the facets constitute "hyperplanes" in the N-dimensional space.

Determination of the mathematical form of the projection requires a derivation which relies in part on the Kuhn-Tucker optimization theorem. This theorem states that if x^* minimizes the objective function, subject to a set of linearly independent constraints, denoted by (3-1), there exists a set of negative constants (Lagrange multipliers, λ) such that

$$\nabla f^{\circ}(\vec{x}^*) - \sum_{j=1}^{m^*} \lambda_j \nabla f^j(\vec{x}^*) = 0, \tag{3-13}$$

$$\sum_{j=1}^{m^*} \lambda_j f^j(\vec{x}^*) = 0, \tag{3-14}$$

$$\lambda_j \leq 0, \quad 1 \leq j \leq m^*.$$

(These Lagrange multipliers have a natural interpretation as sensitivity coefficients of the optimal solution point $\vec{x}^*$ with respect to perturbations in the constraints, Ref. 13, pp 192-194.)

We now proceed with the derivation of the projection algorithm. Since $\vec{x}_k$ and $\vec{x}^*$ satisfy m^* constraints, (3-1) applies to both points:

$$f_*^j = (\vec{g}^j)^T \vec{x}^* - \vec{b}_j = 0, \quad j = 1, m^*,$$
$$f_k^j = (\vec{g}^j)^T \vec{x}_k - \vec{b}_j = 0, \quad j = 1, m^*.$$

Thus,

$$[G_m]^T \left\{ \vec{x}^* - \vec{x}_k \right\} = 0. \tag{3-15}$$

From a Taylor series expansion, one obtains

$$(\hat{\vec{x}} - \vec{x}_k) = -[S_k]\, \vec{g}_k^{\circ},$$
$$(\hat{\vec{x}} - \vec{x}^*) = -[S_k]\, \vec{g}_*^{\circ}.$$

Thus,

$$(\vec{x}^* - \vec{x}_k) = [S_k]\, (\vec{g}_*^{\circ} - \vec{g}_k^{\circ}). \tag{3-16}$$

Now by the Kuhn-Tucker theorem,

$$\vec{g}_*^{\circ} = [G_m]\, \vec{\lambda}.$$
$$\therefore (\vec{x} - \vec{x}_k) = [S_k]\, ([G_m]\, \vec{\lambda} - \vec{g}_k^{\circ}). \tag{3-17}$$

If we substitute (3-17) into (3-15), the following result is obtained:

$$[G_m]^T [S_k] ([G_m] \vec{\lambda} - \vec{g}_k^\circ) = 0. \tag{3-18}$$

Solving (3-18) for $\vec{\lambda}$ yields

$$\vec{\lambda} = [L] [G_m]^T [S_k] \vec{g}_k^\circ, \tag{3-19}$$

where

$$[L] = \left([G_m]^T [S_k] [G_m] \right)^{-1}.$$

([L]is often called the inverse-moment matrix.)

Now we can substitute this value of $\vec{\lambda}$ into (3-17) and obtain the new expression for $(\vec{x}^* - \vec{x}_k)$:

$$\begin{aligned} (\vec{x}^* - \vec{x}_k) &= [S_k]\left([G_m] [L] [G_m]^T [S_k] \vec{g}_k^\circ - \vec{g}_k^\circ \right), \\ (\vec{x}^* - \vec{x}_k) &= [P_k][S_k] \vec{g}_k^\circ \end{aligned} \tag{3-20}$$

where $$[P] = \left([I] - [S_k] [G_m] [L] [G_m]^T \right).$$

3.4 STEP SIZE

The step size α_k, shown in (3-5), is nominally chosen to be unity. However, this value is automatically reduced, if necessary, so that the planned move $\Delta\vec{x}_k$ will neither violate a constraint nor be unduly large. Thus,

$$\alpha_k = \min (1, \alpha^*, \alpha^{**}) \tag{3-21}$$

α^* is determined by first computing the intersection of the step with each inactive constraint j. Thus,

$$(\vec{g}_j^\circ)^T (\vec{x}_k + \alpha_j^* \vec{d}_k) - b_j = 0.$$

$$\therefore \alpha_j^* = \frac{b_j - (\vec{g}_j^\circ)^T x_k}{\vec{(g}_j^\circ)^T \vec{d}_k} \tag{3-22}$$

From these values, the step to the nearest intersection is determined by

$$\alpha^* = \min_{\text{positive}} (\alpha_j^*), \text{ for } m^* \leq j \leq m, \tag{3-23}$$

where

m^* = the number of active constraints

m = the total number of constraints.

α^{**} is determined by limiting the magnitude of the proposed step to 0.3 in terms of normalized variables (see Section 5). Thus,

$$\alpha^{**} = \frac{0.3}{\|\vec{d}\|} \tag{3-24}$$

3.5 LINE SEARCH

Most gradient-directed algorithms employ a line search to determine an optimal step-size, α_k, which results in the maximum decrease in the objective function obtainable by moving from $\vec{x}_k$ in the direction $\vec{d}_k$. Because the performance of this search requires additional function evaluations which are very time-consuming in our case (flutter solutions), only a minimal line search is employed. If a move made with a given step-size results in a point with a lowered f^o, the point is accepted and no line search is made; if f^o is not lowered, the search is conducted. The search consists of performing a cubic polynominial fit in f^o using values of the function and its gradient at the step-off point, $\vec{x}_k$, and the rejected, overshot point, $\vec{x}_{k+1}$. The point at which this polynominal is minimum is then taken as $\vec{x}_{k+2}$. This strategy is illustrated in Fig. 3-4.

3.6 CONVERGENCE CRITERIA

An unconstrained minimum exists whenever the following two conditions are satisfied:

$$\|\vec{g}_k^o\| < \epsilon \tag{3-25}$$

$$\|\Delta \vec{x}_k\| = \|[S_k]\, \vec{g}_k^o\| < \epsilon, \tag{3-26}$$

where ϵ is a small tolerance, typically = 0.001 in terms of normalized variables. The first test establishes the fact that the gradient has nearly vanished. The second test investigates the possibility that the current point is not at a minimum but, rather, is in a very gradually sloping region of space.

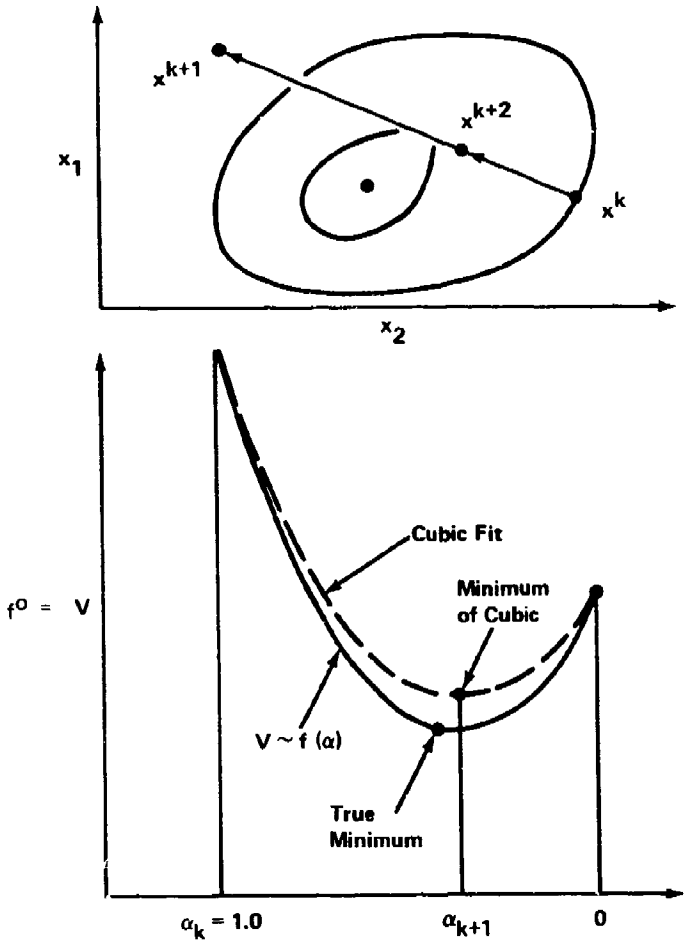

Fig. 3-4 Minimal Line Search

A constrained minimum exists whenever the following three conditions are satisfied:

$$\lambda_j < \epsilon, \text{ for } 1 \leq j \leq m^* \tag{3-27}$$

$$\| \Delta \vec{x}_k \| = \| [P_k]\ [S_k]\ \vec{g}_k^{\,o} \| < \epsilon \tag{3-28}$$

$$\| [PG_k]\ \vec{g}_k^{\,o} \| < \epsilon, \tag{3-29}$$

where $[PG_k]\,\vec{g}_k^{\,0}$ is the normal projection of the gradient onto the subspace formed by the intersection of the m* active constraints. Equations (3-27) and (3-28) comprise the Kuhn-Tucker test. Equation (3-27) states that the Lagrange multipliers of the current m^* constraints are negative (or essentially zero) and, thus, that no constraints should be dropped. Equation (3-28) states that the present point $\vec{x}_k$ is the minimum on these constraints because the projection yields essentially the same point. Equation (3-29) is necessary to preclude the possibility that, due to an inaccurate estimate $[S_k]$, the move computed by (3-20) is accidentally so small that (3-28) is satisfied. Equation (3-29) tests that a projection of the gradient also vanishes; thus, the constraints must be tangent to the local function contour and a minimum exists. Since (3-29) requires that $[PG_k]$ be computed, it is only employed after the first two tests are successful.

4 - SEARCH VARIABLES: COMPUTATION OF GRADIENTS

An expression for the derivatives of flutter speed, V_f, with respect to a design variable, x_i, was derived in Ref. 6. Simplified in Ref. 7, this expression is

$$\frac{\partial V_f}{\partial x_i} = \frac{V_f}{\omega_f^2}\left[\frac{1}{2} R_e\left(\{V\}^T\left(\frac{\partial [K]}{\partial x_i} - \omega_f^2 \frac{\partial [M]}{\partial x_i}\right)\{U\}\right)\right.$$

$$- Im\left(\{V\}^T\left(\frac{\partial [K]}{\partial x_i} - \omega_f^2 \frac{\partial [M]}{\partial x_i}\right)\{U\}\right)$$

$$\left.\times\left(\frac{\frac{\omega_f^2}{2} Re\left(\{V\}^T \frac{\partial [A]}{\partial k}\{U\}\right) + \frac{\omega_f^2}{k}}{Im\left(\omega_f^2 \{V\}^T \frac{\partial [A]}{\partial k}\{U\}\right)}\right)\right] \qquad (4\text{-}1)$$

where

k = reduced frequency

ω_f = flutter frequency (rad/sec)

$[K]$, $[M]$, $[A]$ = stiffness, mass, and aerodynamic matrices

$\{U\}$ and $\{V\}$ = flutter eigenvector and its associated row eigenvector.

If the ith element's stiffness and mass matrices, $[K_i]$ and $[M_i]$, vary linearly with its design variable, x_i, (4-1) can be manipulated into a new "energy-density" form:

$$\frac{\partial V_f}{\partial x_i} = SED_i - KED_i$$

$$= f_1\left(V_f, \omega_f, \frac{\partial [A]}{\partial k}, \frac{\partial [K]}{\partial x_i}\right) + f_2\left(V_f, \omega_f, \frac{\partial [A]}{\partial k}, \frac{\partial [M]}{\partial x_i}\right).$$

In this form, the terms of (4-1) have been grouped into two categories. The first, SED_i, includes what may be interpreted as a linear combination of generalized strain-energy-density terms. The second category, KED_i, contains a similar set of generalized kinetic-energy-density terms. This grouping of terms is adopted to lend visibility to the separate contributions of each element's stiffness and mass to its derivative.

4.1 STORE INERTIAS

For the design variables (mass and moments of inertia), the derivatives of the stiffness matrix in (5-1) are zero and (5-1) can be reduced to the following:

$$\frac{\partial V_f}{\partial x_i} = V_f \left\{ -\frac{1}{2} \mathrm{Re}\left(\{V\}^T \left[\frac{\partial [M]}{\partial x_i} \right] \{U\} \right) + \right.$$

$$\left. \frac{\mathrm{Im}\left(\{V\}^T [\partial [M] / \partial x_i] \{U\} \right)}{\mathrm{Im}\left(\{V\}^T (\partial [A] / \partial k) \{U\} \right)} \times \left(\frac{1}{2} \mathrm{Re}\left(\{V\}^T (\partial [A] / \partial k) \{U\} \right) + \frac{1}{k} \right) \right\}$$

The pilot program described in Section 5 accommodates a maximum of five store locations, each of which can be characterized by up-to-four independent inertia design variables: mass (m) and roll, pitch, and yaw moments of inertia (I_x, I_y, I_z) about the store center-of-gravity. Each store may be dynamically modeled by six degrees of freedom at a node. The center-of-gravity is located by the vector $\vec{s}$ relative to the attachment point. The dynamic coordinate system is defined in Fig. 4-1.

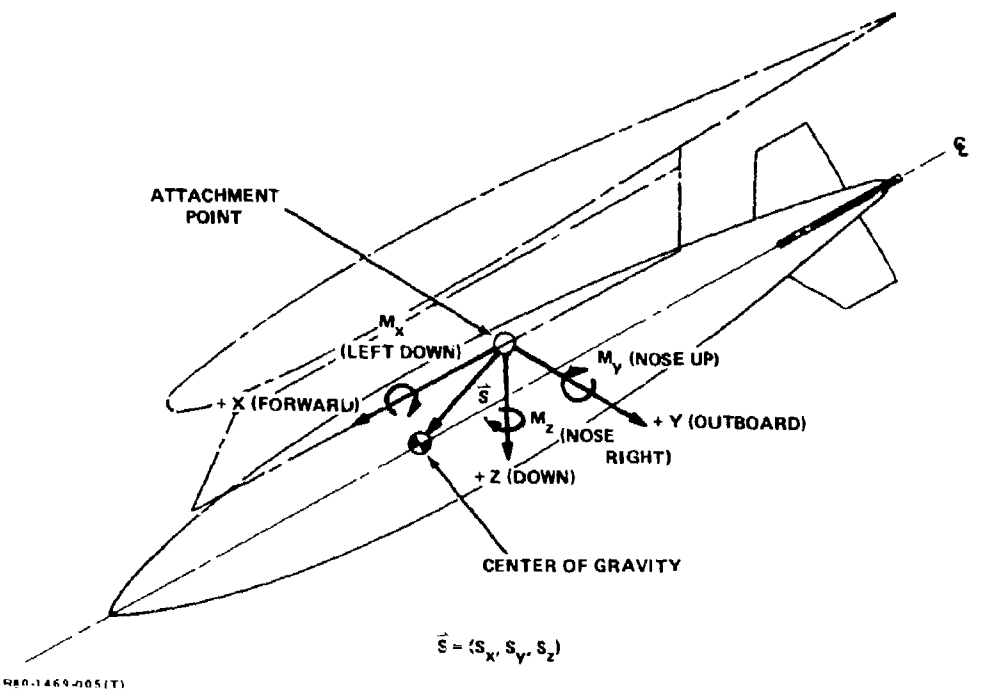

Fig. 4-1 Store Dynamic Coordinate System

The contribution to the total mass matrix corresponding to the ith store, $[\bar{M}_i]$, is then composed of mass, inertia, and unbalance terms as shown below:

$$[M_i] = \left[\begin{array}{ccc|ccc} m_i & & & & & \\ 0 & m_i & & & \text{symmetric} & \\ 0 & 0 & m_i & & & \\ \hline 0 & -m_i s_z & m_i s_y & I_{x_i} + (s_y^2 + s_z^2)\, m_i & & \\ m_i s_z & 0 & -m_i s_x & -s_x s_y m_i & I_{y_i} + (s_x^2 + s_z^2)\, m_i & \\ m_i s_y & -m_i s_x & 0 & s_x s_z m_i & s_y s_z m_i & I_{z_i} + (s_x^2 + s_y^2)\, m_i \end{array}\right] \qquad (4\text{-}2)$$

Thus, for a given design variable, x_i, corresponding to the ith store location, the derivative of the total mass matrix contains zeros for all elements except a few non-zero terms arising from the mass matrix contribution of the ith store, $\frac{\partial}{\partial x_i}[\bar{M}_i]$. For the four inertial design variables, these derivatives are as follows:

$$\frac{\partial[\bar{M}_i]}{\partial m} = \left[\begin{array}{ccc|ccc} 1 & & & & & \\ 0 & 1 & & & \text{symmetric} & \\ 0 & 0 & 1 & & & \\ \hline 0 & -s_z & s_y & s_y^2 + s_z^2 & & \\ s_z & 0 & -s_y & -s_x s_y & s_x^2 + s_z^2 & \\ s_y & -s_x & 0 & s_x s_z & s_y s_z & s_x^2 + s_y^2 \end{array}\right]$$

$$\frac{\partial[\bar{M}_i]}{\partial I_x} = \left[\begin{array}{ccc|ccc} 0 & & & & & \\ 0 & 0 & & & \text{sym} & \\ 0 & 0 & 0 & & & \\ \hline 0 & 0 & 0 & 1 & & \\ 0 & 0 & 0 & 0 & 0 & \\ 0 & 0 & 0 & 0 & 0 & 0 \end{array}\right], \quad \frac{\partial[\bar{M}_i]}{\partial I_y} = \left[\begin{array}{ccc|ccc} 0 & & & & & \\ 0 & 0 & & & \text{sym} & \\ 0 & 0 & 0 & & & \\ \hline 0 & 0 & 0 & 0 & & \\ 0 & 0 & 0 & 0 & 1 & \\ 0 & 0 & 0 & 0 & 0 & 0 \end{array}\right], \quad \frac{\partial[\bar{M}_i]}{\partial I_z} = \left[\begin{array}{ccc|ccc} 0 & & & & & \\ 0 & 0 & & & \text{sym} & \\ 0 & 0 & 0 & & & \\ \hline 0 & 0 & 0 & 0 & & \\ 0 & 0 & 0 & 0 & 0 & \\ 0 & 0 & 0 & 0 & 0 & 1 \end{array}\right]$$

(4-3)

Since many items in a typical stores inventory are roughly cylindrical in shape, the pitch and yaw inertias can be expected to be nearly equal for a given store. Hence, the present computer program allows the user to specify that these design variables are to be held equal throughout a design search. The inertial derivative for this case can then be obtained by using the following derivative of the mass matrix:

$$\frac{\partial[\bar{M}_i]}{\partial l} = \left[\begin{array}{ccc|ccc} 0 & & & & & \\ 0 & 0 & & & \text{sym} & \\ 0 & 0 & 0 & & & \\ \hline 0 & 0 & 0 & 0 & & \\ 0 & 0 & 0 & 0 & 1 & \\ 0 & 0 & 0 & 0 & 0 & 1 \end{array}\right] \qquad (4\text{-}4)$$

4.2 STORE CENTER-OF-GRAVITY LOCATION

In addition to mass and inertia, there are other store parameters that can have a significant effect on flutter speed and, hence, on the critical store configuration. One is the location of the store center-of-gravity. There are three reasons for this location becoming variable. First, the attachment point location may not be fully specified during preliminary design and, consequently, the location of the entire store may be variable. The second is simply that different stores have different center-of-gravity locations. The third is that, for a multiple ejection rack (MER), the aggregate center-of-gravity varies as ejection occurs. As with store mass and inertia, the derivatives of flutter speed with respect to these additional parameters must be computed. Since the stiffness of the system is not a function of these parameters, only the change in the inertial matrix must be considered.

The mass matrix for each store is given by (4-2). The derivatives of this matrix with respect to the components of the center-of-gravity location are:

$$\frac{\partial[\bar{M}]}{\partial s_x} = \left[\begin{array}{ccc|ccc} 0 & & & & & \\ 0 & 0 & & & \text{symmetric} & \\ 0 & 0 & -m & -ms_y & 2ms_x & \\ 0 & -m & 0 & ms_z & 0 & 2ms_x \end{array}\right] \qquad \frac{\partial[\bar{M}]}{\partial s_z} = \left[\begin{array}{ccc|ccc} 0 & & & & & \\ 0 & -m & 0 & 2ms_z & & \\ m & 0 & 0 & 0 & 2ms_z & \\ 0 & 0 & 0 & ms_x & ms_y & 0 \end{array}\right]$$

$$\frac{\partial[\bar{M}]}{\partial s_y} = \left[\begin{array}{ccc|ccc} 0 & & & & & \\ 0 & 0 & & & \text{symmetric} & \\ 0 & 0 & m & 2ms_y & & \\ 0 & 0 & 0 & -ms_x & 0 & \\ m & 0 & 0 & 0 & ms_z & 2ms_y \end{array}\right] \qquad (4\text{-}5)$$

Note that these derivatives are not constants but vary with (s_x, s_y, s_z).

4.3 PYLON FLEXIBILITY OR STIFFNESS

Another parameter having a significant effect on store flutter is the flexibility (or stiffness) of the pylon attaching the store to the wing. Early in the design process, store carriage flexibilities (or stiffnesses) are generally "ballpark" numbers subject to change. After the design is finalized, there is still a variability in these parameters due to store installation procedures and the addition of various store racks. Unlike changes in store mass, inertia, and center-of-gravity position, a variation in pylon flexibility will affect the stiffness matrix of the system but not the inertial matrix.

In practice, pylon stiffnesses or flexibilities are specified in terms of overall store motions (e.g., pitch, roll). Thus, it is inappropriate to implement changes in these parameters by varying the stiffness matrix derived in the structures (i.e., finite element) model. Such a model is too detailed to conveniently effect changes in overall lumped stiffnesses (or flexibilities). Therefore, it is necessary to modify the stiffness or flexibility matrix in the dynamics model. Figure 4-2 illustrates these two different models.

We shall denote the dynamic flexibility and stiffness matrices by

$$\left[C_D\right] = \begin{bmatrix} C_{ww} & C_{wp} \\ C_{pw} & C_{pp} \end{bmatrix} \quad \text{and} \quad \left[K_D\right] = \begin{bmatrix} K_{ww} & K_{wp} \\ K_{pw} & K_{pp} \end{bmatrix} \quad , \tag{4-6}$$

where the subscript w denotes those degrees of freedom associated with the wing nodes and the subscript p denotes those associated with the pylon/store attachment node(s). Since we desire variations in the pylon flexibilities, we denote the incremental pylon flexibility matrix by $[\Delta]$, which we assume is diagonal. As $[\Delta]$ is varied, we need expressions for the revised flexibility matrix and the derivative of the revised stiffness matrix with respect to a particular flexibility variable, say Δ_i. The revised flexibility matrix can easily be written as

$$\left[\overline{C_D}\right] = \begin{bmatrix} C_{ww} & C_{wp} \\ C_{pw} & C_{pp} \end{bmatrix} + \begin{bmatrix} 0 & 0 \\ 0 & \Delta \end{bmatrix} \tag{4-7}$$

To derive an expression for the derivative of the revised stiffness matrix, we differentiate the equation

$$\left[\overline{K_D}\right] \cdot \left[\overline{C_D}\right] = [I] \tag{4-8}$$

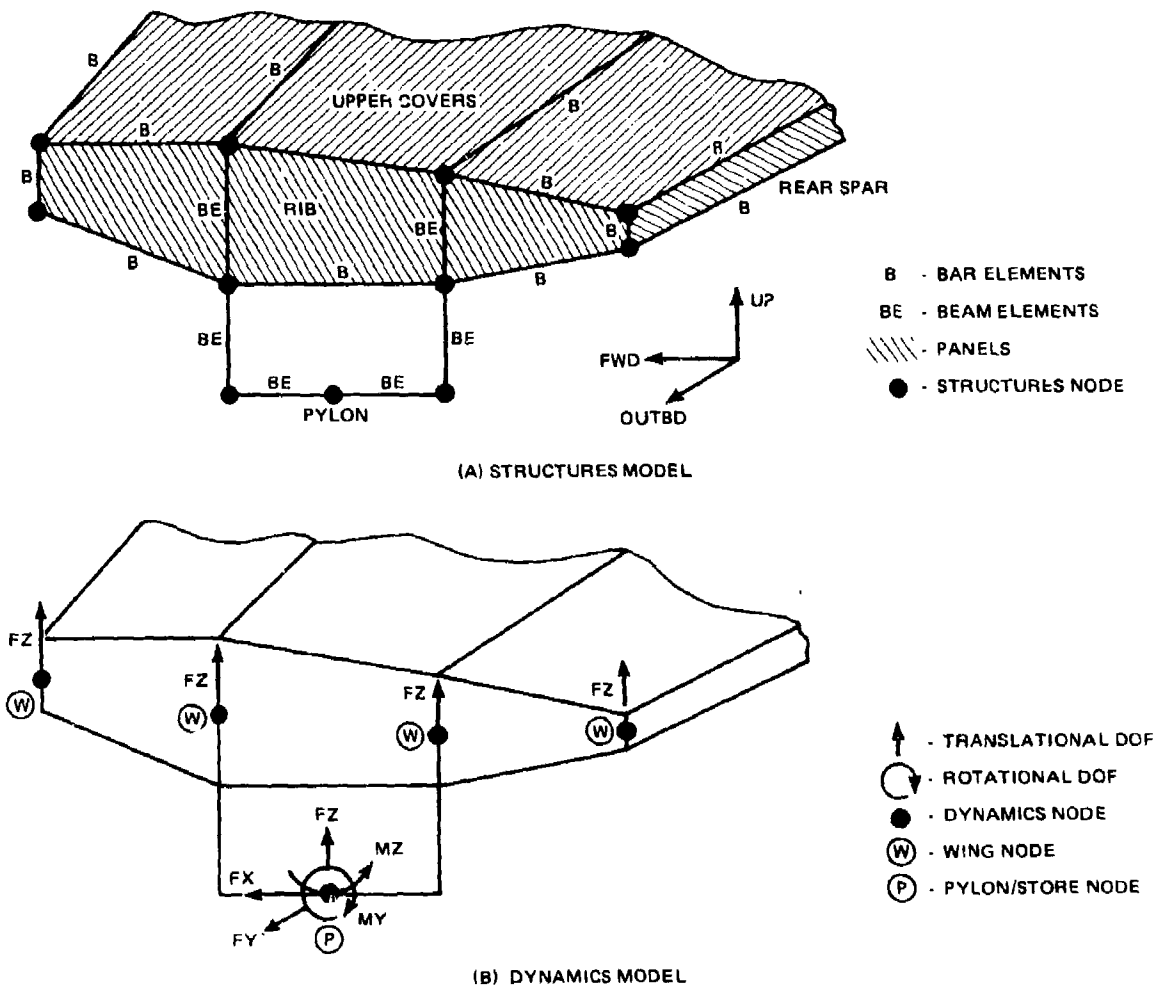

Fig. 4-2 Typical Structures and Dynamics Models at a Pylon Rib Station

where the bars denote revised quantities. Thus,

$$\frac{\partial [\bar{K}_D]}{\partial \Delta_i} [\bar{C}_D] + [\bar{K}_D] \frac{\partial [\bar{C}_D]}{\partial \Delta_i} = 0$$

$$\frac{\partial [\bar{K}_D]}{\partial \Delta_i} = - [\bar{K}_D] \frac{\partial [\bar{C}_D]}{\partial \Delta_i} [\bar{K}_D] \qquad (4\text{-}9)$$

Since the matrix $\partial [\bar{C}_D] / \partial \Delta_i$ contains all zero terms except for a "1" at the ith diagonal entry, (4-9) becomes

$$\frac{\partial[\bar{K}_D]}{\partial \Delta_i} = \left\{\bar{K}_i\right\} \cdot \left\{\bar{K}_i^T\right\} \quad (4\text{-}10)$$

where $\left\{\bar{K}_i\right\}$ is the ith column of $\left[\bar{K}_D\right]$.

Hence, only this one column of the revised stiffness matrix need be computed. An expression for this column is derived in Appendix A. If only one flexibility is taken as a variable (i.e., if $[\Delta]$ is all zero except for the ith entry), the expression is particularly simple:

$$\left\{\bar{K}_i\right\} = r\left\{K_i\right\} \quad (4\text{-}11)$$

where r is a constant given by

$$r = \frac{1}{1 + \Delta_i k_{ii}} \quad (4\text{-}12)$$

and k_{ii} is the i-i term of the original stiffness matrix. In this case, (4-10) becomes

$$\frac{\partial[\bar{K}_D]}{\partial \Delta_i} = r^2 \left\{K_i\right\} \cdot \left\{K_i^T\right\} \quad (4\text{-}13)$$

For the more general case of p variables considered in Appendix A,

$$\frac{\partial[\bar{K}_D]}{\partial \Delta_i} = \left[K_p\right] \cdot [R]^2 \cdot [K_p]^T, \quad (4\text{-}14)$$

where

$$[R] = \left([I] + [\Delta]\ \left[K_{pp}\right]\right)^{-1} \quad (4\text{-}15)$$

and $\left[K_p\right]$ is the matrix of p columns of $\left[K_D\right]$. Upon inspecting this equation, we conclude that $\left[K_p\right]$ need be computed only once (for the original, nominal pylon) while [R] - a relatively small matrix - must be computed at each step of the search.

5 - ESP PILOT PROGRAM

The theory described in Section 3 is implemented in the present application using the pilot computer code to be discussed. As an aid to understanding, the discussion will follow a top-down approach. Successive subsections will discuss the program in increasing levels of detail. However, the discussion is not carried to the level of a programmer's manual; rather, it is intended as an overview.

5.1 ESP

A pilot computer program developed in Ref. 1 was expanded in the present study. For identification purposes, the program has been given the acronym ESP (External Stores Program).

ESP is built around an extensive analysis and structural optimization package, FASTOP (Flutter And Strength Optimization Program, Ref. 7). In particular, a modified version of the Flutter Optimization Module of FASTOP (FOP) is used to perform three tasks: (1) vibration analysis, (2) flutter analysis, and (3) computation of the derivatives of flutter speed with respect to store parameters. The modifications to FOP enable it to perform task (3) and allow the multiple, sequential performance of all three tasks necessary for implementing the iterative search. Additional routines were written to direct the search and change the store parameters as the search progresses.

The logical flow of ESP is shown in Fig. 5-1. For an initial user-specified store combination, FOP computes the mass matrix, normal modes, flutter speed, and aerodynamic, inertial, stiffness, and flutter-speed derivatives. Using the search algorithm described below, the program then computes revised values of the store parameters. Control then returns to the start of the program, a revised mass and/or flexibility matrix is computed, and a second cycle of analysis is performed. This iteration continues for a user-specified number of cycles or until convergence is achieved.

5.2 VIBRATION ANALYSIS MODULE

As discussed in Ref. 7, the Vibration Analysis Module (VAM) of FOP computes normal-mode frequencies and shapes for a user-specified dynamics model. Free-free or cantilevered models are allowed. As modified for ESP, VAM can accept a

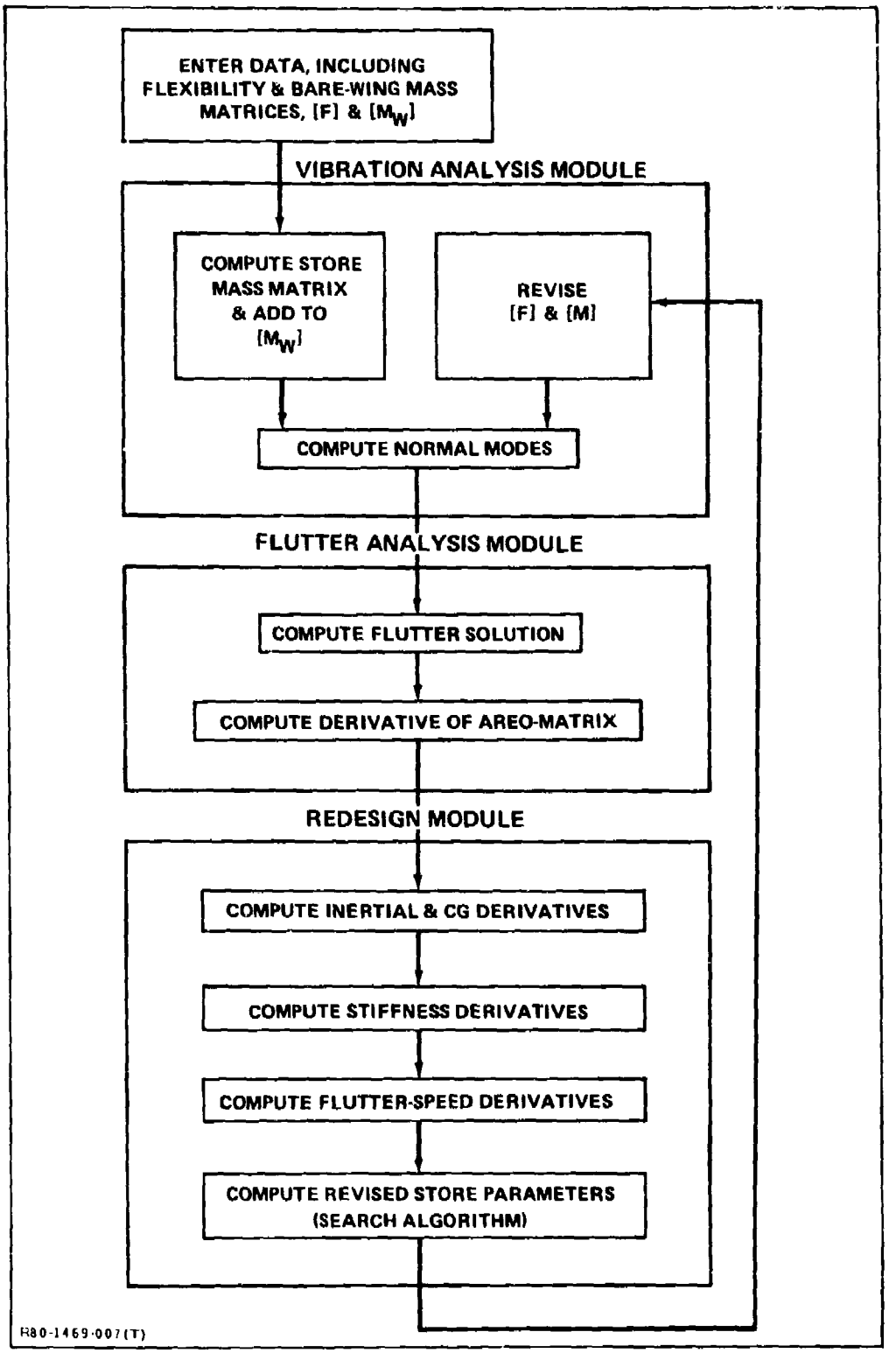

Fig. 5-1 ESP Flowchart

flexibility matrix generated external to the FASTOP system. An input mass matrix is modified at each step of the search to reflect the current inertial characteristics of the stores. (This is accomplished by altering the mass, inertias, and center-of-gravity values at the designated pylon/store attachment nodes.) Similarly, the flexibility matrix is updated when pylon flexibility is taken to be a search variable.

5.3 FLUTTER ANALYSIS MODULE

This module computes generalized aerodynamic forces and then performs flutter analysis. First, an initial setup run is performed, during which unsteady aerodynamic influence coefficient matrices are calculated for six reference reduced frequencies and stored on magnetic tape (or disk). Then, during the performance of each cycle of the searches, these matrices are read from tape and pre- and post-multiplied by the columns of the current normal modes and downwashes, respectively, to produce generalized aerodynamic forces for each of the six reference reduced frequencies. In the present study, the doublet-lattice method is used in the aerodynamic calculations.

For each cycle of the search, a flutter analysis is performed using the p-k solution method in FASTOP. The generalized forces needed at various reduced frequencies are obtained by interpolation from those at the six reference values. For use in (4-1), the module computes the flutter speed, frequency, eigenvector and associated row eigenvector, and the derivative of the aerodynamic force matrix with respect to the reduced frequency at flutter.

5.4 REDESIGN MODULE

The redesign module computes the derivatives of the inertia (4-3, 4-4, and 4-5) and stiffness (4-14) matrices, from which it then computes flutter speed derivatives (4-1). It then calls the search module to calculate revised store parameters.

5.5 SEARCH MODULE

Figure 5-2 shows the routines in the top level of the search module (STRDES). First, the store search variables are scaled (non-dimensionalized) by subroutine VSCALE. Next (for all the steps but the first), the flutter speed at the current point is compared to that of the last acceptable point. If it is larger, an overshoot has occurred and LINESR is called to do a line search to obtain a new step size. If it is smaller, the current point is accepted, ROC is called to compute a new unconstrained search direction, and CONSTR is called to compute the (possibly) constrained move

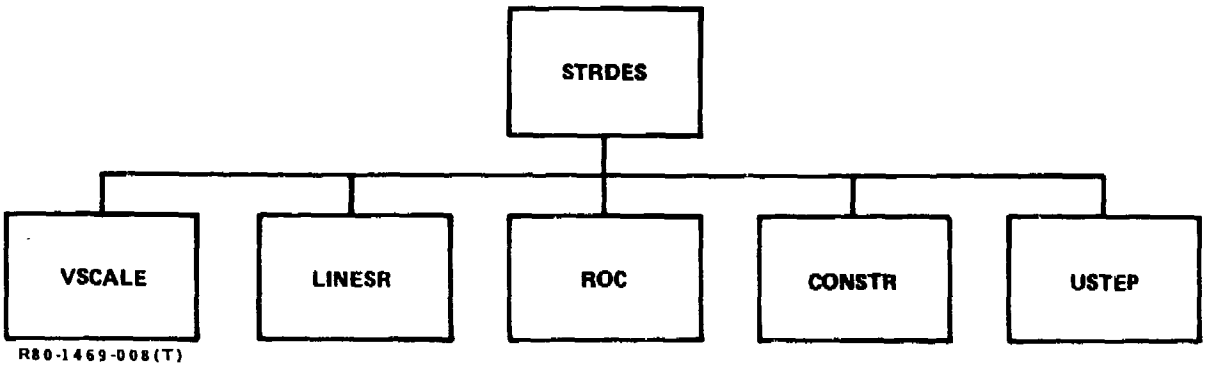

Fig. 5-2 Submodules of Search Module

direction and step size. In either case, USTEP is then called to make the move to the next point. Finally, VSCALE is again called to unscale the new point's parameters.

5.5.1 VSCALE

The scalings done are

$$x_k^j = \xi_k^j / a^j$$

$$f_k^o = V_k / a^o \qquad (5\text{-}1)$$

$$\left(g_k^o\right)^j = \frac{a^j}{a^o}\left(\frac{\partial V}{\partial \xi^j}\right)_k$$

where

a^o is the flutter speed scale factor

a^j is the scale factor on the jth variable

ξ^j is the jth store variable.

The scale factors are chosen as the largest anticipated values of the flutter speed and the respective store variables in the analysis.

5.5.2 LINESR

A cubic fit, in the step size α, to the function f^o is performed based on the function values and derivatives at each end of the step:

$$f^o(\alpha = 0) = f^o(x_k), \qquad f'^o(\alpha = 0) = \vec{g}_k^o \cdot \Delta\vec{x}_k$$

$$f^o(\alpha_k), \qquad f'^o(\alpha_k) = \vec{g}_{k+1}^o \cdot \Delta\vec{x}_k \qquad (5\text{-}2)$$

The α that minimizes this cubic is then determined analytically.

5.5.3 ROC

This routine first computes the new estimate [S] of the inverse Hessian matrix using (3-12), and then computes the move direction using (3-6).

5.5.4 USTEP

This routine uses (3-5) to determine the new step.

5.5.5 CONST

Figure 5-3 shows the constituent subroutines in the constrained-search submodule (CONSTR). The five routines (SETJGL, ADDCON, DELCON, LDFIX, and LMKP1) determine and update the status of the constraints. A constraint may be inactive or active. If active, it may be linearly dependent on or independent of the other active constraints. A set of linearly independent active constraints, which is a subset of all active constraints, is required for various operations and must be kept current. These routines also form and update the [L] matrix of (3-19).

Routines LAGMUL and HYPER compute the Lagrange multipliers, using (3-19), and the direction of the constrained move, using (3-20), respectively. After the direction has been obtained, CONSTR calls routine INSECT to determine the step size, using (3-21) through (3-24).

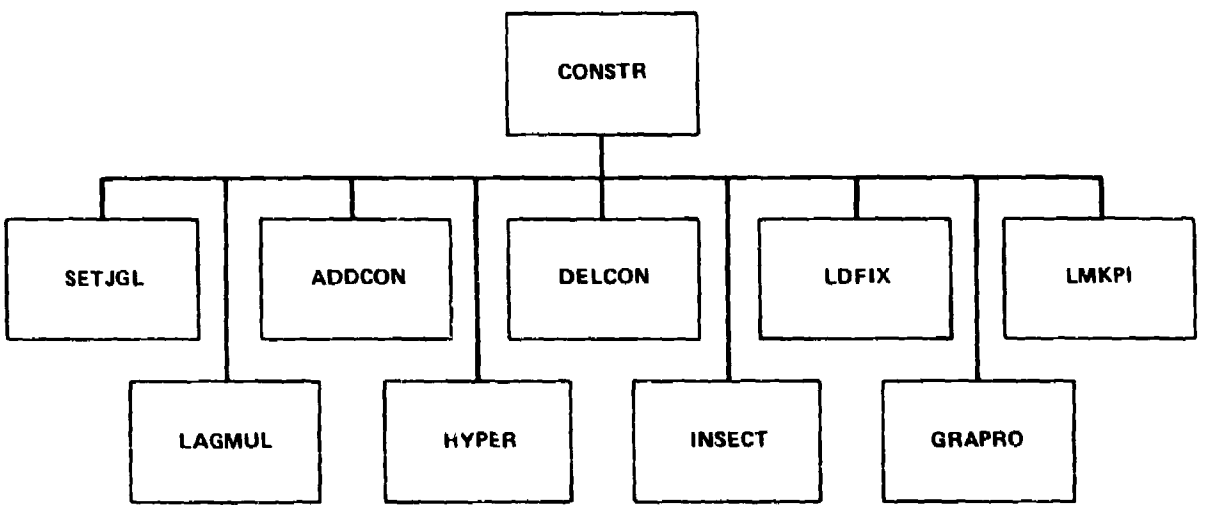

Fig. 5-3 Submodules of Constrained-Search Module

Among other tasks, CONSTR performs the tests, (3-25) through (3-29), for the existence of a minimum. For the test given by (3-29), a normal projection of the local gradient onto the subspace of active constraints is needed. This projection is calculated in GRAPRO.

6 - DEMONSTRATION PROBLEM

The aircraft chosen for demonstration of the method was the A-6 Intruder, shown in Figure 6-1. The A-6 is a subsonic, moderately-swept-wing, carrier-based attack aircraft carrying stores at two stations on each wing and at a station under the fuselage. The five store locations allow the aircraft to carry a large variety of missiles, drop tanks, and bombs weighing up to 3600 lb per store station. The addition of multiple- and triple-ejection racks (MER and TER) results in a vehicle with over a million different store configurations, making it a sufficiently complex study case.

The math models of the aircraft used in the demonstration are described below. The models were obtained from flutter-clearance studies performed during the course of a recent store-inventory addition to the A-6E aircraft, i.e., the A-6/Harpoon Integration project. This choice of models assures commonality with current project design data.

6.1 DYNAMICS MATH MODEL

The idealization used by project personnel was a beam-model representation of the complete aircraft, consisting of 92 dynamics nodes and 284 degrees of freedom (including plug) for the symmetric free-free analysis. A drawing of the model is provided in Figure 6-2. (The node numbering is peculiar to the beam-model dynamics program used to generate the flexibility matrix. Some details that perhaps need clarification are: nodes 901-912 are on the fin; 101-105 are on the rudder; nodes 001-002 represent the flaps; node 211 represents the speed brake; and nodes 182-184, 192-194, and 201-204 are placed along extremely light artificial beams connected to the outboard, inboard, and centerline pylons, respectively. These last three sets of nodes are present so that pylon modal motions (pitch, yaw, etc.) can be seen in computer-generated plots of the normal modes.)

As stated above, this model was selected for the present study so that direct correlation could be made with A-6 project results. However, the use of this model in ESP resulted in computer-programming complications. ESP, which is a derivative of the FASTOP system (Flutter and Strength Optimization Program, Ref. 7), was originally programmed to receive a flexibility matrix on a specially formated tape generated for a finite-element structural model created by the structural-analysis module of FASTOP. Use of the desired A-6 math model required modification of the ESP code to enable it to use an externally created flexibility matrix.

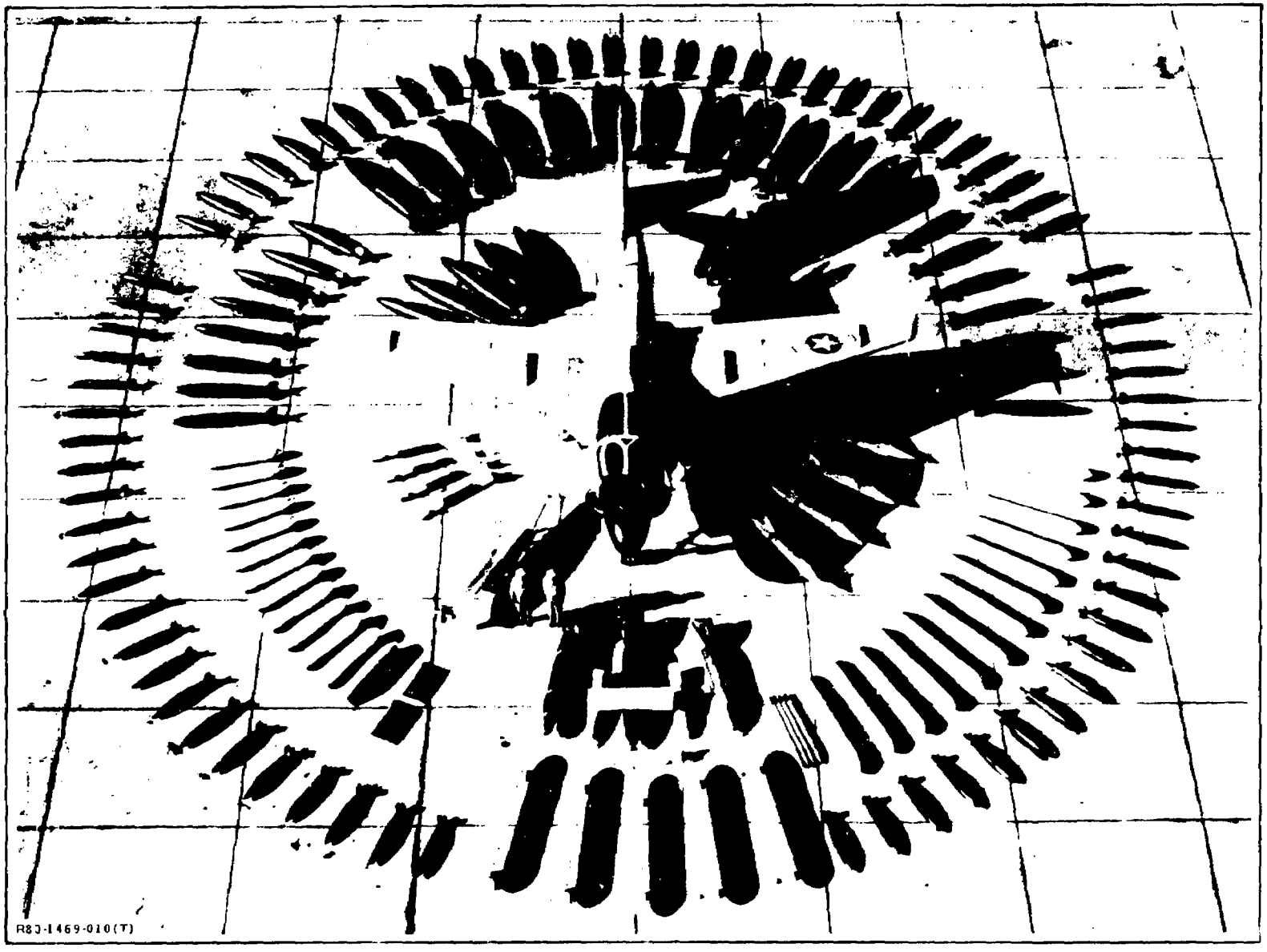

Fig. 6-1 A-6 Attack Airplane with Representative Stores

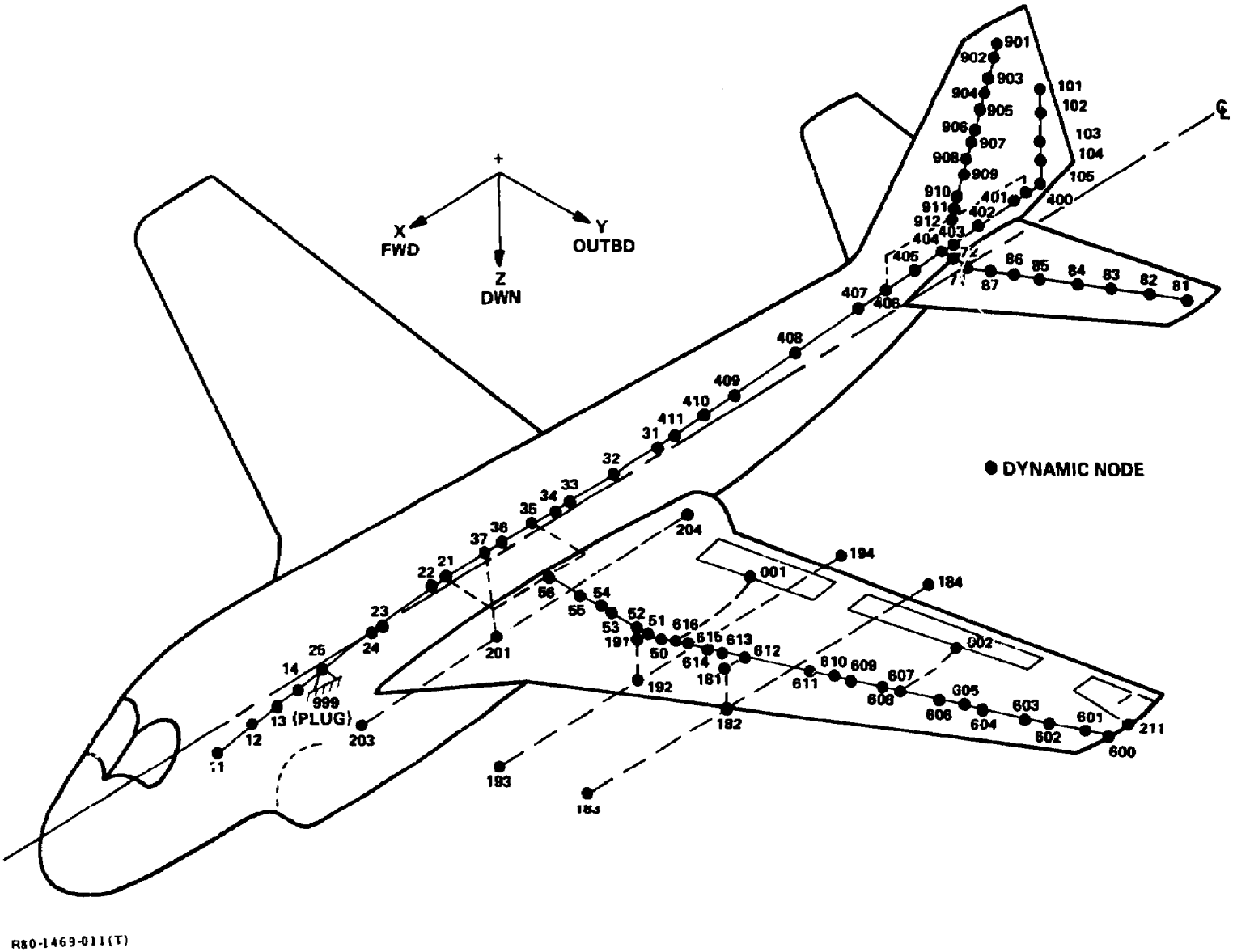

Fig. 6-2 A-6E Dynamics Math Model

A second complication was due to the fact that the cited dynamics model included several rigid-link members and, thus, the resulting flexibility matrix was singular. Consequently, computation of flutter derivates with respect to pylon flexibilities could not initially be performed because (as discussed in Section 4) the calculation required that the stiffness matrix be obtained by an inversion of the flexibility matrix. To remedy this situation, the model was modified slightly by replacing the rigid links with stiff members. To verify that the revised model was sufficiently equivalent to the original model, normal modes computed in ESP using the new model were compared with those obtained by project personnel using the original idealization in a different vibration-analysis computer program. The configuration used for this comparison was the symmetric, free-free, clean wing with no wing fuel. Table 6-I shows the computed frequencies of the lowest 16 normal modes. As can be seen, results using the revised model (Rev. 1) agree well with those of the original.

To economize the computing time required for the study, it was decided to generate a reduced-size dynamics model, equivalent to the original idealization in most respects. This was accomplished by replacing the detailed modelling of the airplane tail by a lumped mass (with the proper inertial characteristics) on the aft fuselage and replacing the speed brake by added inertias at the wing tip node. This simplified model has 209 degrees of freedom, whereas the original has 284. Since the computational time needed for a vibration analysis varies as the third power of the problem size, this simplified model required only 40% of the time required by the original idealization for each of the many vibration analyses performed during the study. Modal results for the clean wing are presented (Rev. 2) in Table 6-I. In comparison with the previous results, it is seen that the new model adequately duplicates the lowest modes of the original model with the exception of third wing bending; of course, stabilizer and speed-brake modes are missing. This representation was considered adequate for the purpose of the present study. For reference computer-generated plots of the mode shapes of the lowest nine modes for the final idealization are presented in Fig. 6-3 through 6-11.

The reductions in the number of modes obtained from the revised model also led to a substantial economy in the flutter analyses. As in the case of vibration analysis, the computational time needed for a flutter analysis varies as the third power of the problem size. However, since the flutter analysis is performed in modal coordinates, the

TABLE 6-I A-6E SYMMETRIC, FREE-FREE, CLEAN-WING, NORMAL MODES COMPUTED USING VARIOUS DYNAMICS MATH MODELS

ORIGINAL		REVISION 1 (STIFF MEMBERS)		REVISION 2 (LUMPED TAIL)		MODEL DESCRIPTION
MODE	FREQ, Hz	MODE	FREQ, Hz	MODE	FREQ, Hz	
1	4.9	1	4.9	1	4.9	WING 1ST BENDING
2	10.2	2	10.2	2	10.6	FUSELAGE 1ST BENDING
3	14.1	3	14.2	3	14.8	WING 2ND FUSELAGE
4	16.3	4	16.2	–	–	STABILIZER ROOT BENDING
5	18.9	5	18.0	4	18.2	WING 1ST FORE-AFT
6	23.4	6	23.4	5	23.9	WING 1ST TORSION/FUSELAGE 2ND BENDING
7	26.3	7	25.9	6	26.1	FUSELAGE 2ND BENDING/WING 1ST TORSION
8	27.4	8	26.6	–	–	STABILIZER ROOT FORE-AFT
9	29.7	9	29.7	7	31.5	WING TIP TORSION/WING 3RD BENDING
10	36 8	10	36.7	–	–	WING 3RD BENDING
11	40.3	11	40.3	8	39.6	FLAPS ROTATION – OUT OF PHASE
12	41.6	12	41.6	9	41.0	FLAPS ROTATION - IN PHASE
13	45.4	13	45.0	11	46.3	FUSELAGE 3RD BENDING
–	–	–	–	10	41.3	WING 2ND TORSION/3RD BENDING
14	48.7	14	48.6	–	–	SPEED BRAKE ROLL
15	49.7	15	49.6	–	–	SPEED BRAKE ROTATION
16	52.6	16	52.2	–	–	STABILIZER PITCH

R80-1469-012(T)

flutter-problem size is the number of modes selected. For example, by selecting all modes less than 53 Hz, 11 modes would be needed rather than the original 16 and the reduced model would require only 32% of the time taken by the original for each flutter analysis performed. Since each flutter analysis requires much more time than the associated vibration analysis, this savings is very significant.

6.2 FLUTTER MATH MODEL

The aircraft idealization used in the flutter-clearance studies on the A-6/Harpoon Integration project was obtained. The model is comprised of an aerodynamic idealization of the wing and stabilizer, and the previously described dynamics model of the complete vehicle. The aerodynamics are computed by the doublet-lattice method, using 40 singularity panels on the wing (Fig. 6-12) and 25 panels on the stabilizer (Fig. 6-13). For each normal mode, the downwash distributions on these surfaces are obtained from the modal deflections and streamwise rotations of the dynamics-model nodes. (These nodes also are shown in Fig. 6-12 and 6-13.)

The flight conditions chosen for the present study are a Mach number of 0.90 and an altitude of 10,000 ft. As a check on the correctness of the present data setup, a flutter analysis was performed in ESP using the clean-wing modes from the original dynamics model. The resultant flutter speed (693 keas) and frequency (9.4 Hz) agree to within 1% with those computed by A-6/Harpoon project personnel, Ref. 8.

Consistent with the simplifications made in the dynamics model, the stabilizer was deleted from the flutter model used in the subsequent analyses. The clean-wing flutter analysis was rerun using modes from the final revised dynamics model and the final flutter model (no stabilizer). The resultant flutter speed (698 keas or 812 ktas) and frequency (9.5 Hz) are in excellent agreement with those cited above. V-g and V-f plots are presented in Fig. 6-14. The flutter mechanism for this clean-wing configuration involves mode 1 (wing first bending), mode 3 (wing second bending), and mode 5 (wing first torsion).

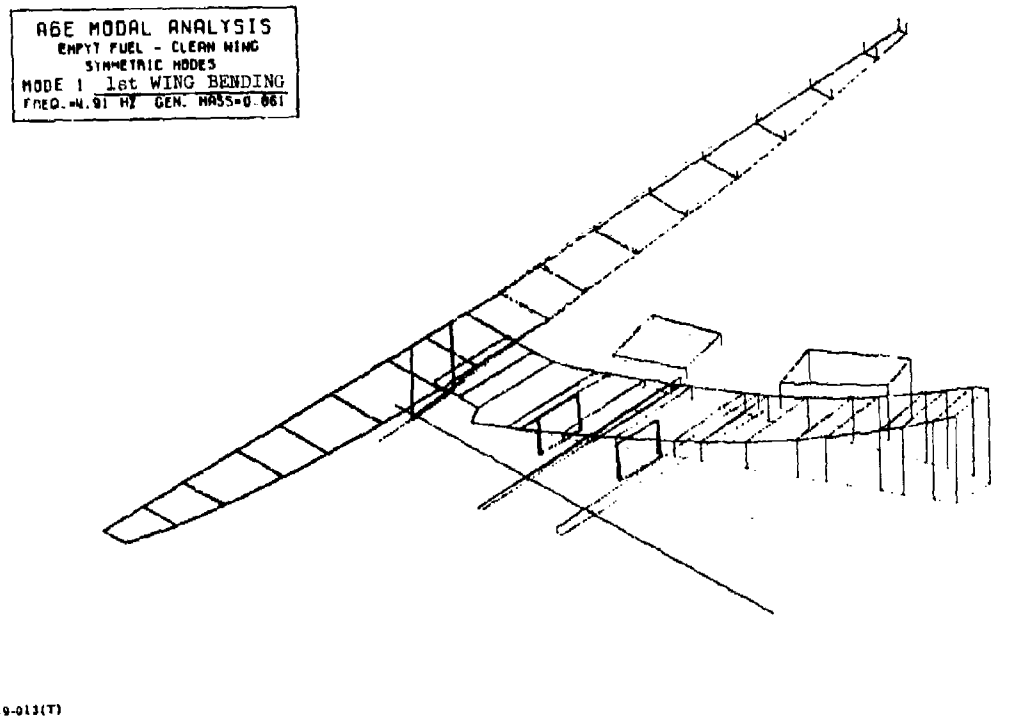

R80-1469-013(T)

Fig. 6-3 A-6E Clean Wing: Mode 1

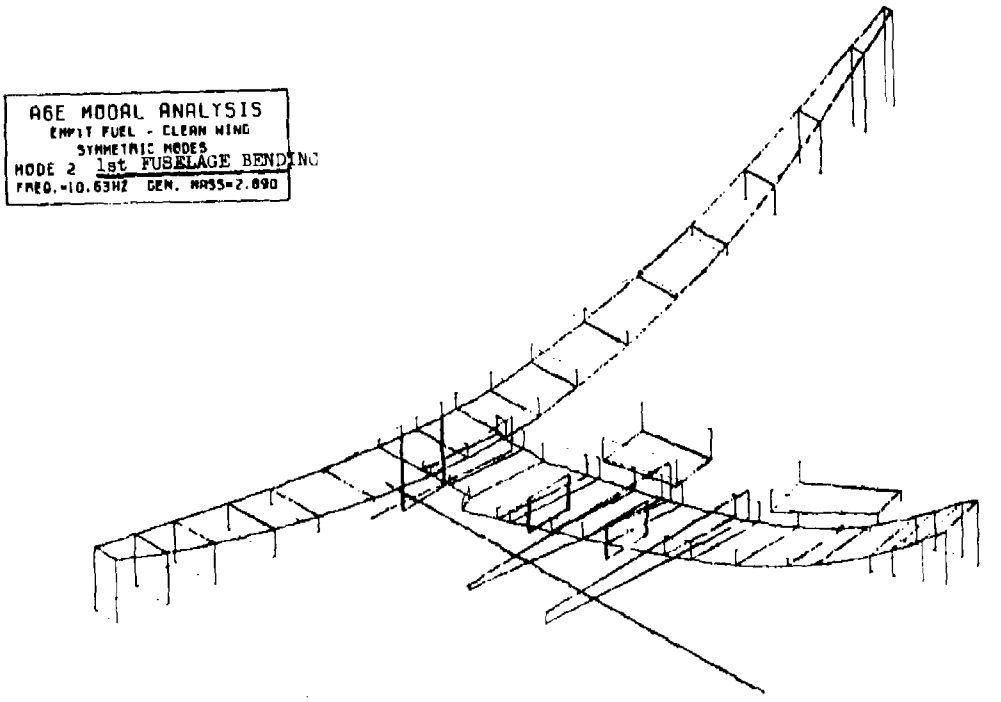

R80-1469-014(T)

Fig. 6-4 A-6E Clean Wing: Mode 2

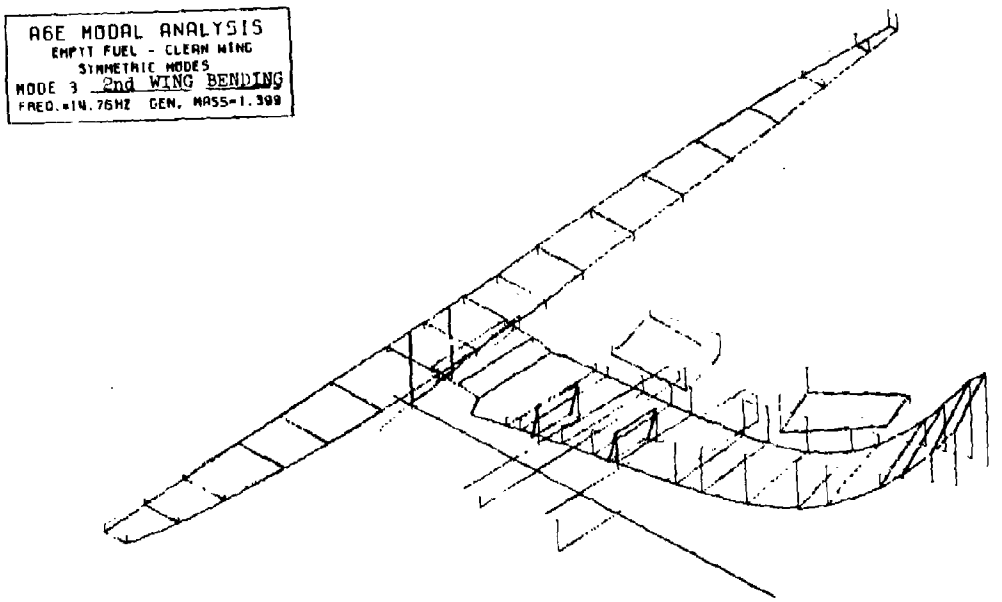

R80-1469-015(T)

Fig. 6-5 A-6E Clean Wing: Mode 3

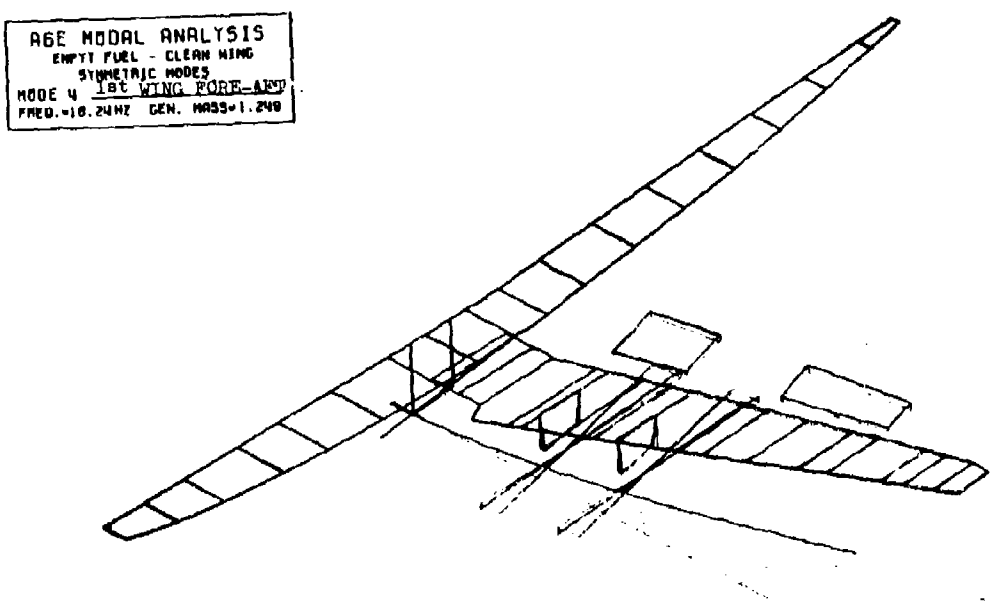

R80-1469-016(T)

Fig. 6-6 A-6E Clean Wing: Mode 4

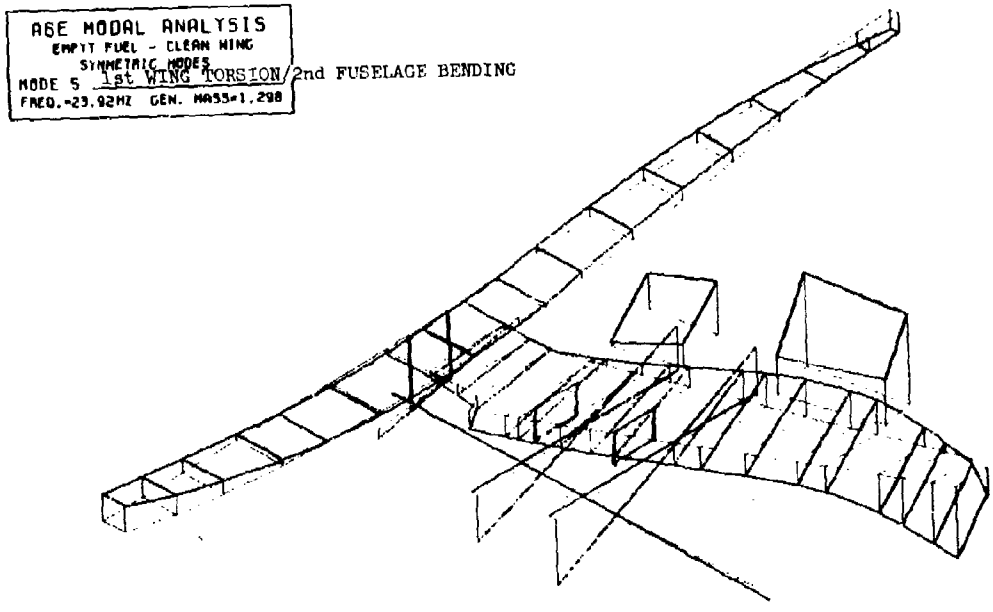

R80-1469-017(T)

Fig. 6-7 A-6E Clean Wing: Mode 5

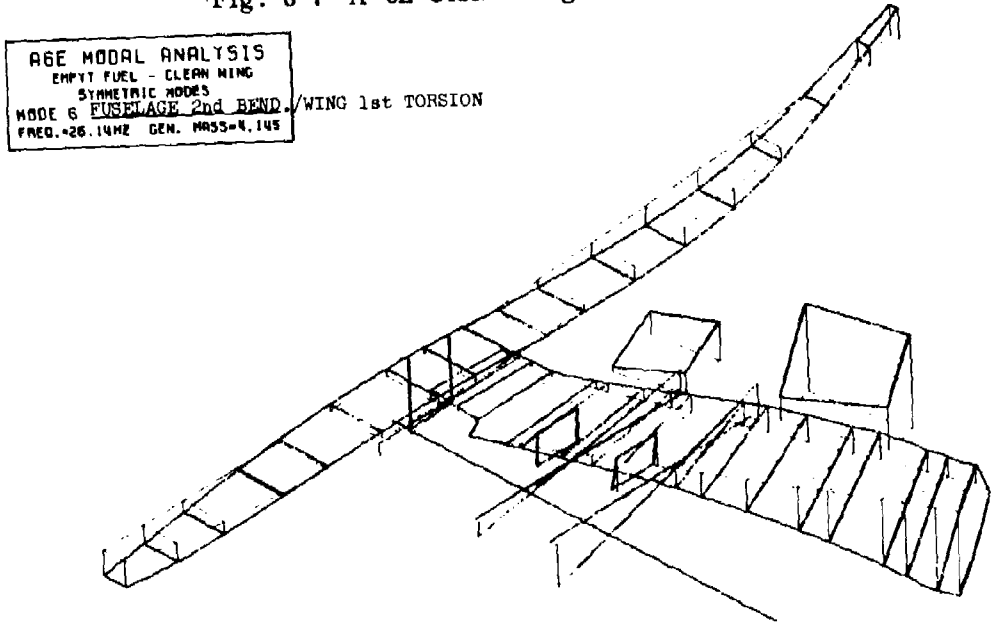

R80-1469-018(T)

Fig. 6-8 A-6E Clean Wing: Mode 6

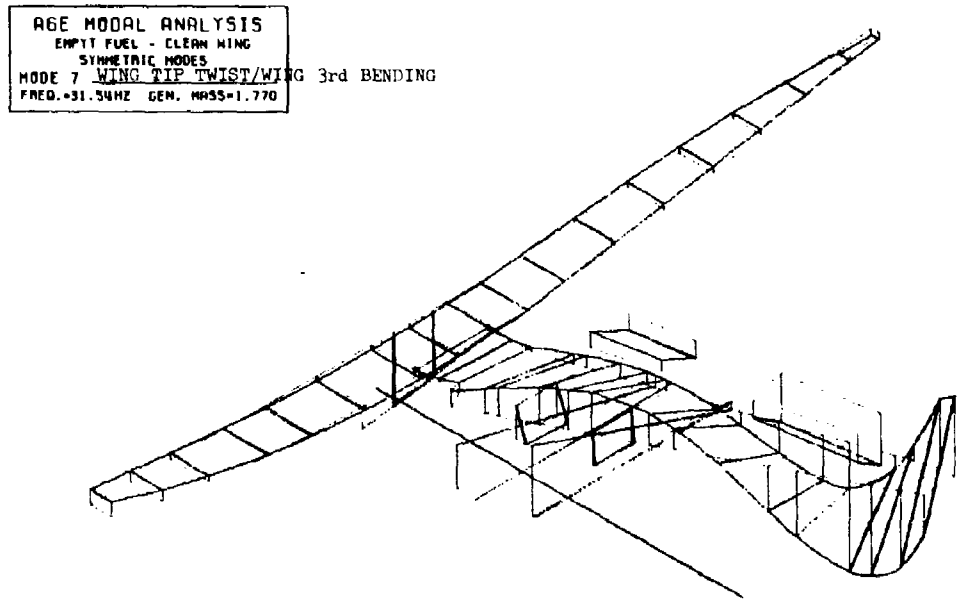

R80-1469-019(T)

Fig. 6-9 A-6E Clean Wing: Mode 7

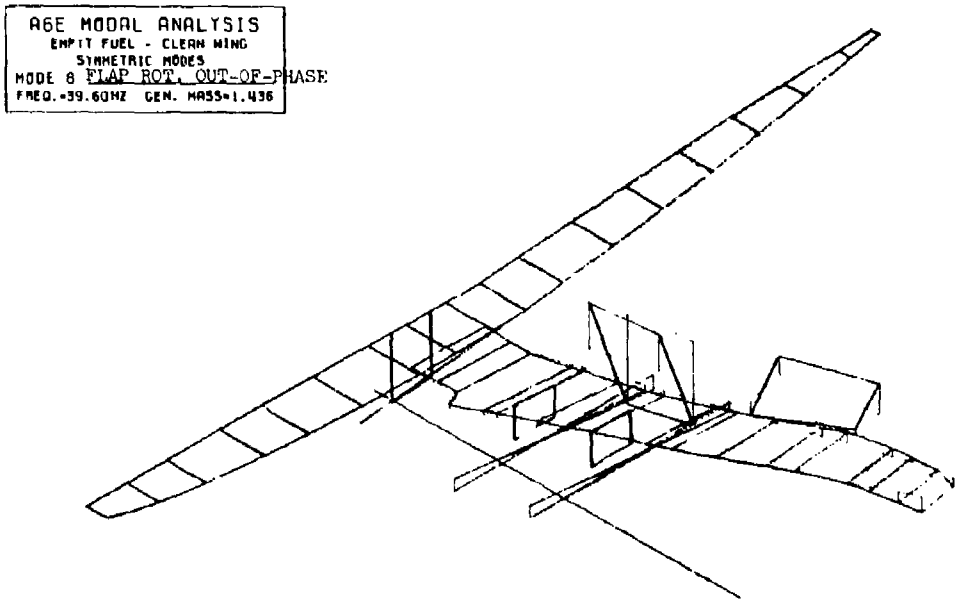

R80-1469-020(T)

Fig. 6-10 A-6E Clean Wing: Mode 8

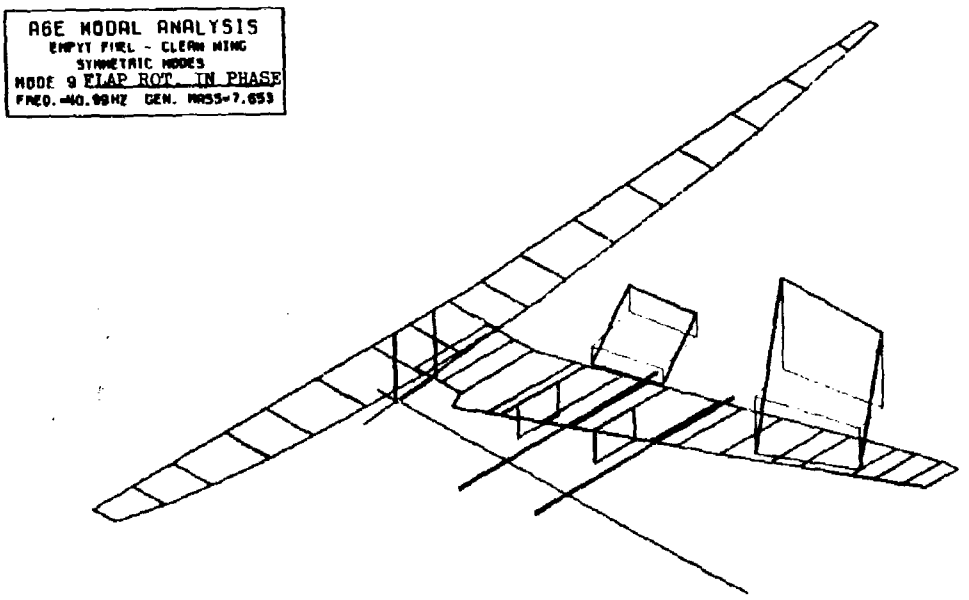

RGD-1469-021(T)

Fig. 6-11 A-6E Clean Wing: Mode 9

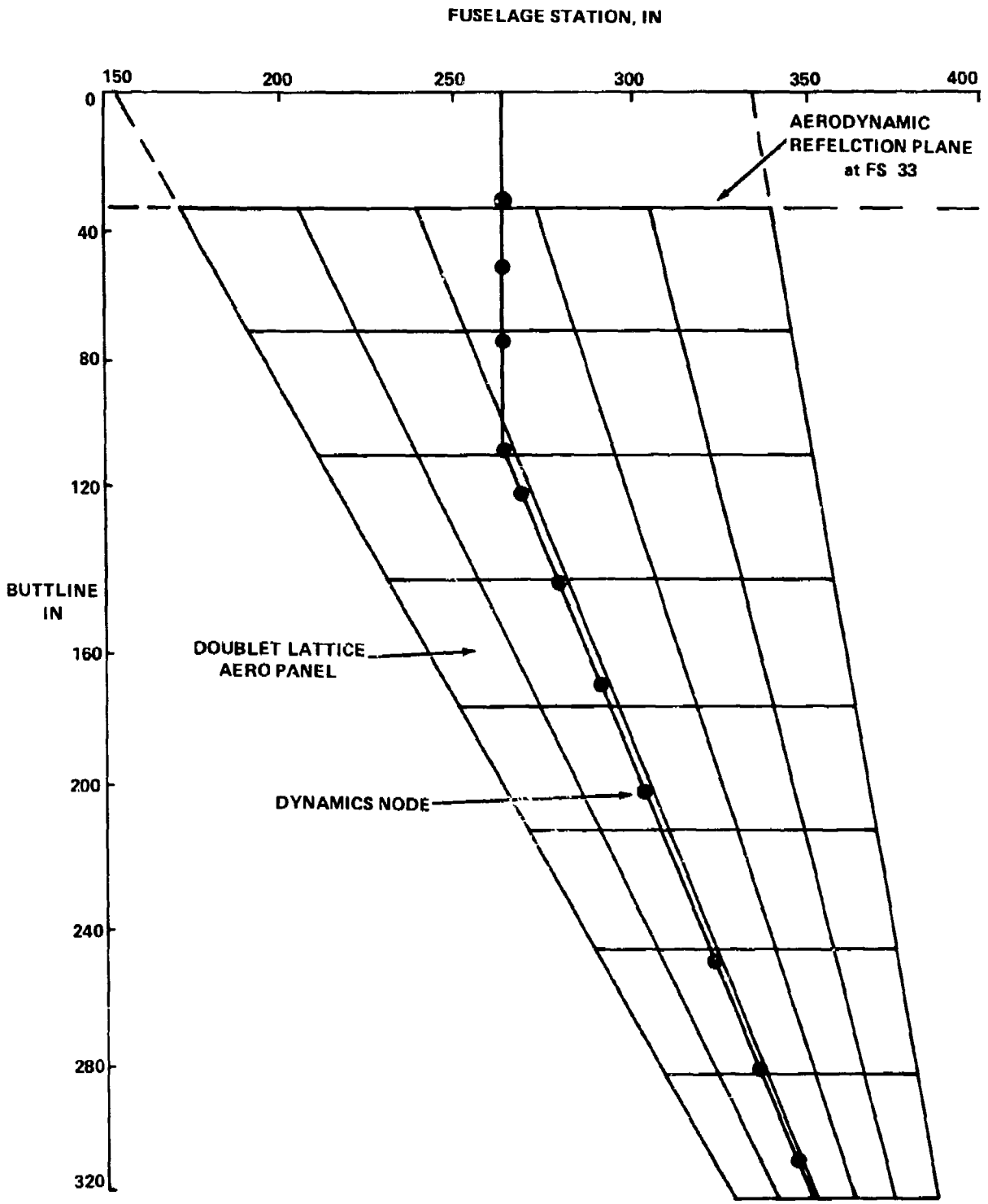

Fig. 6-12 Flutter Math Model for the A-6E Wing

R80-1469-022(T)

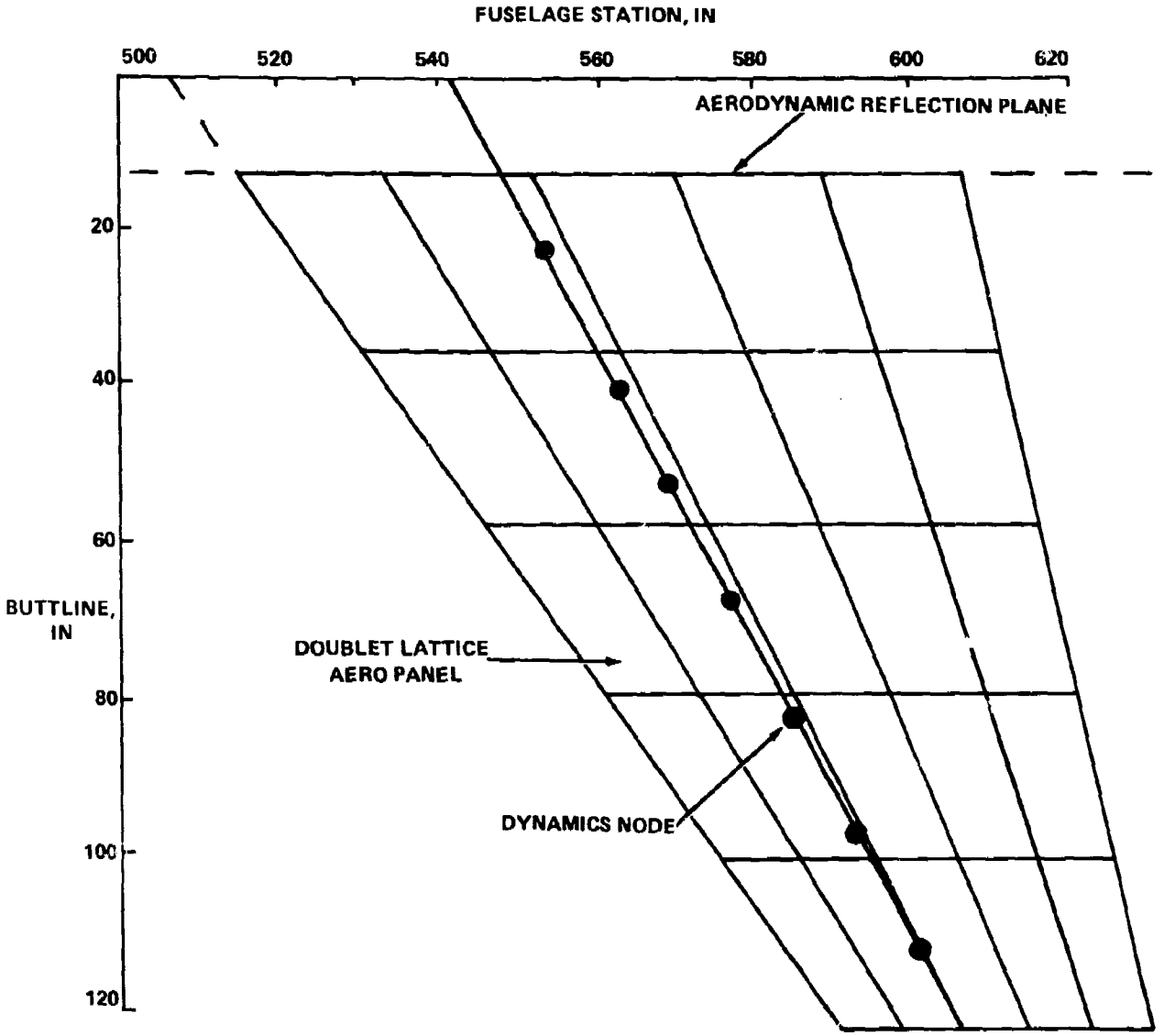

Fig. 6-13 Flutter Math Model for the A-6E Stabilizer

R80-1469-023(T)

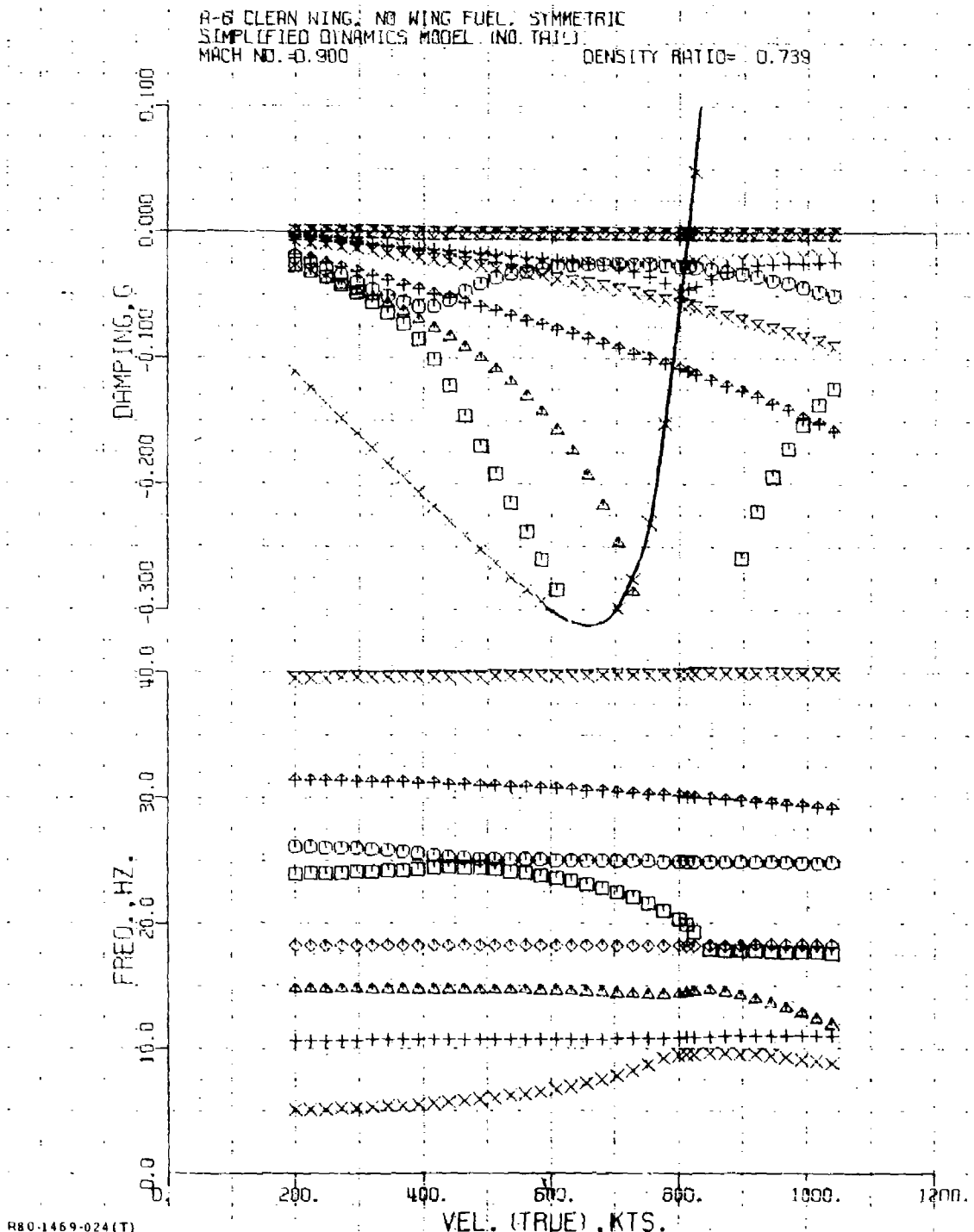

Fig. 6-14 V-g-ω Plots for A-6E, Clean Wing

7 - DEMONSTRATION INVENTORY

7.1 ENUMERATION OF CONFIGURATIONS

The store inventory was obtained from the A-6 Tactical Manual (U), NWP55-3-A6, Vol. 1, NAVAIR 01-85ADA-1T (Ref. 9) and is itemized in Table 7-I, taken directly from that source. As can be seen, more than eighty distinct stores are possible. To this number must be added the configurations that are obtained when many of these stores are placed (one, two, or three at a time) on a TER and the 15 distinct configurations per store type that arise when a MER is employed. This brings the number of unique configurations to the order of a thousand for each pylon. The pylons in combination bring the total to the order of a million.

To define the allowable combinations of inertial parameters arising from the configurations in the inventory, a data base containing weight/moment-of-inertia data for the individual stores listed in Table 7-I was established. After extensive examination of the Tactical Manual (Ref. 9) and various government and in-house store manuals (Ref. 10-12), moment of inertia data for many stores were still undetermined. Consequently, estimates of these quantities were made, based on inspection of parts drawings and comparisons with similar stores.

The data base was expanded (by means of a simple computer code) to include allowable stores-on-TER configurations. Figure 7-1 presents a plot of I vs M for the single store and TER configurations, identified by store type. Missiles and tanks are seen generally to have a larger moment of inertia per given mass (higher radius of gyration) than bombs.

The data base was further expanded to include MER configurations and the fore-aft center-of-gravity data for all configurations. Figures 7-2 and 7-3 are projections of the MER data onto the weight/moment-of-inertia (M, I) and weight/center-of-gravity (M, x) planes. The symbols indicate whether a given configuration has stores on both the forward and aft racks of the MER, only on the forward, or only on the aft. As can be seen, moment of inertia is much higher when the loading is distributed. A certain amount of asymmetry about cg = 0 can be detected; this is due to the asymmetry of the empty MER rack itself, the inertial properties of which are combined with the individual stores in each configuration. Since the empty MER rack weighs over 200 lb, its effect is not insignificant -

TABLE 7-1 A-6E STORES INVENTORY

STORE WEIGHTS

BOMBS	WT LB
MK 81 GP BOMB	
CONICAL FIN	260
SNAKEYE FIN	301
MK 82 GP BOMB	
CONICAL FIN	531
SNAKEYE FIN	572
MK 83 LDGP	985
MK 84 LDGP	2006
MK 36 DST	
CONICAL FIN	531
SNAKEYE FIN	572
MK 40 DST WITH MAU-91 FIN	1057
MK 41 DST	2005
MK 82 LGB (KMU-388/B OR GBU-12B/B)	601
MK 83 LGB (KMU-431/B OR GBU-16/B)	1100
MK 84 LGB (KMU-351A/B OR GBU-10 C/B)	2130
MK 20 MOD 2, 3 AND 6 (ROCKEYE II)	496
CBU 59/B APAM	760
CBU 72/B FAE	522
MJU 5/B CHAFEYE	
(WITH RR 145/147AL)	330
(WITH RR 68AL)	423
(WITH RR 94AL)	303
MK 77 MOD 2, 4 FIRE BOMB	520

MISSILES	WT LB
AGM-45 A/B (SHRIKE)	402
AIM-9D/G/H/L (SIDEWINDER)	197
AGM-78 (STANDARD ARM)	1368

ROCKET LAUNCHERS	WT LB FULL EMPTY
LAU-10/A (ZUNI)	533/105
LAU-61/A (2.75 FFAR)	540/133
LAU-69/A (2.75 FFAR)	507/98
LAU 68 (2.75 FFAR)	218/67

NUCLEAR WEAPONS, SHAPES AND MINES	WT LB
B-43 OR-BDU-24/C	2120
B-57 OR-BDU-20/C	500
B-61 OR-BDU-36/C	715
B 61 TYPE 3/E	715
MK 104	2100
BDU 6E	2100
BDU-8/B	2100
BDU 11E	500
BDU-12/B	500
MK 25 MINE	2015
MK 25 DRILL MINE	2132
MK 36 DRILL MINE	1258
MK 52 MINE	1243
MK 52 DRILL MINE	1202
MK 55 MINE	2194
MK 55 DRILL MINE	2128
MK 56 MINE	2215
MK 56 DRILL MINE	2150

TRAINING AND PYROTECHNICS	WT LB
MK 76 MOD 4 PB, BDU-33	26
MOD 5 PB	26
MK 106 MOD 3 PB	6
MOD 4 PB	6
MK 86 WSF PB	217
MK 87 WSF PB	333
MK 88 WSF PB	783
MK 124 PB	666
MK 104 PB	2020
MK 24 MOD 2A, 3, 4, PARAFLARE	28
MK 45 MOD 0 PARAFLARE	28
LUU-2B/B	28
SUU-44/A FLARE CONTAINER (MK 24, MK 45, OR LUU-2 B/B PARAFLARES WITH TRAYS)	371
MK 58 MARINE MARKER	13

TANKS/PODS AND SENSORS	WT LB FULL EMPTY
AERO 1D DROP TANK	2238/198
D 704 REFUELING STORE	2774/700
SARGENT FLETCHER MODEL 31 300 REFUELING STORE	2720/680
CTU 2/A DELIVERY CONTAINER	713/213
ADSID III (FOLDING FIN)	38
SUU 53A	150/100
CNU-188/A	649/218
LB 31A STRIKE CAMERA POD	120
ALE 37A	282/186
ALE 41	589/210
SSQ 36	20
SSQ 41A	21
SSQ 47B	29
SSQ 50	39
SSQ 53	29
SSQ 53A	29
SSQ 62	39

EJECTOR RACKS AND LAUNCHERS	WT LB
AERO-7A EJECTOR RACK	53
AERO-7B EJECTOR RACK	50
A/A 37B-3 PMBR	87
A/A 37B-5 TER	98
A/A 37B-6 MER	214
LAU-7/A MISSILE LAUNCHER	87
AERO-5 MISSILE LAUNCHER	90
ADU-299E	20
AERO-1A ADAPTER	10
GAEC ADAPTER	20
LAU-77A/A ELA	181

K-ADATM 143

Figure 14-2. (U) Store Weights

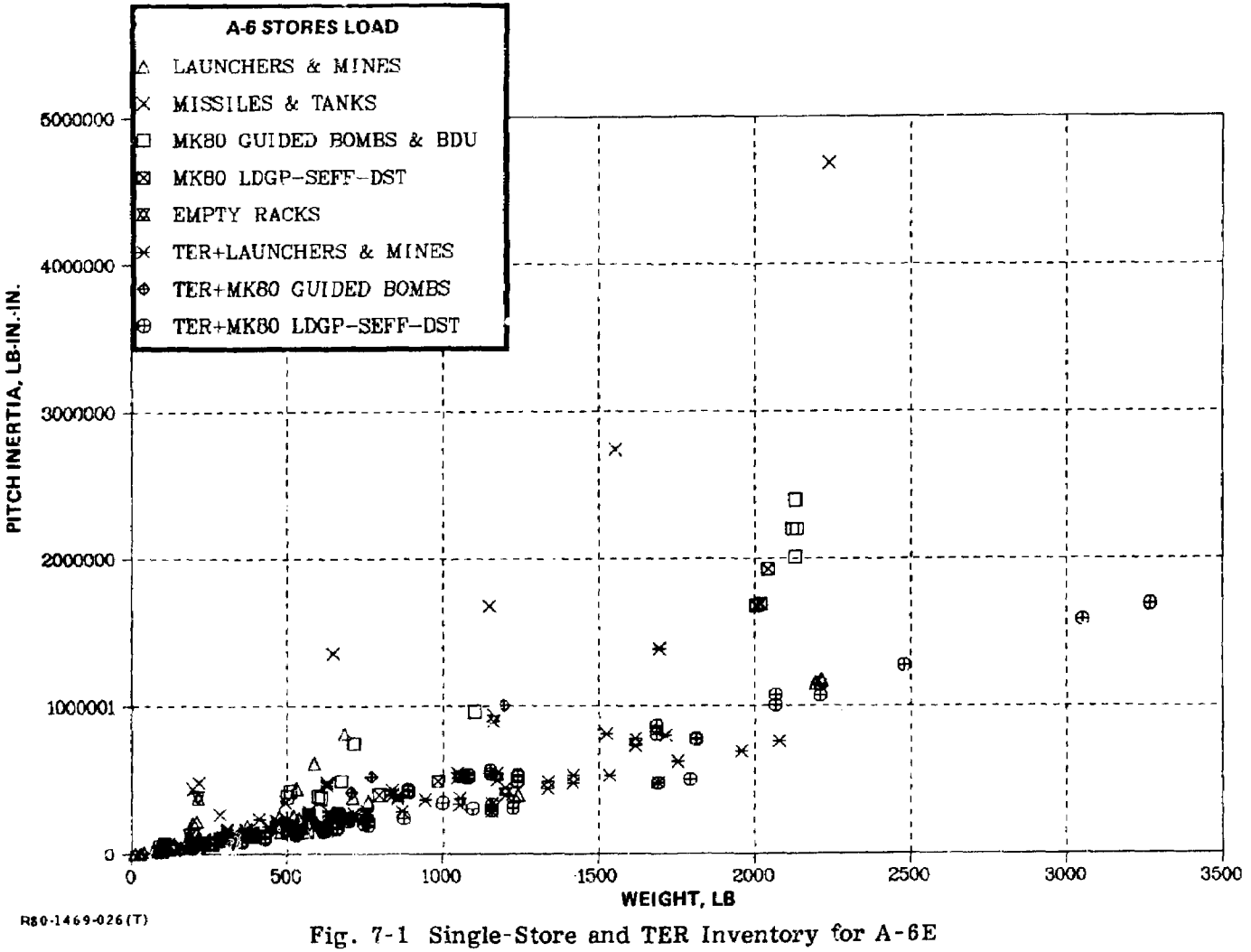

Fig. 7-1 Single-Store and TER Inventory for A-6E

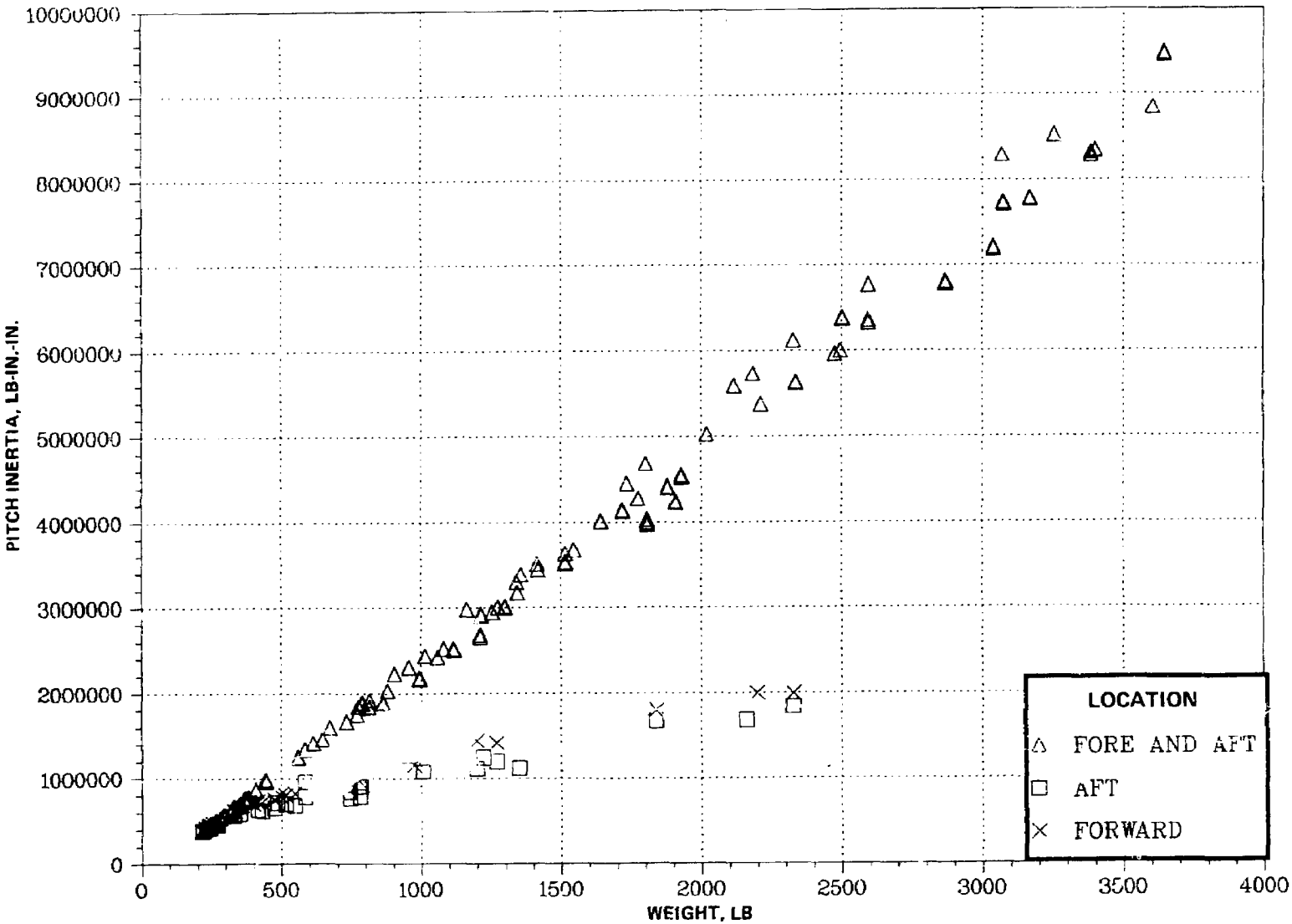

Fig. 7-2 Moment-of-Inertia/Weight Projection, MERs Only

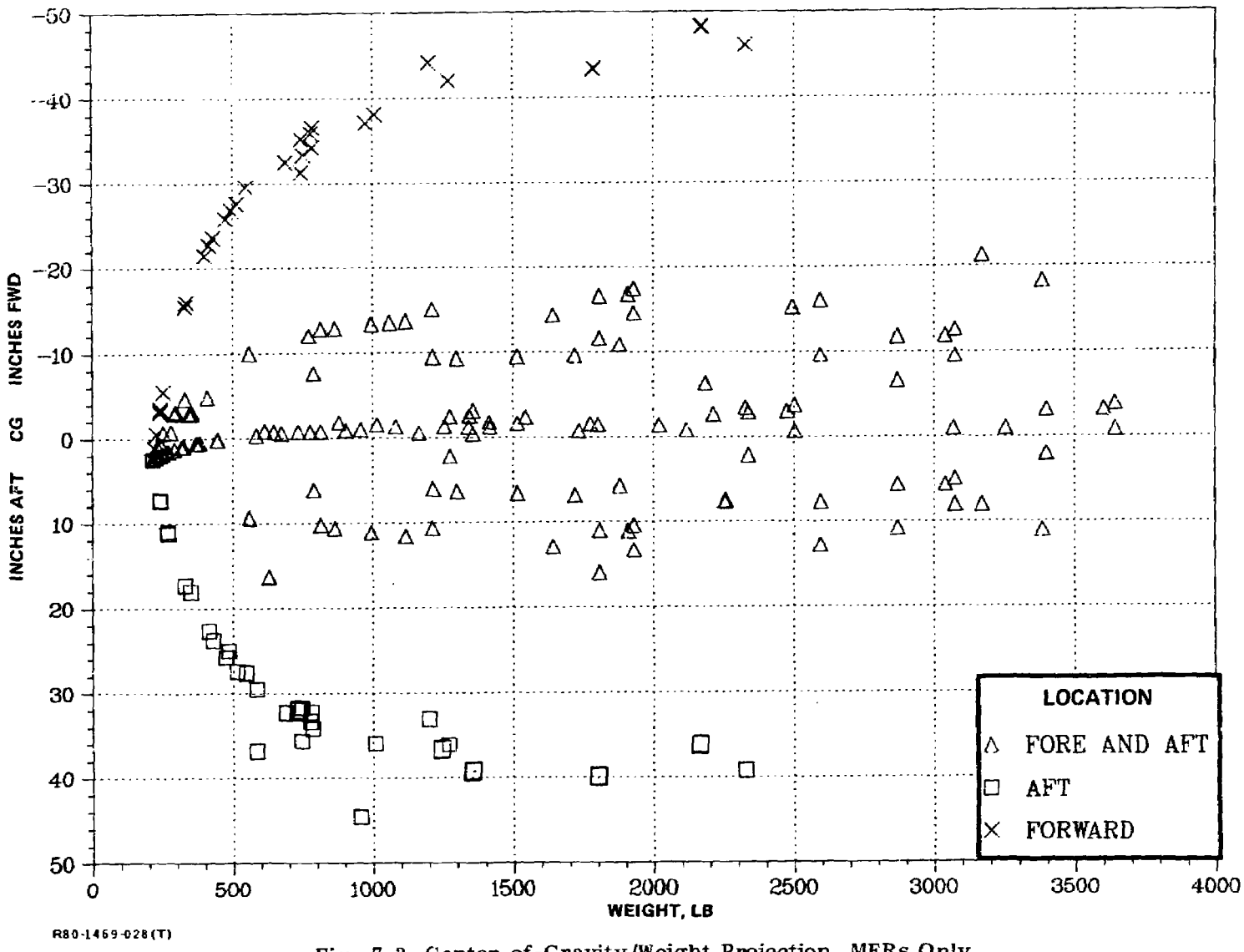

Fig. 7-3 Center-of-Gravity/Weight Projection, MERs Only

particularly on the lighter stores. This fact also explains the curved patterns in the weight/center-of-gravity plot.

A brief digression on allowable MER loadings is in order. A MER can accommodate up to six stores of a given type. These stores are mounted such that three are hung forward and three aft in clusters of two high (shoulder-to-shoulder, close to the wing plane) and one low. The order of ejection is indicated in the following chart:

	FORWARD			AFT		
	LEFT	CENTER	RIGHT	LEFT	CENTER	RIGHT
HIGH	4	-	6	3	-	5
LOW	-	2	-	-	1	-

This means that there are only six distinct configurations in the normal ejection sequence, when six stores of a particular type are loaded. However, when fewer than six of a given type are allowed on the rack, location no. 1 is not always the location left empty. Usually, this deviation is due to physical clearance restrictions on certain stores. Consequently, sets of configurations different from those indicated by the chart can occur during ejection, depending on the type of store and its initial loading.

Figures 7-4 through 7-6 are weight/moment-of-inertia, weight/center-of-gravity and center-of-gravity/moment-of-inertia plots of the combination of MER, TER and single-store configurations that comprise the authorized store loadings at the wing pylons of the A-6. As can be seen, the MER loadings are generally the most severe.

Inspection of the weight/moment-of-inertia data, (M, I), reveals that the inventory is clustered in two regions. To reflect this natural grouping, the data base was split in two. As indicated in Fig. 7-7, this divides the space into an upper and a lower part. The former contains store configurations with relatively high radii of gyration, e.g., a 300-gallon fuel tank or a MER loaded with stores both forward and aft on the rack. The latter contains configurations with small radii of gyration, e.g., a general-purpose bomb or a MER loaded with only a single store.

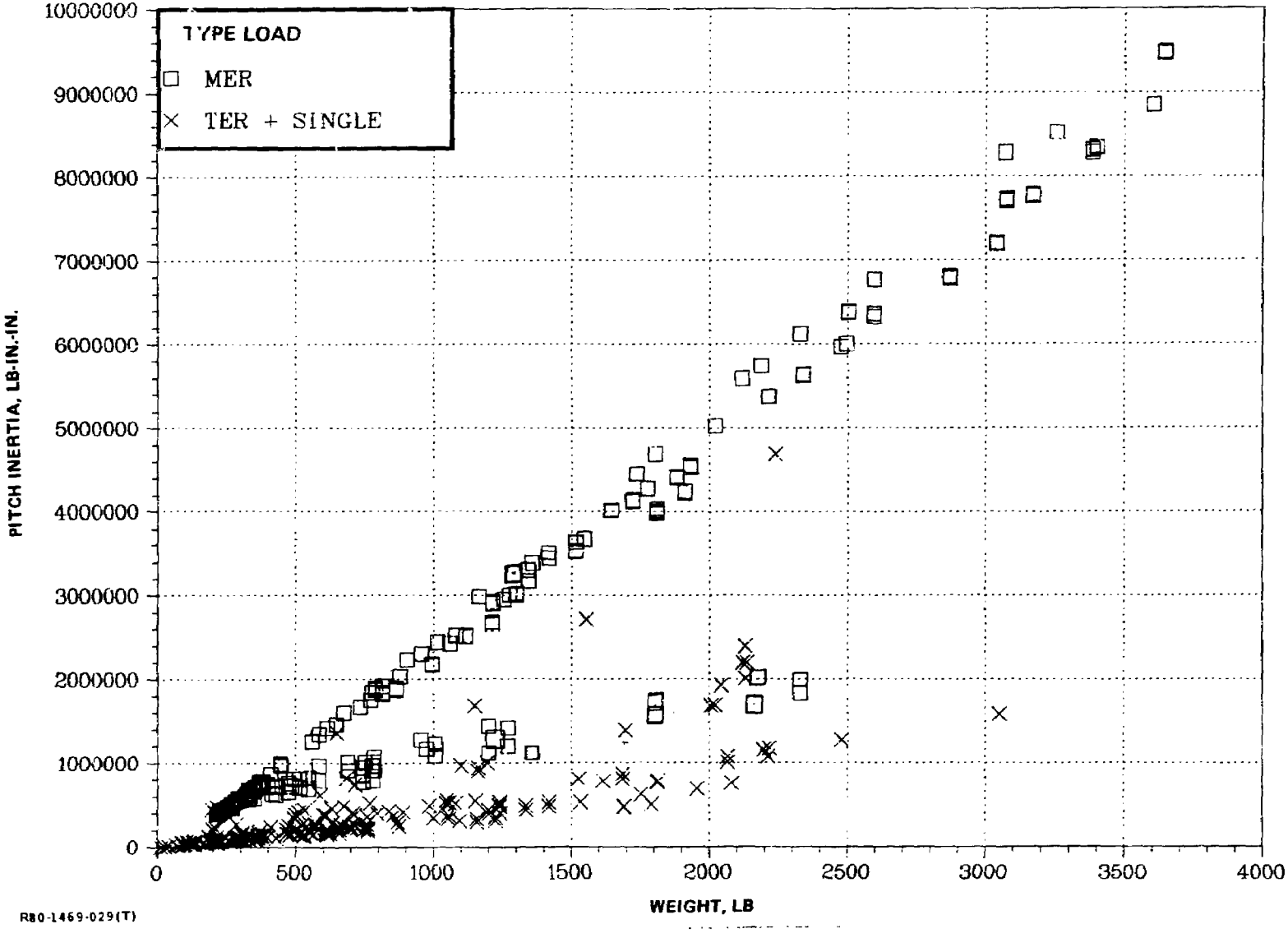

Fig. 7-4 Moment-of-Inertia/Weight Projection, All Stores in Inventory

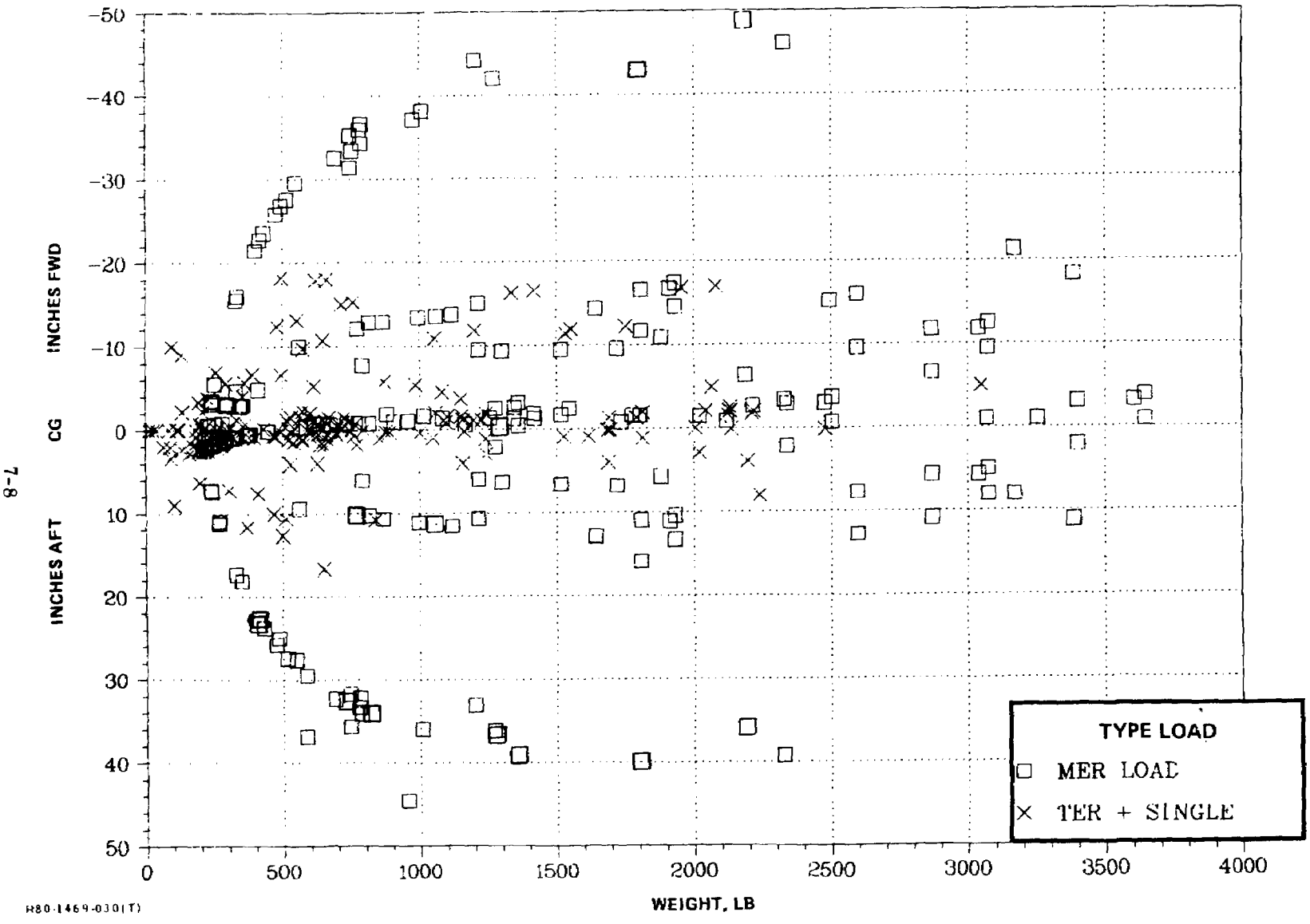

Fig. 7-5 Center-of-Gravity/Weight Projection, All Stores in Inventory

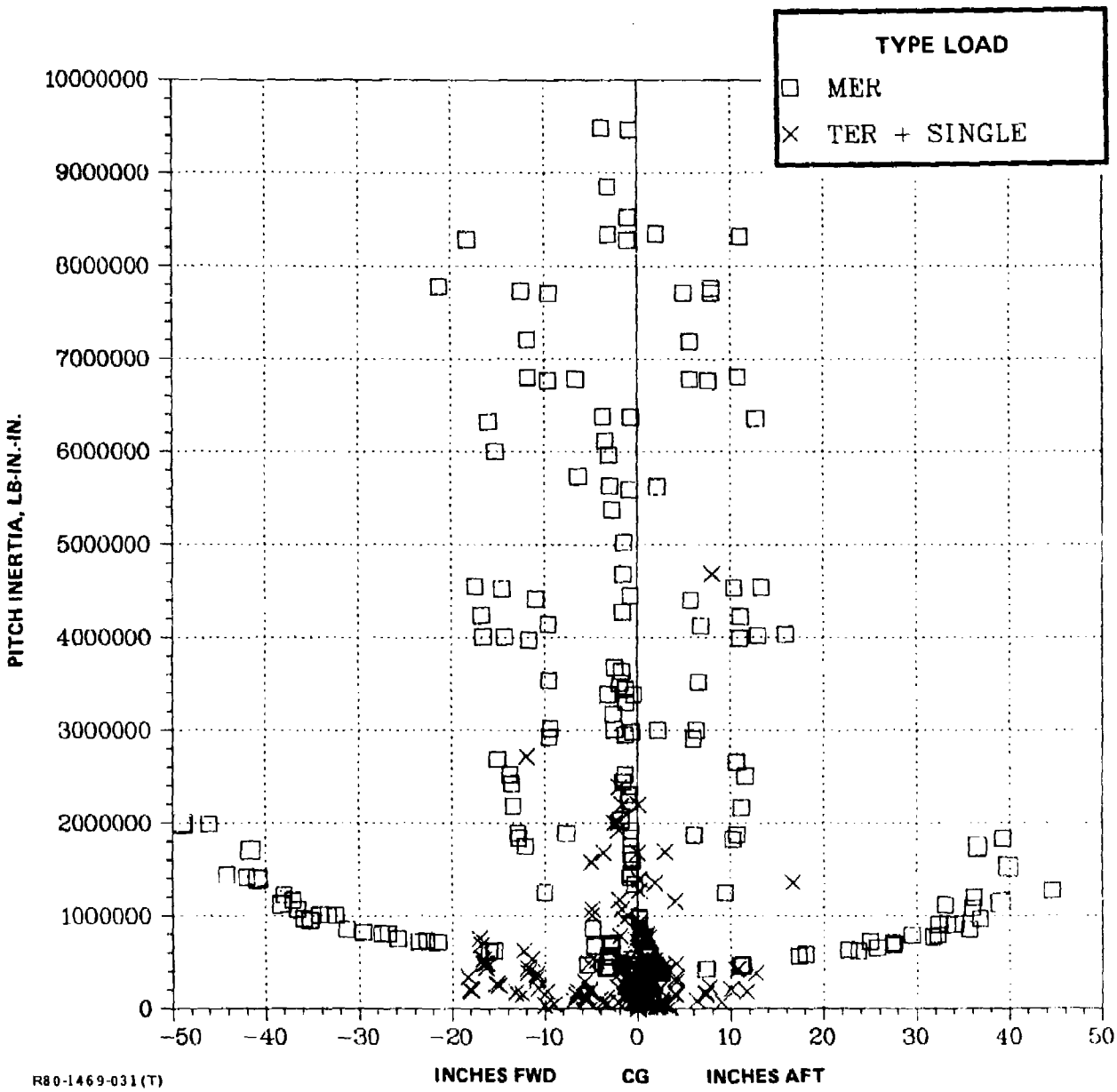

Fig. 7-6 Moment-of-Inertia/Center-of-Gravity Projection, All Stores in Inventory

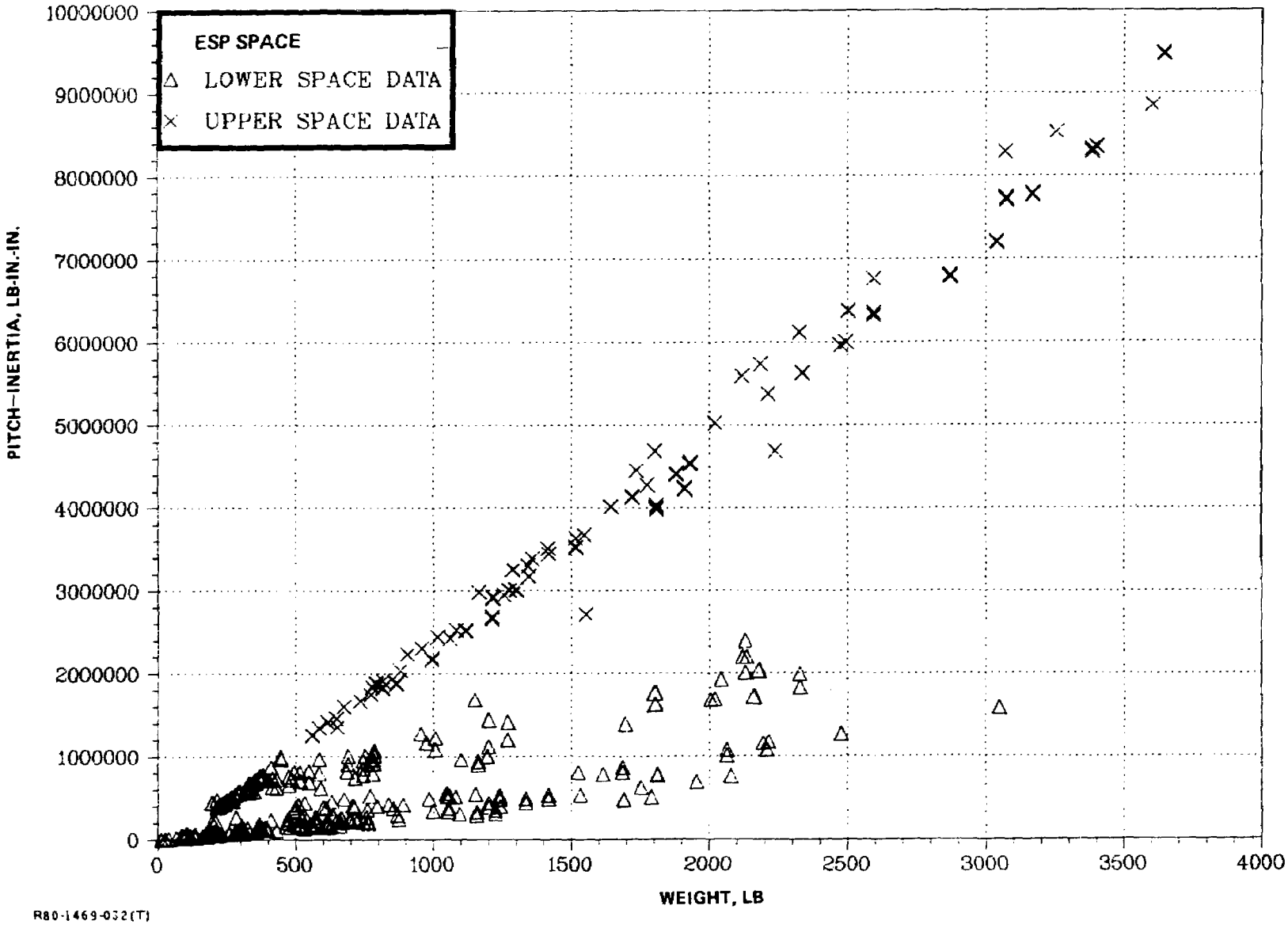

Fig. 7-7 Division of Moment-of-Inertia/Weight Projection, All Stores

Examinations of the authorized-store-loading charts in the A-6 Tactical Manual reveals that the inventory of stores allowed on the outboard pylon is significantly different from that allowed on the inboard pylon. Consequently, the data base was further divided into inboard and outboard portions. There are four resulting regions (or spaces) of store inertial parameters: an inboard-pylon upper space, an inboard-pylon lower space, an outboard-pylon upper space, and an outboard-pylon lower space. Plots of these regions are given in Fig. 7-8 through 7-19. The (M, I) plots are given in Fig. 7-8, 7-11, 7-14, and 7-17; (M, x) plots are given in Fig. 7-9, 7-12, 7-15, and 7-18; (x, I) plots are given in Fig. 7-10, 7-13, 7-16, and 7-19. As can be seen by comparing appropriate inboard/outboard plots, a major difference between the allowed loadings is that the range of center-of-gravity locations for the lower-space inboard-pylon stores is aft of that for the outboard pylon stores. This trend is partially a consequence of loading restrictions imposed to prevent geometric interference between stores and the extended landing-gear door of the A-6; i.e., no large store may be mounted on the inboard, forward shoulder of the MER located at the inboard pylon.

7.2 CONSTRUCTION OF CONSTRAINTS

A feasible space in which to conduct the searches was defined by constructing constraints on the store parameters. The objective was to enclose the store-inventory data by a convex polyhedron, constructed (if possible) such that there would be little empty space near the surfaces. (This consideration ensured that the minimum-flutter-speed parameters determined by the subsequent search were near an allowable store configuration.) To meet this objective as closely as possible, an occasional isolated extreme data point was allowed to fall outside of the polygon - such points were later individually analyzed for flutter.

Using the outboard-pylon upper space as an example, the procedure for constructing these constraints was as follows. Starting in the (M, I) projection (Fig. 7-14) a circumscribing polygon was constructed, the sides of which are planes perpendicular to this projection. A five-sided polygon was chosen. The polygon corner points in Fig. 7-14 were then transferred to the (M, x) projection (Fig. 7-15) as vertical lines, and a polygon enclosing most of the points in this projection and truncating the vertical lines was drawn.

In this projection, a five-sided polygon was also used, and the transferred vertical line at 3700 lb was truncated to a point. The process then moved to the (x, I) projection (Fig. 7-16), where horizontal lines at the maximum and minimum inertia values from Fig. 7-14 formed part of the polygon. Additional sides were constructed based on the plotted values for the actual store parameters and considering that the lengths of the horizontal lines had been previously determined by the truncations in Fig. 7-15. The complete three-view definition of the polyhedron was obtained by moving points and lines from view to view, and iterating on their positions as desired.

It should be emphasized that the construction can be made as simple or complex as is warranted by the nature of the inventory, the requirements of the overall analysis (preliminary or detailed), and the time available. Computer graphics were used to help visualization during the process, but such capability is not a necessity.

Figures 7-9 through 7-19 show the constructed constraints for all regions. There are eight, seventeen, seven, and seventeen constraint planes enclosing the outer-upper, outer-lower, inner-upper, and inner-lower spaces, respectively. Input data to define these constraints in ESP consists merely of the coordinates of any three non-colinear points on each plane.

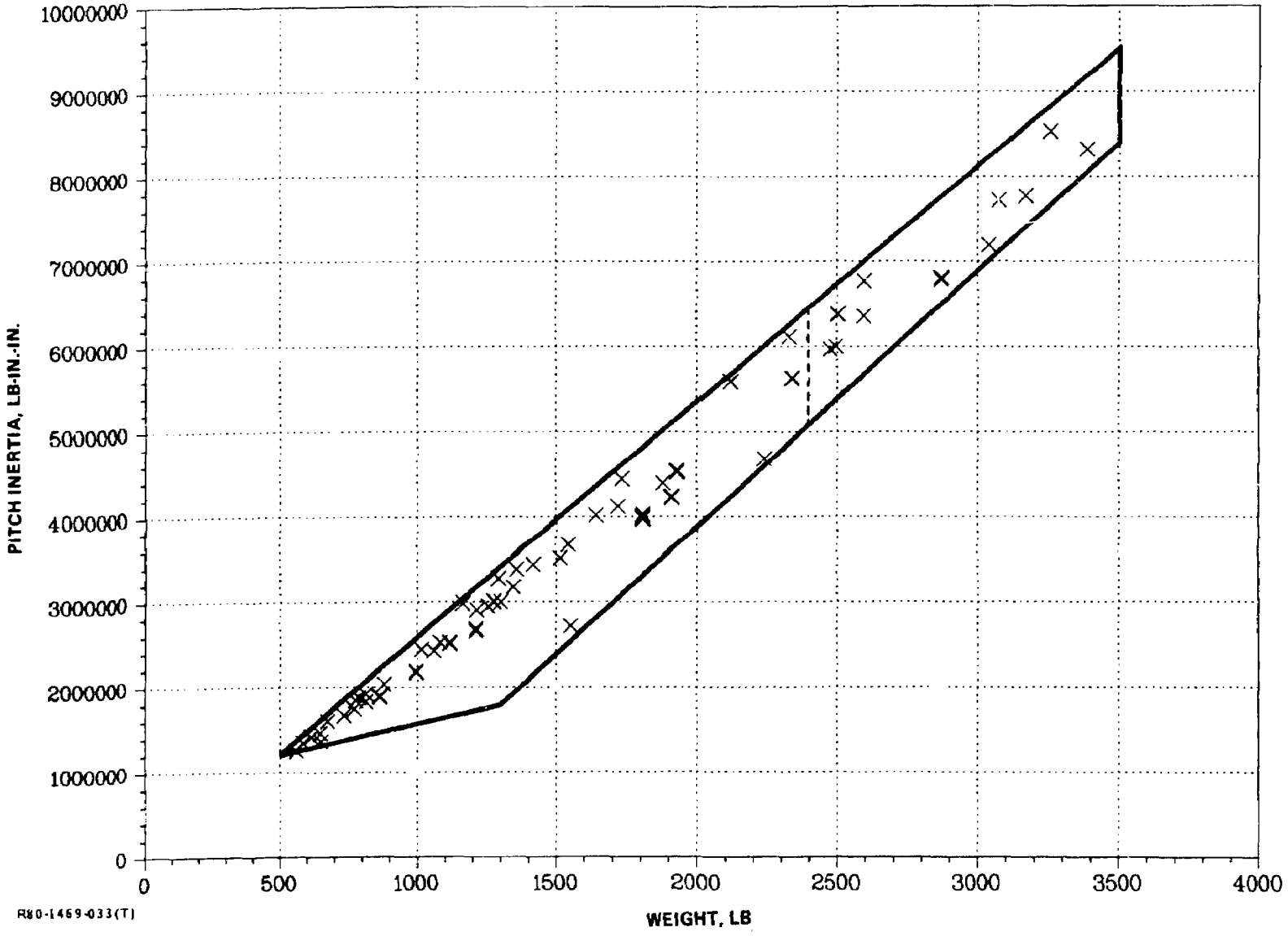

Fig. 7-8 (M, I) Upper Space, Inboard Pylon

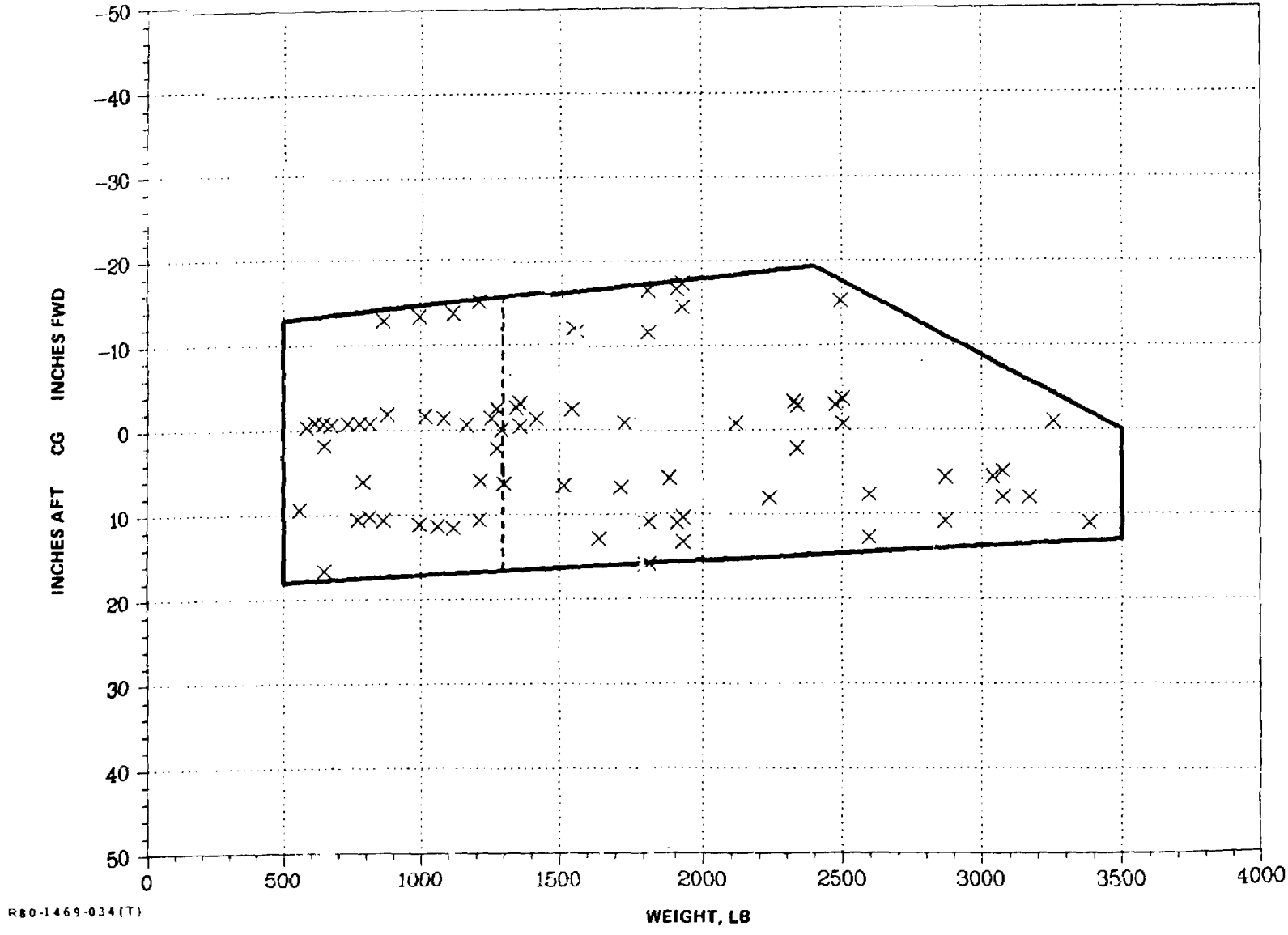

Fig. 7-9 (M, x) Upper Space, Inboard Pylon

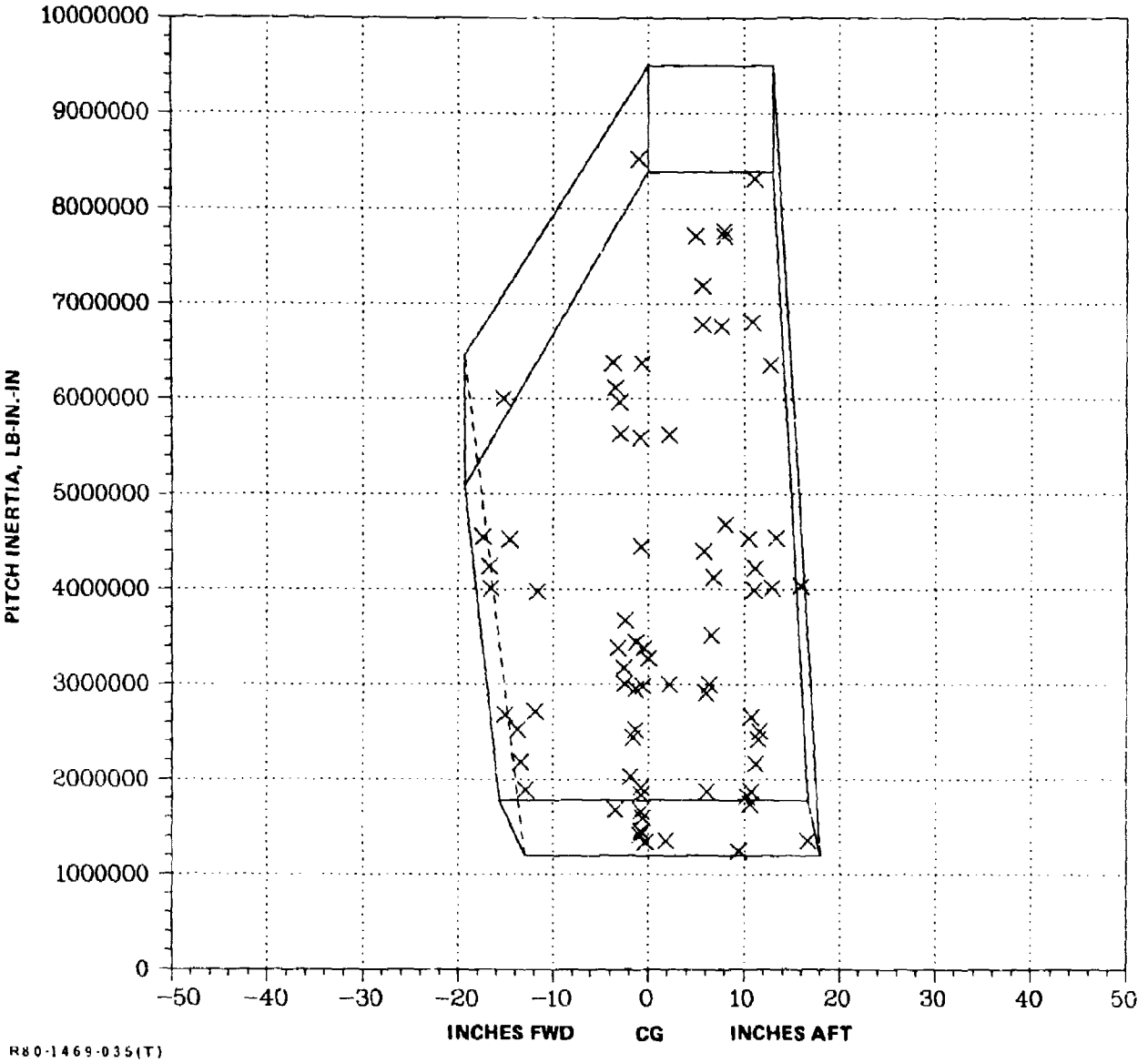

Fig. 7-10 (x,I) Upper Space, Inboard Pylon

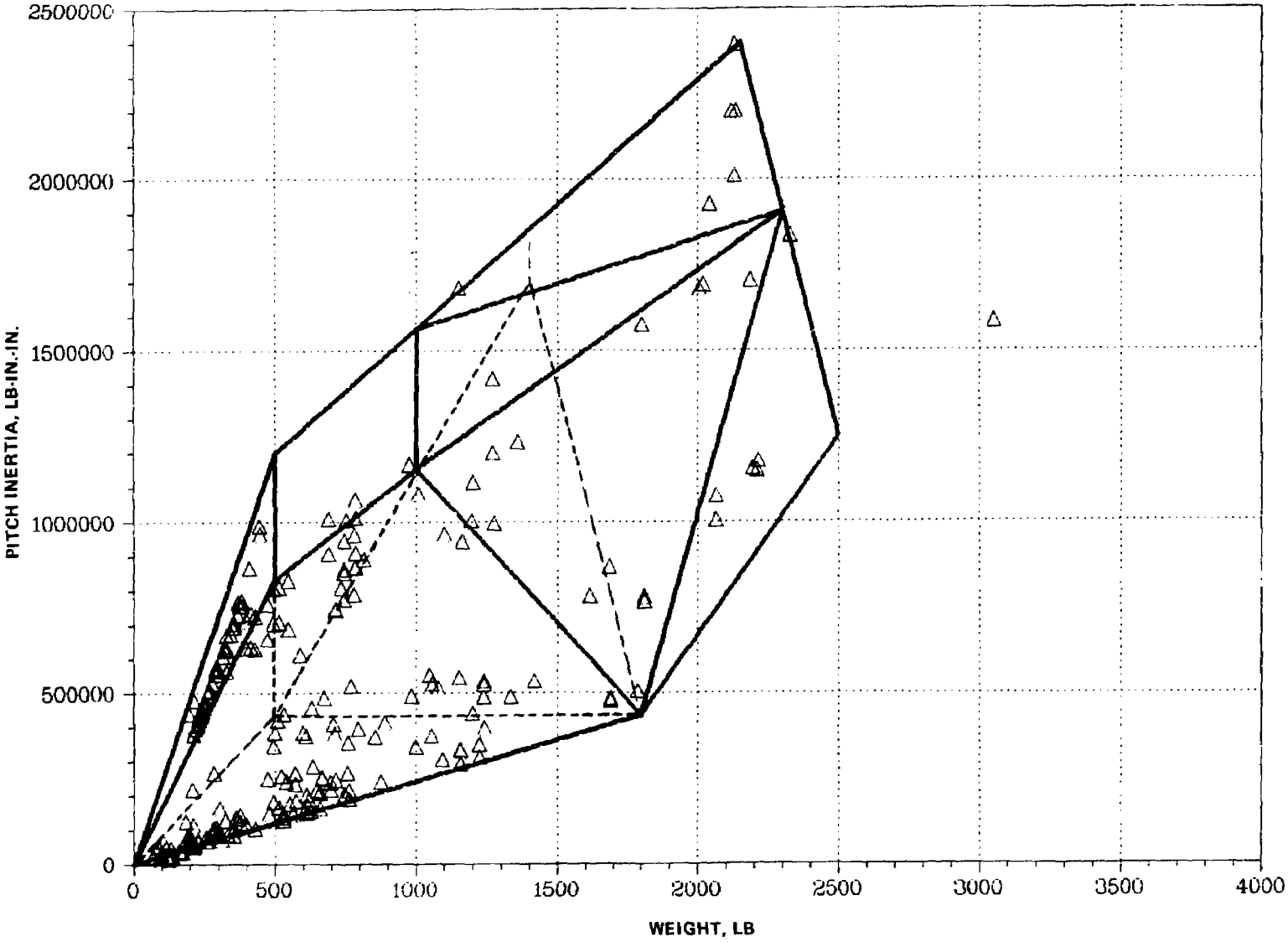

R80-1469-036(T)

Fig. 7-11 (M,I) Lower Space, Inboard Pylon

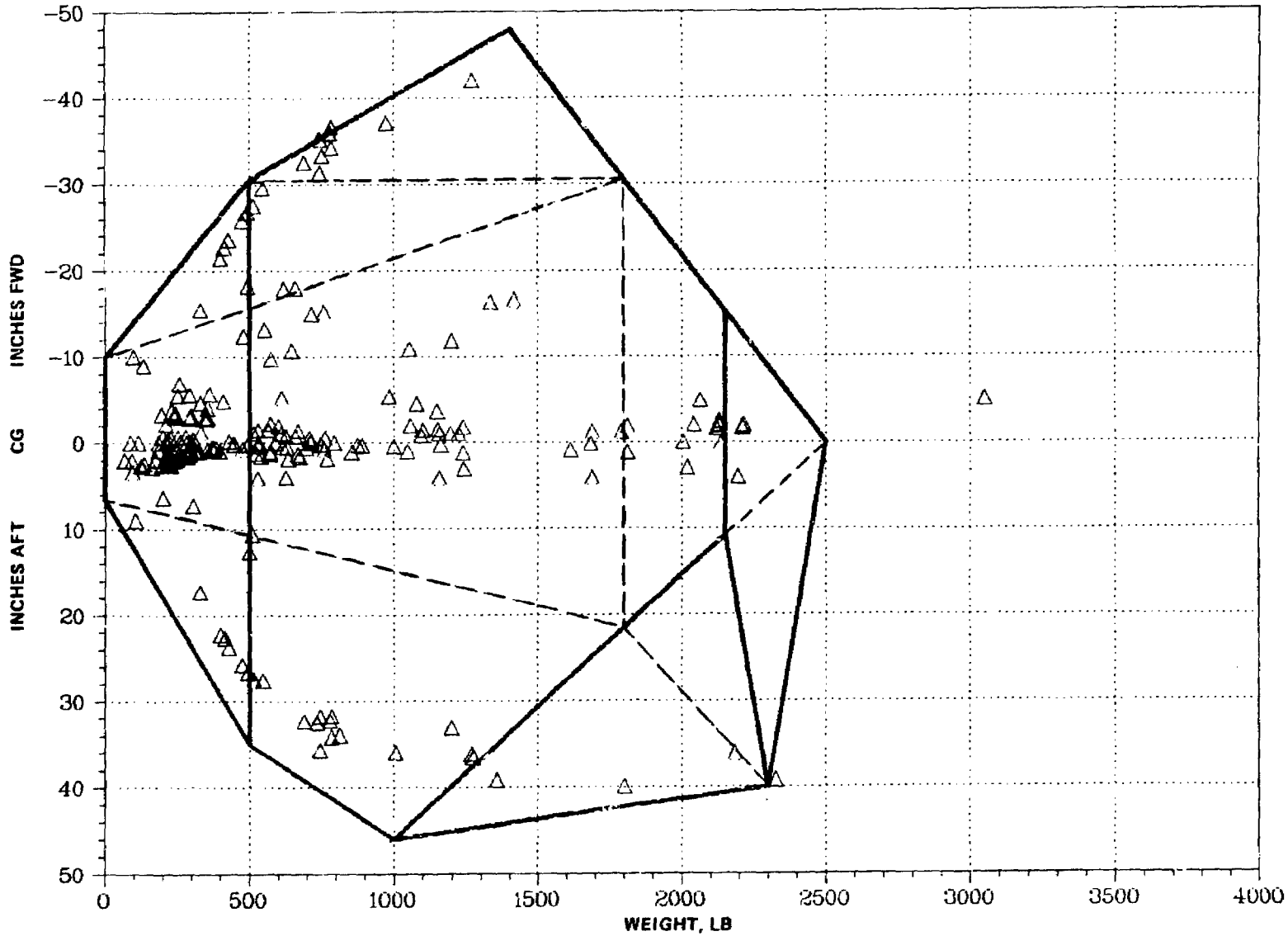

R80-1469-037(T)

Fig. 7-12 (M,x) Lower Space, Inboard Pylon

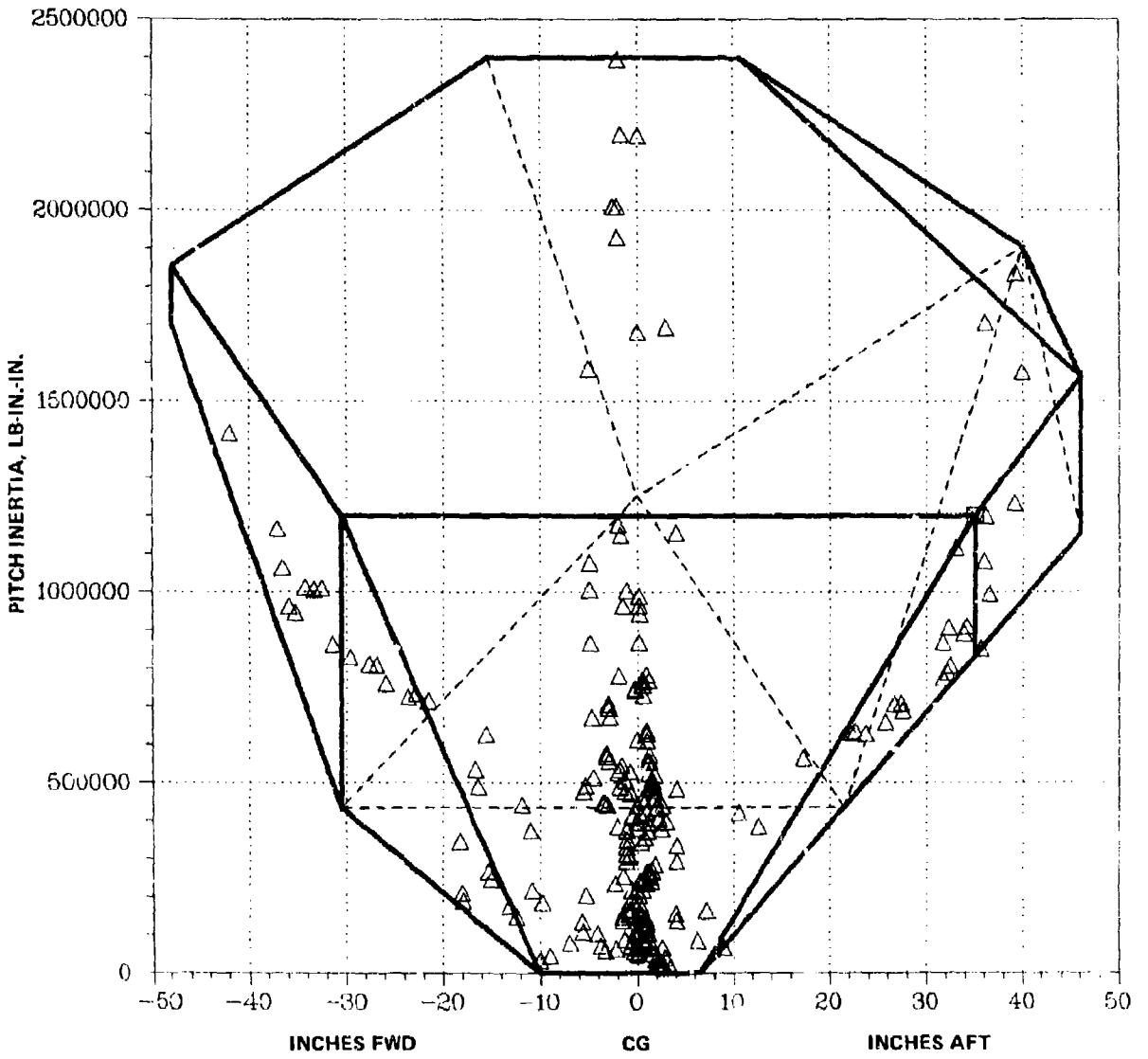

Fig. 7 13 (x,I) Lower Space, Inboard Pylon

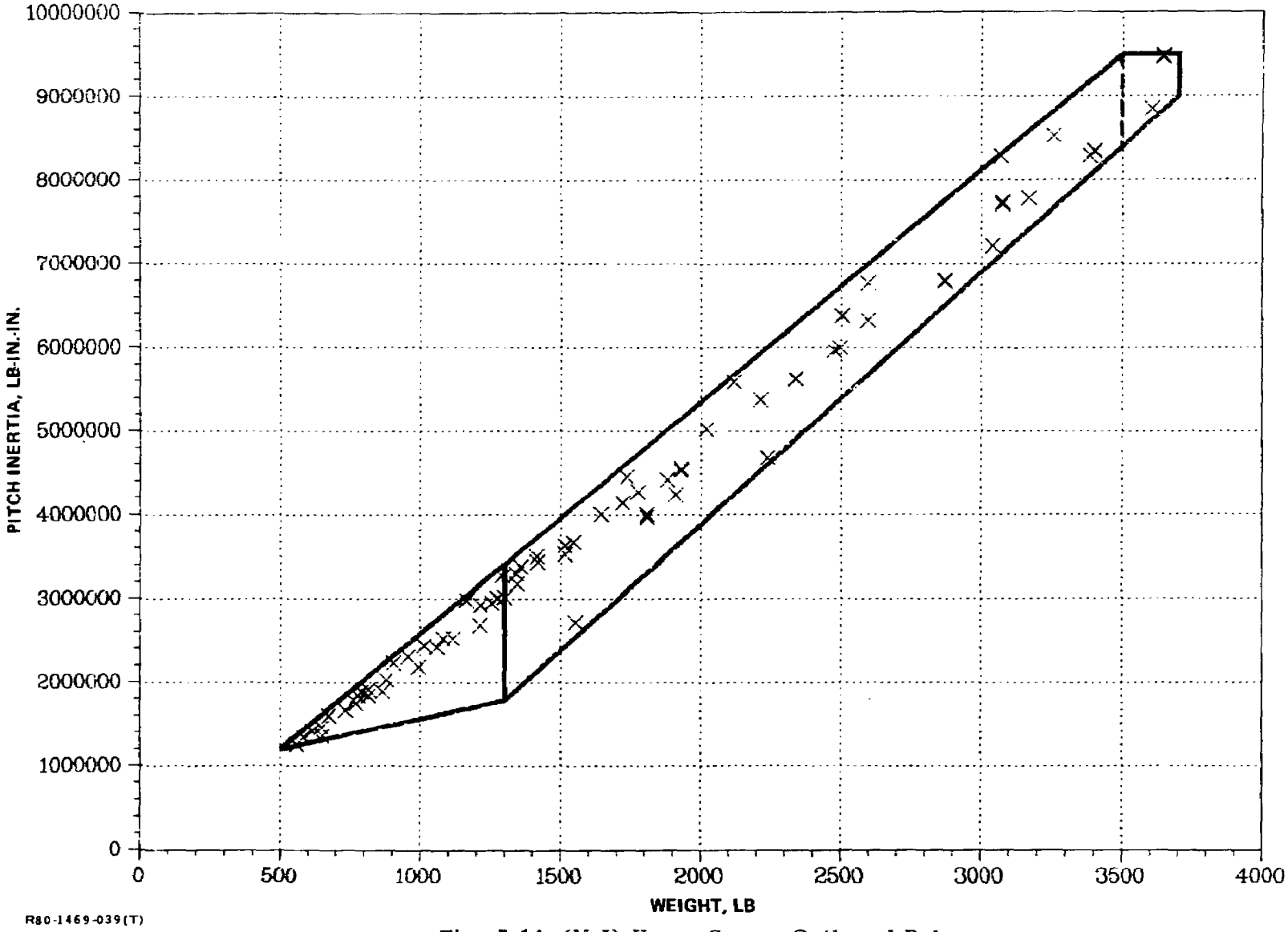

Fig. 7-14 (M,I) Upper Space, Outboard Pylon

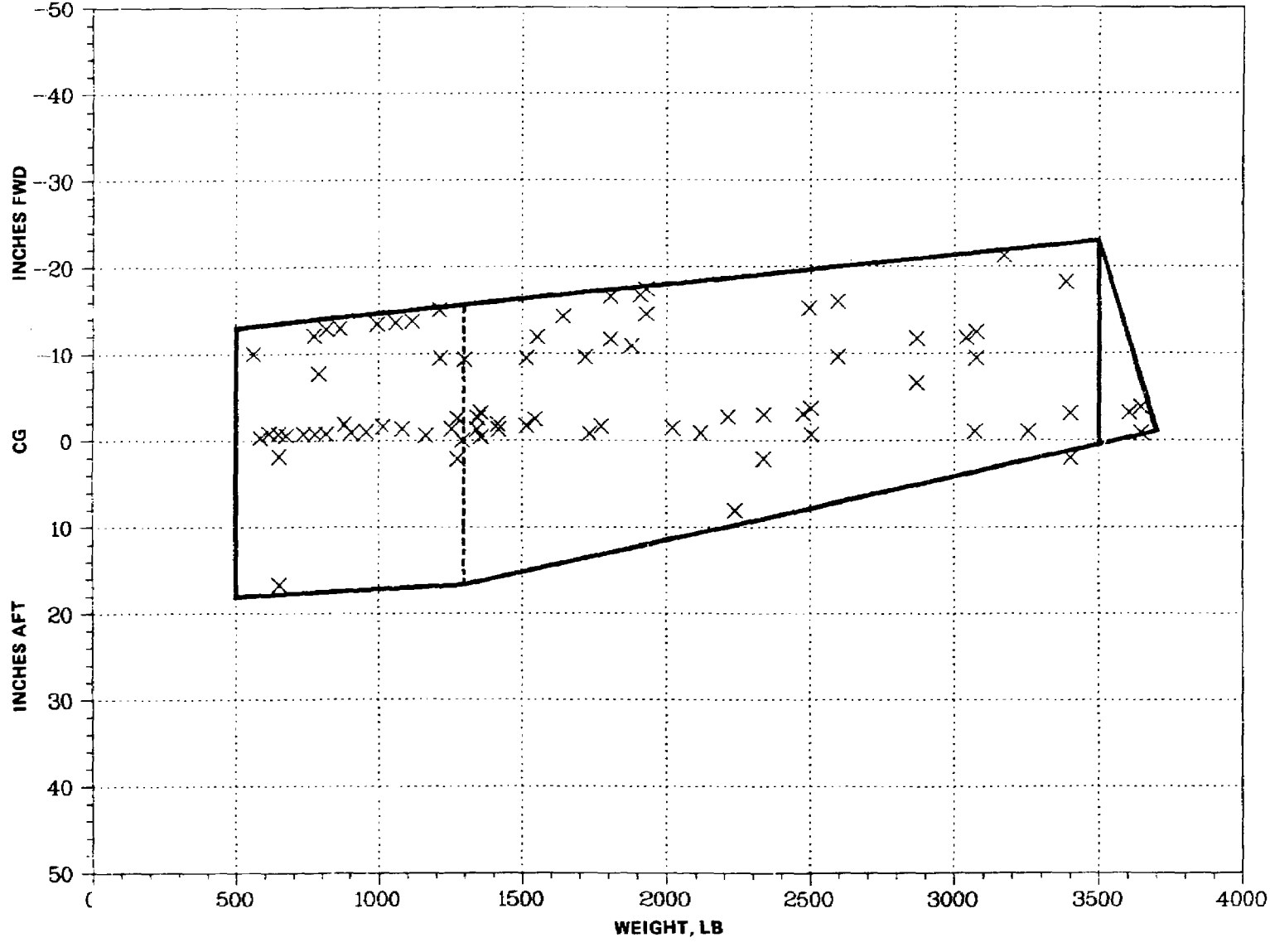

R80-1469-040(T)

Fig. 7-15 (M,x) Upper Space, Outboard Pylon

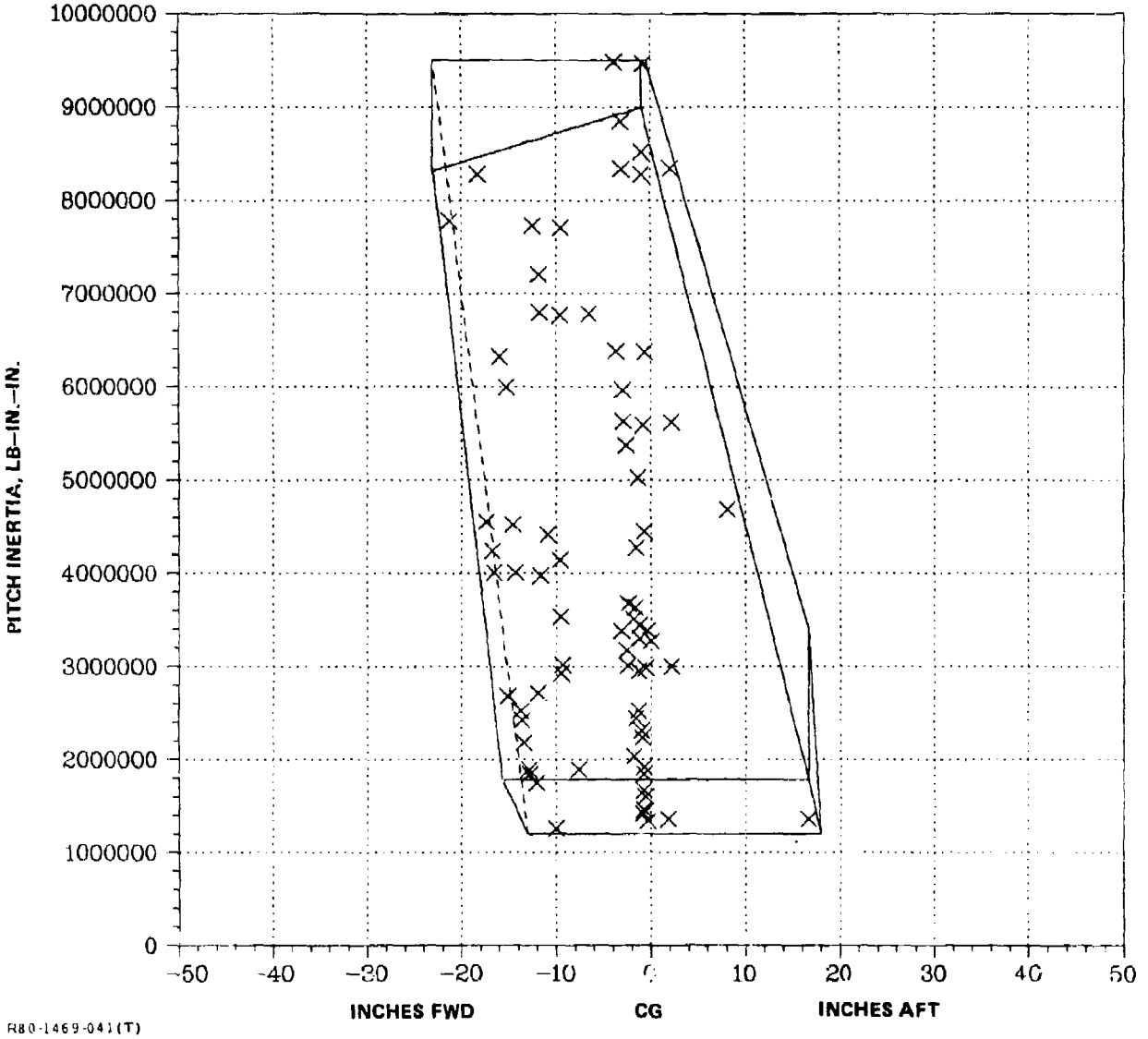

Fig. 7-16 (x,I) Upper Space, Outboard Pylon

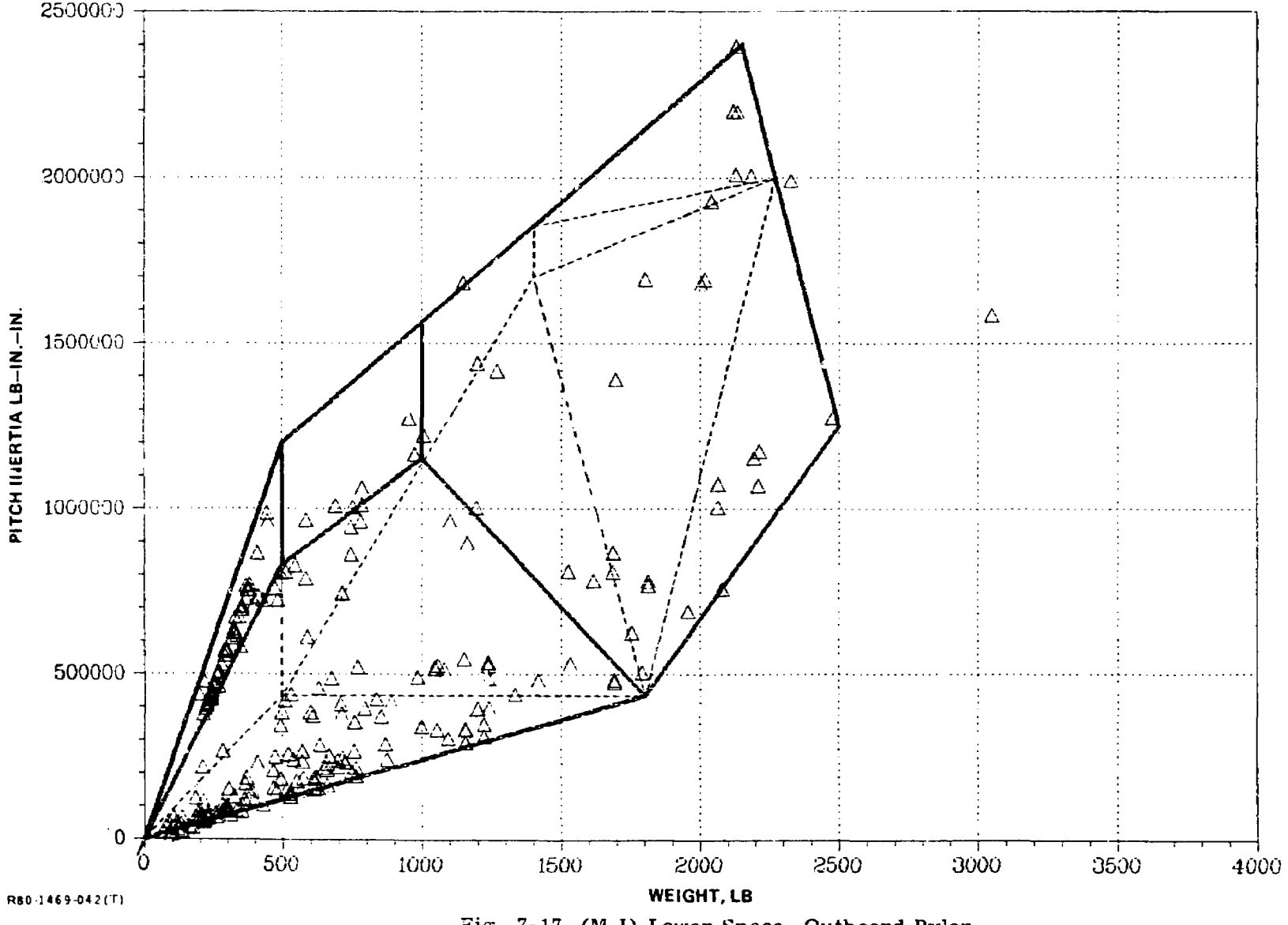

Fig. 7-17 (M,I) Lower Space, Outboard Pylon

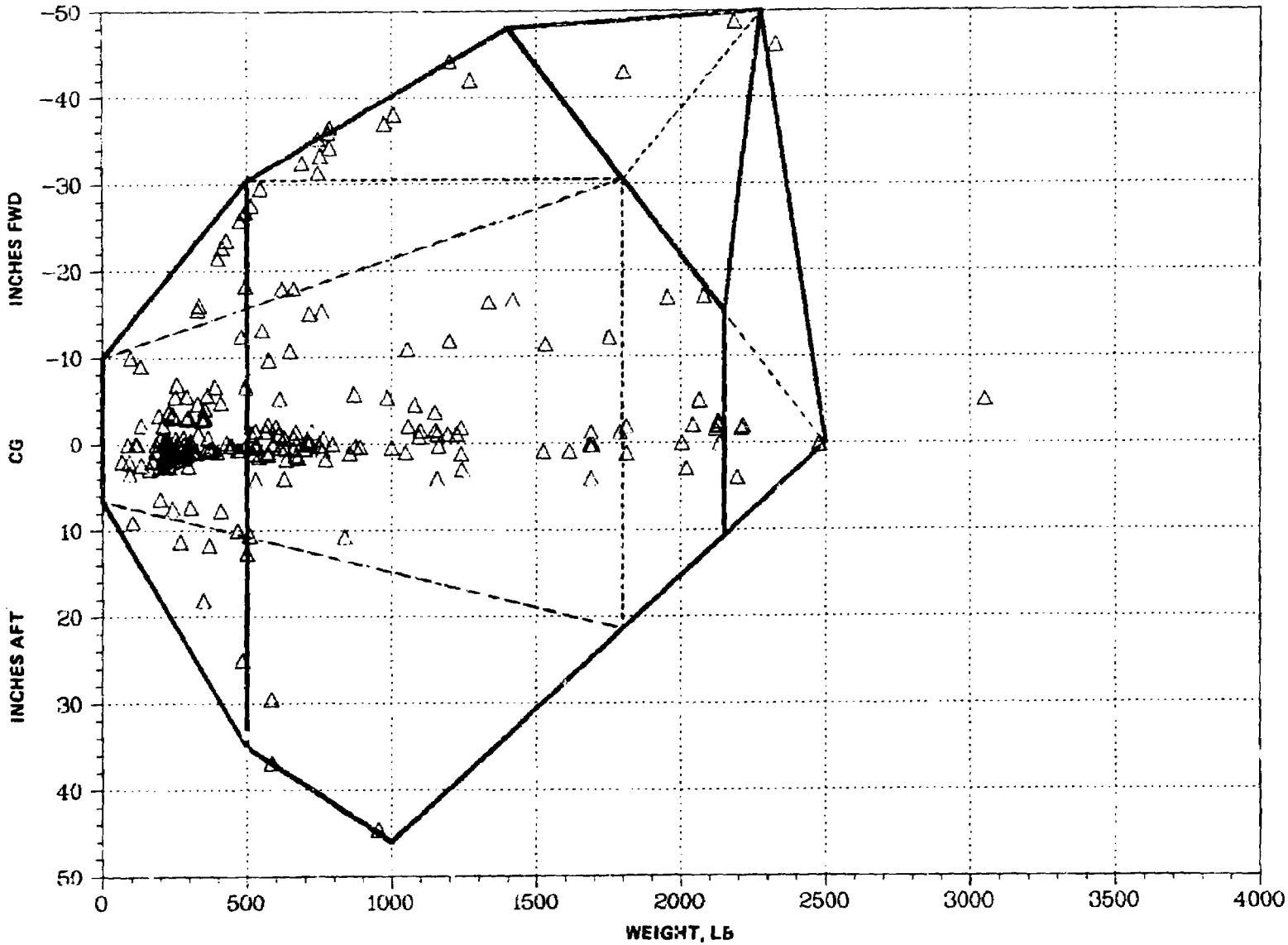

R80-1469-043(T)

Fig. 7-18 (M,x) Lower Space, Outboard Pylon

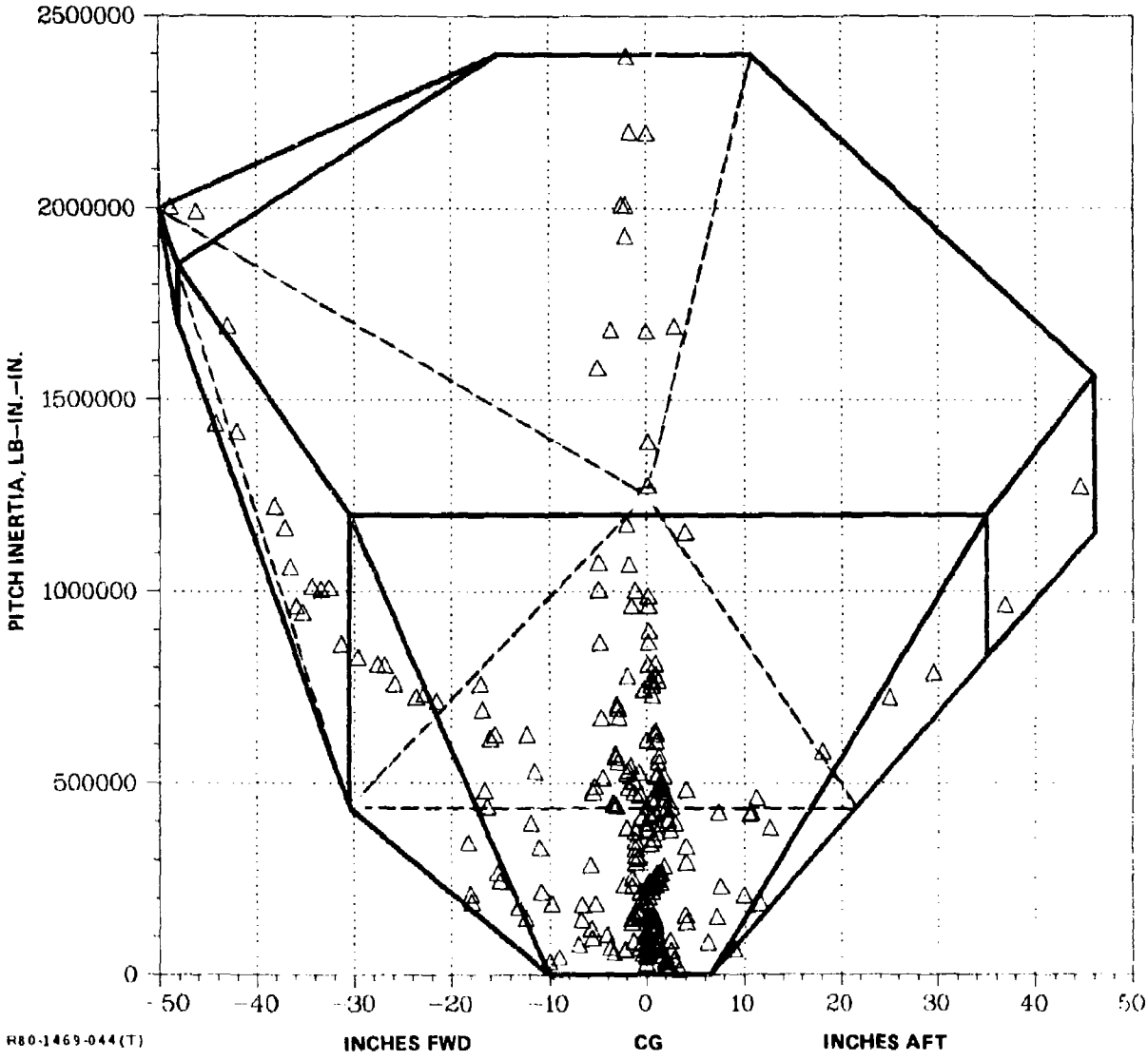

Fig. 7-19 (x,I) Lower Space, Outboard Pylon

8 - DEMONSTRATION RESULTS

8.1 SEARCH STRATEGY

Because various flutter mechanisms are possible due to the large range of inertial characteristics of the store configurations, local minima may occur in the search space. To assure that the global minimum is detected, several searches must be initiated from various different regions of the space. The following strategy was used to reduce the number of these searches required in the present study.

Flutter analyses were performed on a few initial configurations, consisting of various inboard stores but no outboard stores. The most flutter-critical of these arbitrarily selected inboard configurations was determined and held fixed for the first set of searches. These initial searches commenced from arbitrarily selected outboard stores in the upper and lower spaces. The most critical outboard configurations found from these searches were identified and held fixed in subsequent searches of the inboard space. From the inboard searches, tentative combined (inboard/outboard) minima were determined. From each of these configurations, final searches were made in the inboard/outboard parameters simultaneously to determine the final critical configurations. One isolated configuration external to the constraints was analyzed separately and found not to be critical.

8.2 INITIAL INBOARD STORE SELECTION

The inboard-store configurations selected for the initial flutter analyses are listed in Table 8-I and marked on Fig. 8-1 and 8-2. These analyses were run with no structural damping present, using both 10 and 15 modes. Resultant flutter speeds and their derivatives with respect to inboard-store mass are given in Table 8-II. As can be seen from the Table, there is little difference in the flutter speed of a particular configuration due to the use of five fewer modes. However the derivatives computed using only 10 modes can be quite different from their 15-mode counterpart, but only when they are small in magnitude (e.g., configuration no. 8). Consequently, the searches described below are initiated using 10 modes and then refined using 15. From Table 8-II, the most critical case is seen to be no. 3, MK40 DST on MER (one forward, two aft); but the flutter speed of configuration no. 5 is only 2.6 knots higher. The fact that these configurations are significantly different from one another but are nearly equally critical substantiates the presence of local minima.

TABLE 8-I INITIAL INBOARD CONFIGURATIONS

NO.	WEIGHT, LB	MOMENT-OF-INERTIA, LB –IN.^{2}	CG, IN (+AFT)	DESCRIPTION
IB-0	0	0	0	CLEAN WING
IB-1	2328	1.83×10^6	+39.3	MK40 DST ON MER (0 FWD, 2 AFT)
IB-2	2238	4.68×10^6	+ 8.1	300 GALLON TANK
IB-3	3385	8.32×10^6	+11.1	MK40 DST ON MER (1 FWD, 2 AFT)
IB-4	1271	1.42×10^6	-42.0	MK40 DST ON MER (1 FWD, 0 AFT)
IB-5	2494	6.00×10^6	-15.2	CBU-59/B ON MER (2 FWD, 1 AFT)
IB-6	745	0.85×10^6	+35.7	MK36 DST ON MER (0 FWD, 1 AFT)
IB-7	1418	0.54×10^6	-16.5	LAU-61/A ON TER (2)
IB-8	2594	6.77×10^6	+ 7.7	MK20 MOD2 ON MER (2 FWD, 3 AFT)

R80-1469-045(T)

TABLE 8-II RESULTS OF INITIAL FLUTTER ANALYSES

NO.	FLUTTER SPEED, KEAS		REPRESENTATIVE FLUTTER-SPEED DERIVATIVE, KEAS/LB*	
	15 MODES	10 MODES	15 MODES	10 MODES
IB-0	696.7	697.9	2.1×10^{-4}	1.5×10^{-4}
IB-1	597.3	600.5	-3.9×10^{-2}	-4.0×10^{-2}
IB-2	560.5	565.3	-3.0×10^{-3}	-5.0×10^{-3}
IB-3	436.4	438.5	6.1×10^{-4}	-1.3×10^{-3}
IB-4	664.2	670.2	-5.6×10^{-2}	-5.6×10^{-2}
IB-5	439.0	442.2	-1.0×10^{-2}	-1.1×10^{-2}
IB-6	682.8	687.3	-1.1×10^{-2}	-1.2×10^{-2}
IB-7	689.9	692.9	-3.4×10^{-4}	-1.2×10^{-3}
IB-8	471.5	474.4	4.1×10^{-3}	1.9×10^{-3}

*DERIVATIVES WITH RESPECT TO INBOARD STORE MASS ARE PRESENTED. DERIVATIVES WITH RESPECT TO STORE MOMENT OF INERTIA AND CENTER OF GRAVITY ARE NOT SHOWN BUT HAVE BEEN FOUND TO EXHIBIT SIMILAR TRENDS.

R80-1469-048(T)

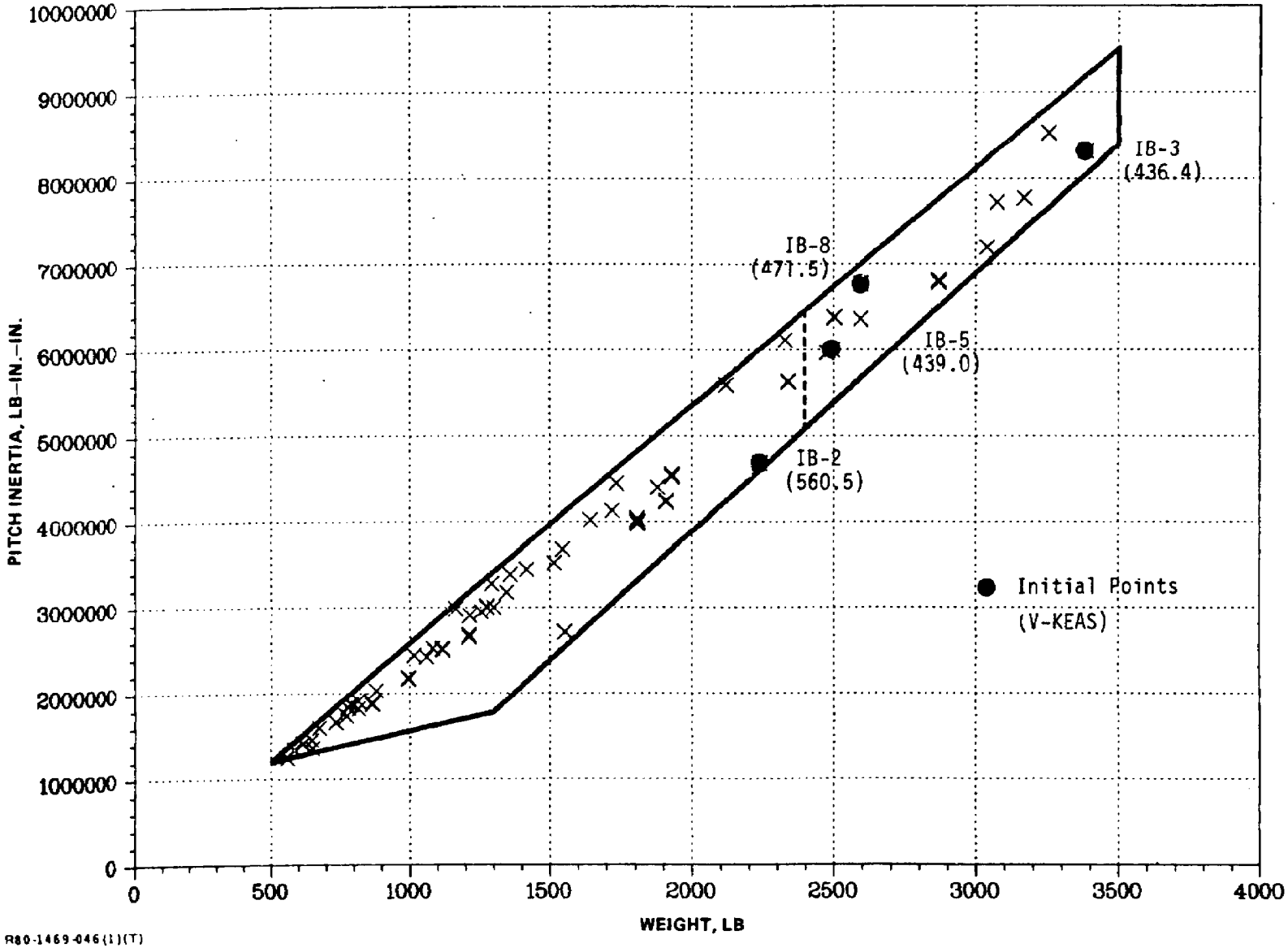

Fig. 8-1 Initial Configurations: Upper Space, Inboard Pylon (Sheet 1 of 3)

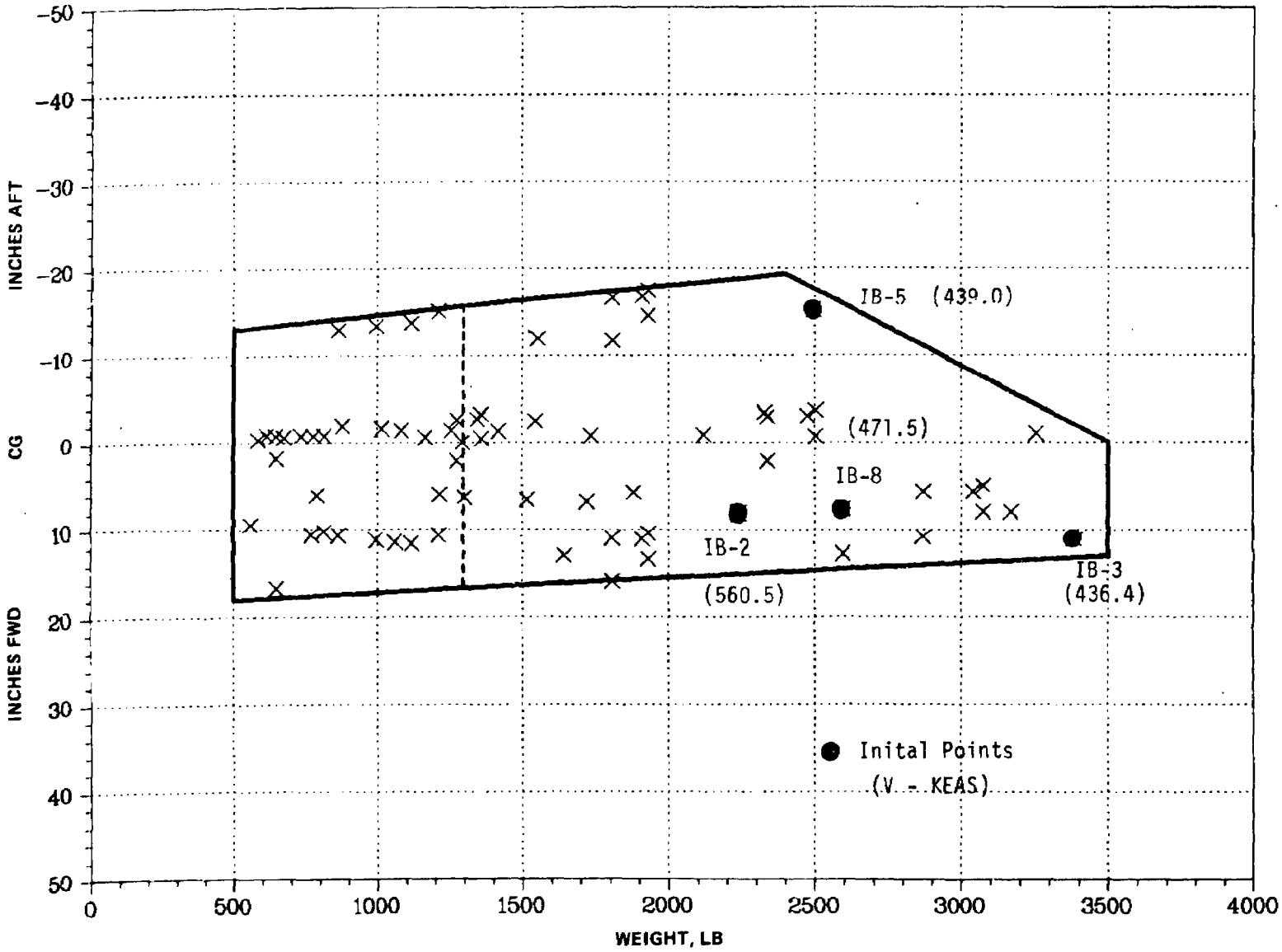

R80-1469-046(2)(T)

Fig. 8-1 Initial Configurations: Upper Space, Inboard Pylon (Sheet 2 of 3)

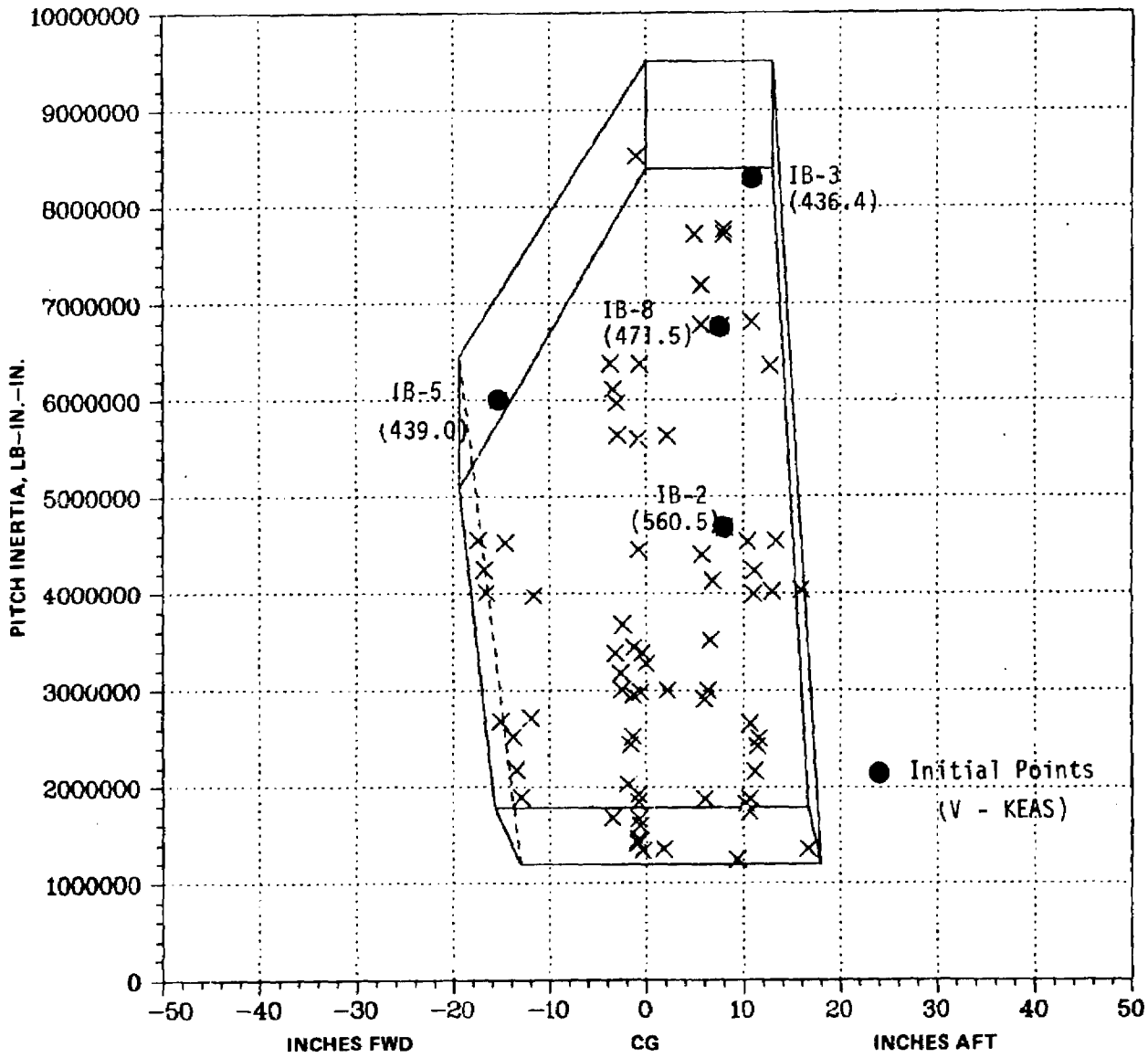

R10-1469-046(3)(T) Fig. 8-1 Initial Configurations: Upper Space, Inboard Profile (Sheet 3 of 3)

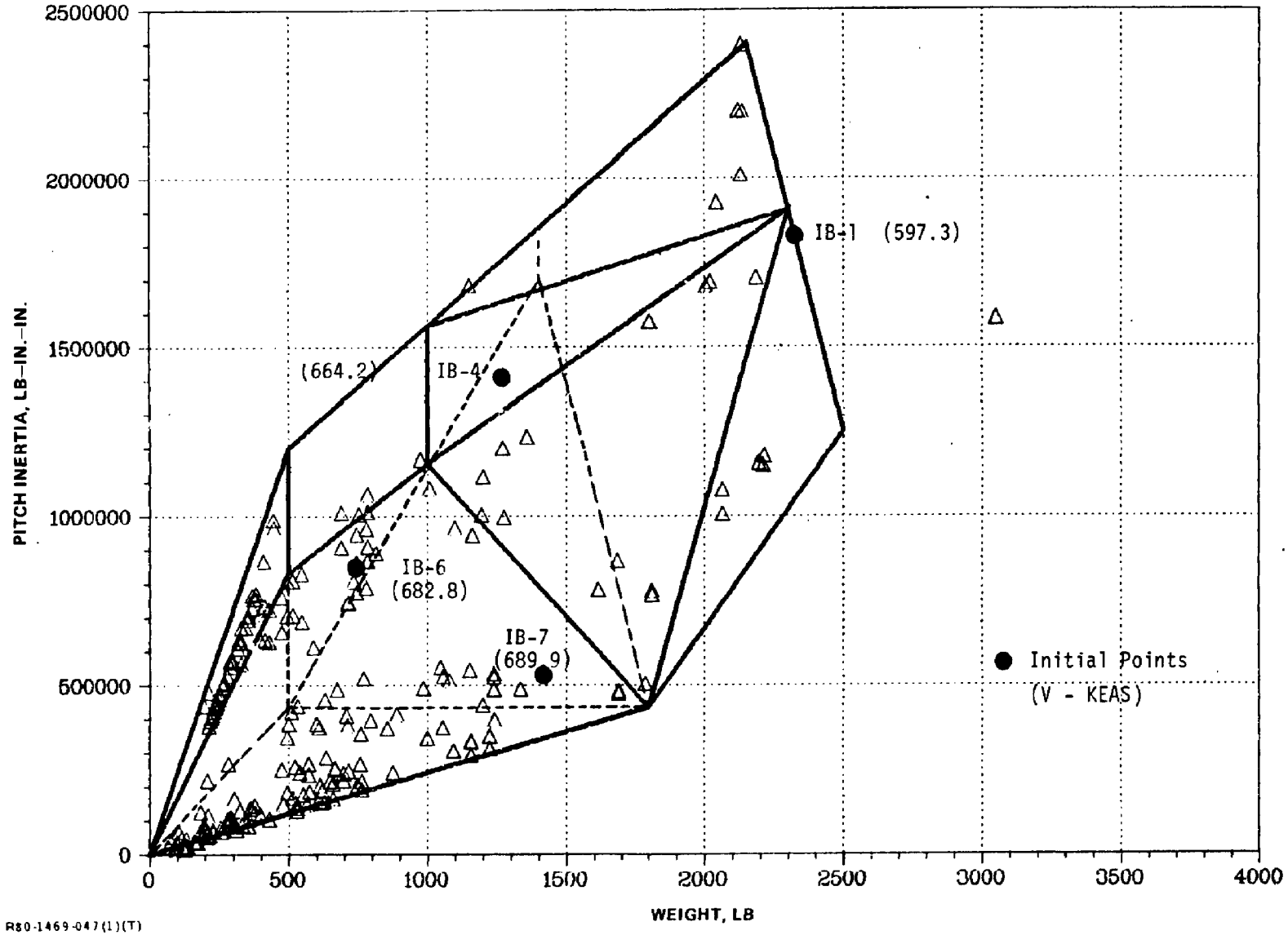

R80-1469-047(1)(T)

Fig. 8-2 Initial Configurations: Lower Space, Inboard Pylon (Sheet 1 of 3)

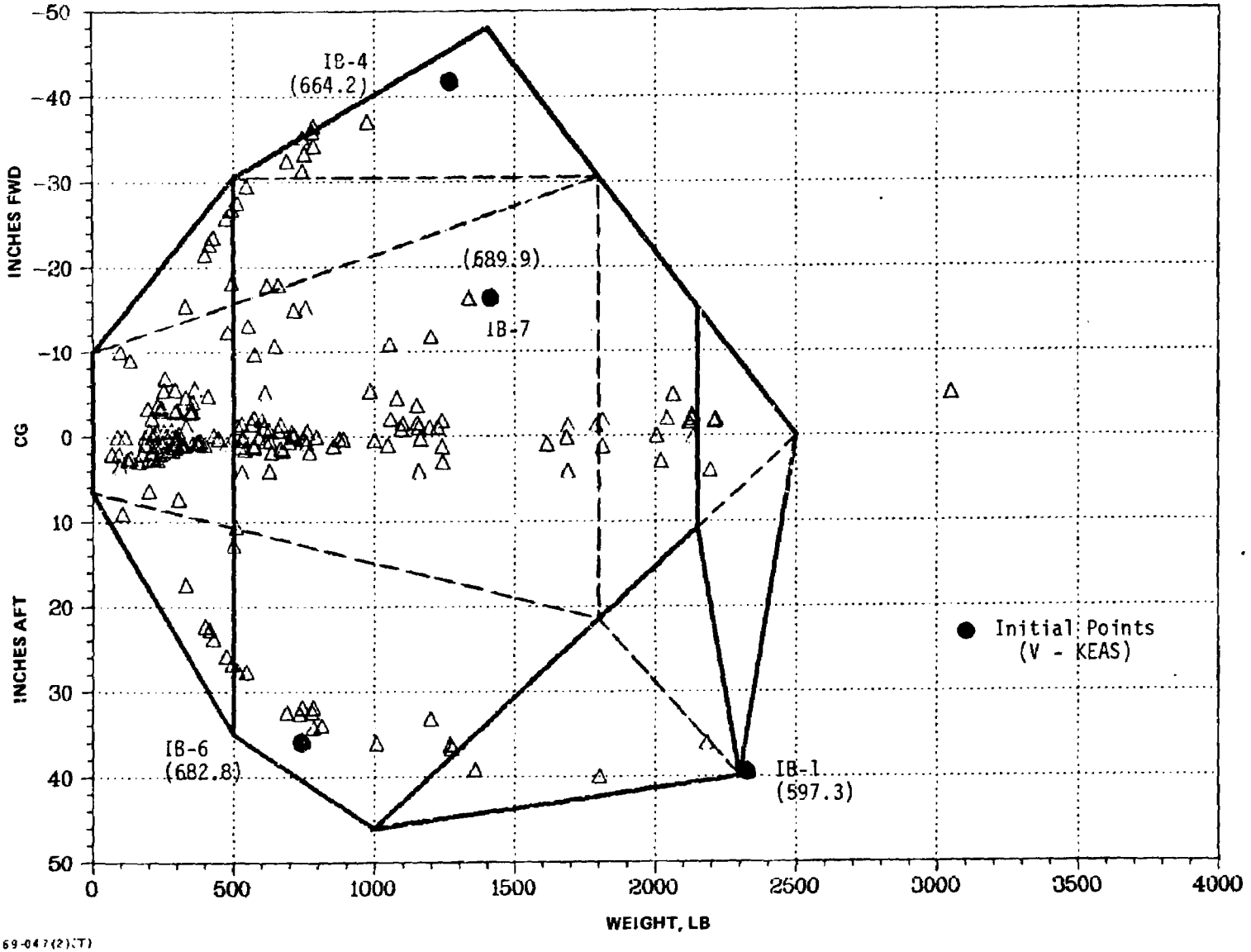

R80-1469-047(2)(T)

Fig. 8-2 Initial Configurations: Lower Space, Inboard Pylon (Sheet 2 of 3)

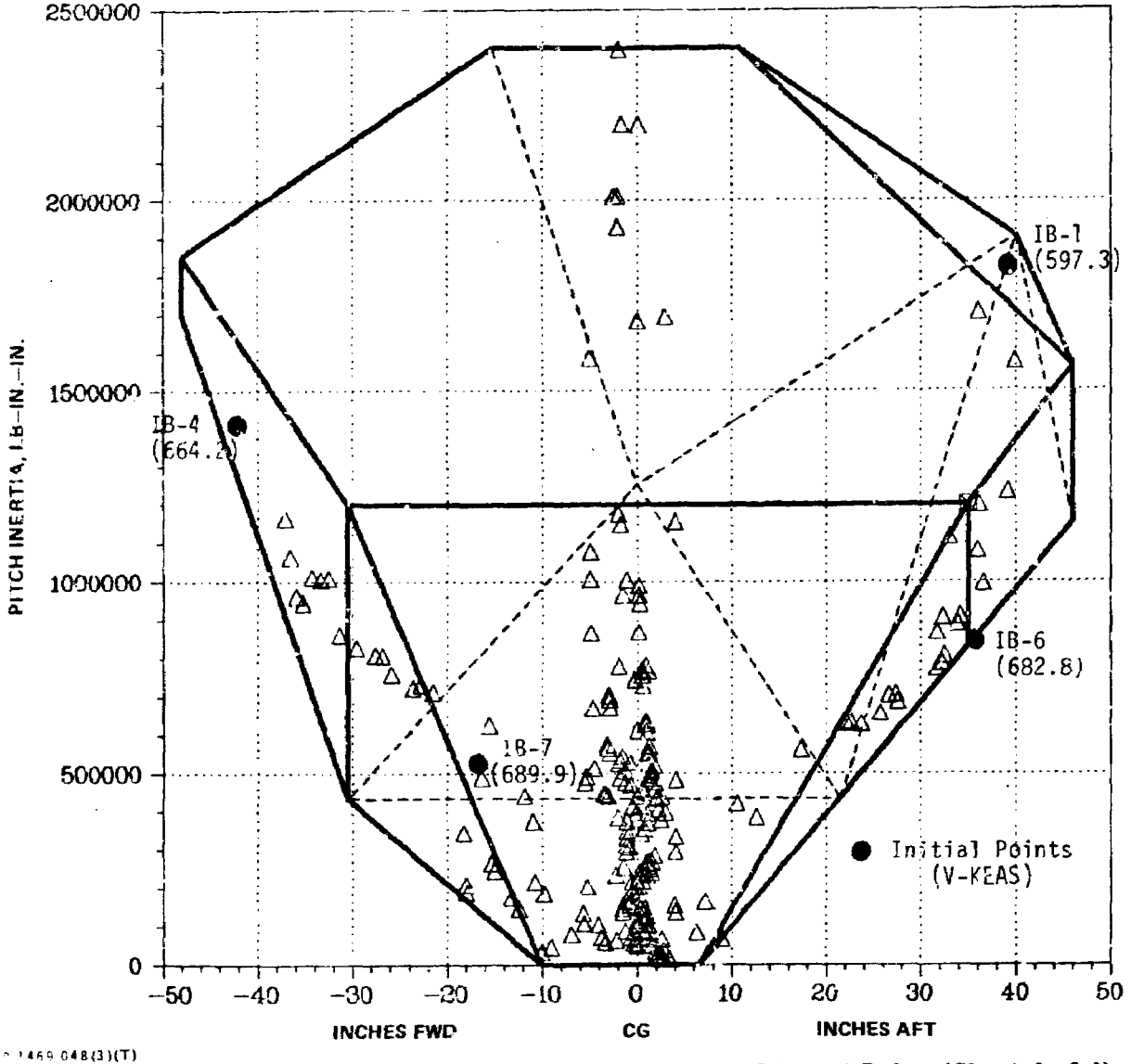

Fig. 8-2 Initial Configurations: Lower Space, Inboard Pylon (Sheet 3 of 3)

8.3 OUTBOARD SEARCHES

Fixing the inboard store parameters to represent configuration no. 3, chosen above, searches of the outboard store spaces were run. The starting points for these searches are specified in Table 8-III and are marked on Fig. 8-3 and 8-4. To economize on computer time, each search was run for five cycles using 10 modes. Each search was then restarted from the fifth point, using 15 modes, and run (on the average) for 10 additional steps.

The minima determined by these searches are marked on Fig. 8-3 and 8-4 and summarized in Table 8-IV. Several searches (i.e., 4, 5, 8, and 9) traverse large distances in the space before homing in on various local minima.

The detailed path of one search (OB-5) is shown in Fig. 8-5. Starting from an unconstrained point 1, the search first moved to constraint C8 and proceeded, via the projection technique, to traverse the constraint. It landed on constraint C2 at point 3, causing two constraints to be active simultaneously. Points 4 and 5 were reached by projecting along the intersection of constraints C2 and C8. The switch to 15 modes resulted in a 9.4-knot drop in flutter speed at point 5. Points 6, 8, 10, and 12 were overshoots; the subsequent line search found an acceptable point in each instance (points 7, 9, 11, and 13). The search was terminated at point 14 because it was close to the minimum previously detected by search OB-4.

Referring to Table 8-IV, three minima (the final points of searches OB-3, OB-4/OB-5, and OB-6) are substantially more critical than the others. They all have exceptionally low flutter speeds of less than 300 keas. Moreover, the less critical minima also exhibit unrealistically low flutter speeds - well within the limits of the A-6 flight envelope. An examination of a typical V-g-ω plot for one of these cases (Fig. 8-6), however, reveals that the flutter cross-over is very gradual; thus, the presence of even a small amount of structural damping can cause a large increase in flutter speed.

Consequently, a structural damping of 2% was added to the present analyses to determine more realistic flutter speeds. (This choice of damping coincides with that used by project personnel in analyzing flutter clearance of the A-6E with Harpoon Missiles Ref. 8.) The three critical minima were then reanalyzed and searches were initiated from

these previous minima. Table 8-V summarizes the results. For OB-4/OB-5 and OB-6, flutter speeds were dramatically increased but, in each case, the location of the minimum point was virtually unchanged. For OB-3, the added damping eliminated the store-mode instability, causing the flutter speed to increase over 500 keas (to a basic wing instability). Thus, OB-3 was no longer considered critical. Since the flutter speeds of the two critical damped configurations were close to that of the undamped OB-8/OB-9, this configuration was also reanalyzed with damping and found not to be critical (see Table 8-V).

In Fig. 8-3 and 8-4, the locations of the two revised critical minima are marked 4D and 6D. These values were held fixed in two separate sets of searches described below. (All subsequent analyses were run using 2% damping.)

TABLE 8-III STARTING POINTS FOR INITIAL OUTBOARD SEARCHES

UPPER OR LOWER	NO.	WEIGHT, LB	MOMENT-OF-INERTIA, LB–IN.^{2}	CG, IN. (+AFT)	DESCRIPTION
U	OB-1	3646	9.48×10^6	-3.9	MK36 DST SNAKEYE ON MER (3 FWD, 3 AFT)
U	OB-2	2238	4.68×10^6	+8.1	300 GALLON TANK
U	OB-3	3169	7.79×10^6	-21.2	MK83 LDGP ON MER (2 FWD, 1 AFT)
U	OB-4	649	1.36×10^6	+16.7	CNU-188/A BAGGAGE STOWED AFT
U	OB-5	1807	4.01×10^6	-16.6	MK82 LDGP ON MER (2 FWD, 1 AFT)
L	OB-6	2184	2.01×10^6	-48.7	MK83 LDGP ON MER (2 FWD, 0 AFT)
L	OB-7	956	1.28×10^6	+44.6	SUU-44/A ON MER (0 FWD, 2 AFT)
L	OB-8	2130	2.40×10^6	-2.0	KMU-351A/B GUIDED BOMB
L	OB-9	2478	1.28×10^6	0.0	MK88 SAND FILLED ON TER (3)

R30-1469-049(T)

TABLE 8-IV RESULTS OF INITIAL OUTBOARD SEARCHES

NO.	FLUTTER SPEED, KEAS	WEIGHT, LB	MOMENT-OF-INERTIA, LB–IN.^{2} X 10^{-6}	CG, IN. (+AFT)
OB-1	343.0	3626	9.499	- 9.2
OB-2	422.1	2281	6.126	+ 9.4
OB-3	265.6	3315	7.848	-14.1
OB-4	205.2	3049	7.045	-20.3
OB-5	251.1	2973	6.820	-20.0
OB-6	236.7	2273	1.995	-49.6
OB-7	458.8	1000	1.564	+46.0
OB-8	409.1	820	1.448	-36.7
OB-9	409.2	821	1.433	-36.7

R80-1469-052(T)

TABLE 8-V EFFECT OF STRUCTURAL DAMPING ON RESULTS OF INITIAL OUTBOARD SEARCHES

NO.	FLUTTER SPEED, KEAS	WEIGHT, LB	MOMENT OF INERTIA, LB–IN.^{2} X 10^{-6}	CG IN. (+AFT)
3D/OB-3	779.3	3352	9.086	-22.5
4D/OB-4	387.0	2823	6.373	-20.7
6D/OB-6	383.3	1992	1.962	-49.3
8D/OB-8	476.1	784	1.422	-36.0

R80-1469-055(T)

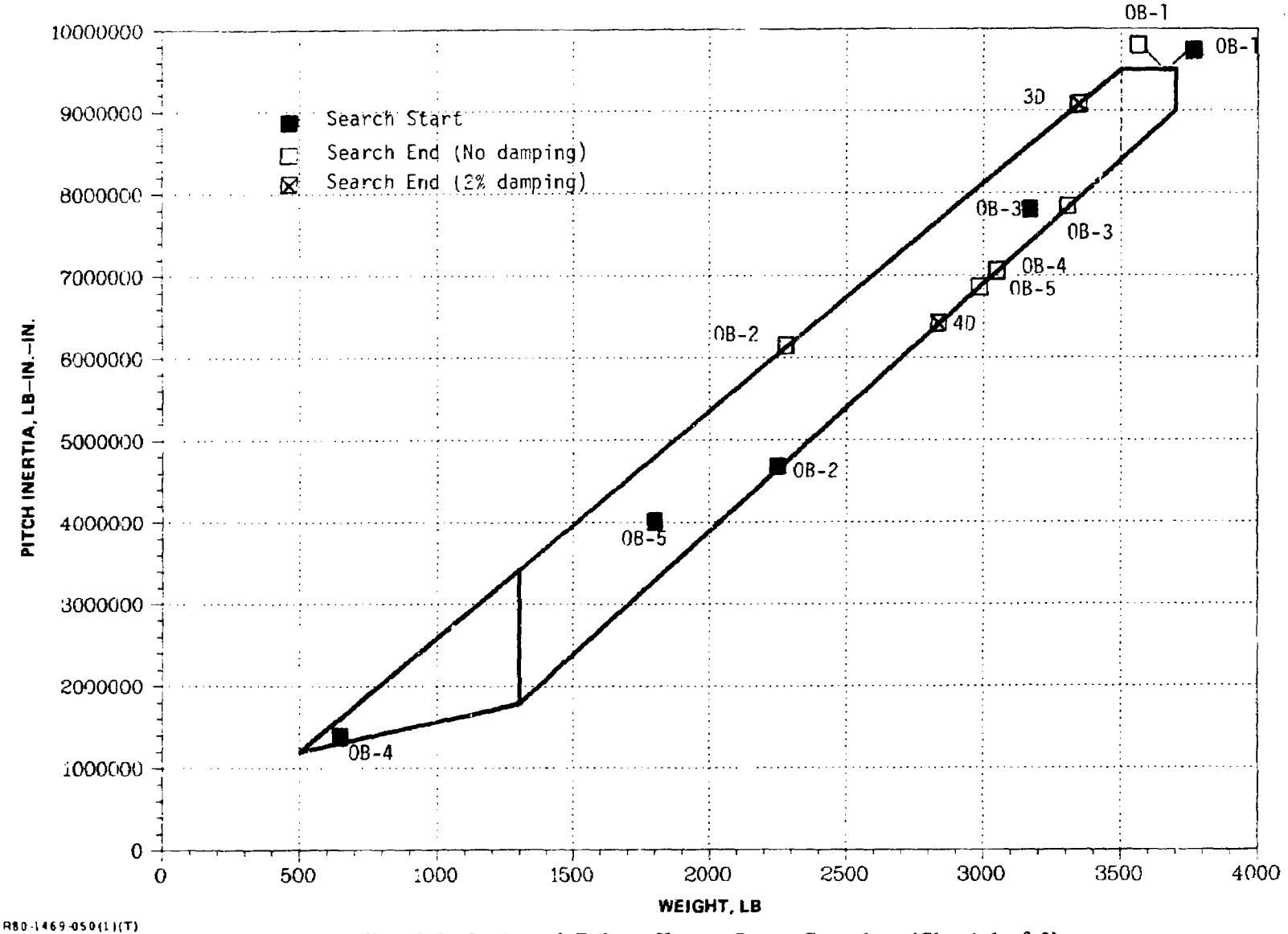

R80-1469-050(1)(T)

Fig. 8-3 Outboard-Pylon, Upper-Space Searches (Sheet 1 of 3)

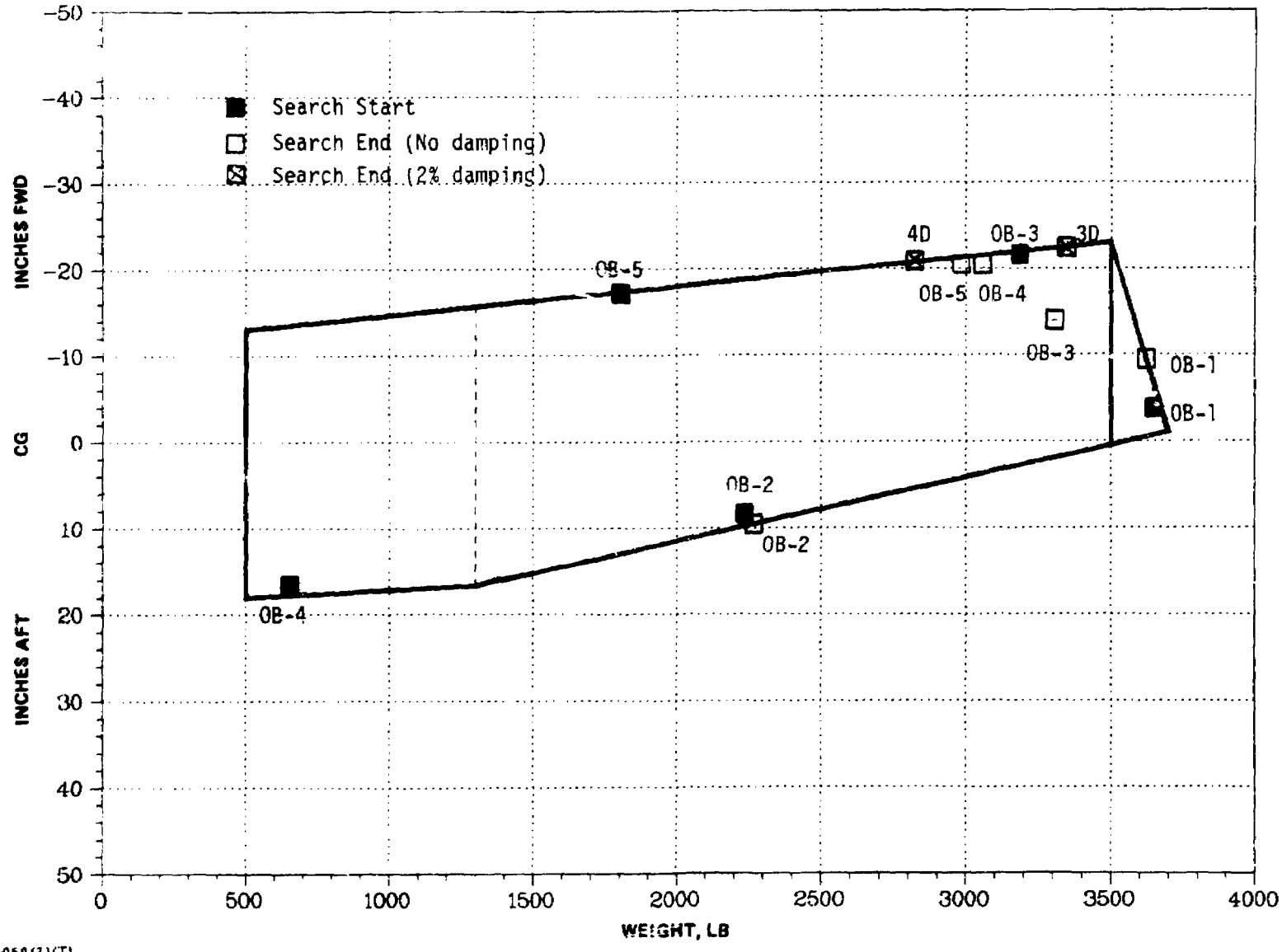

R80-1459-050(2)(T)

Fig. 8-3 Outboard-Pylon, Upper-Space Searches (Sheet 2 of 3)

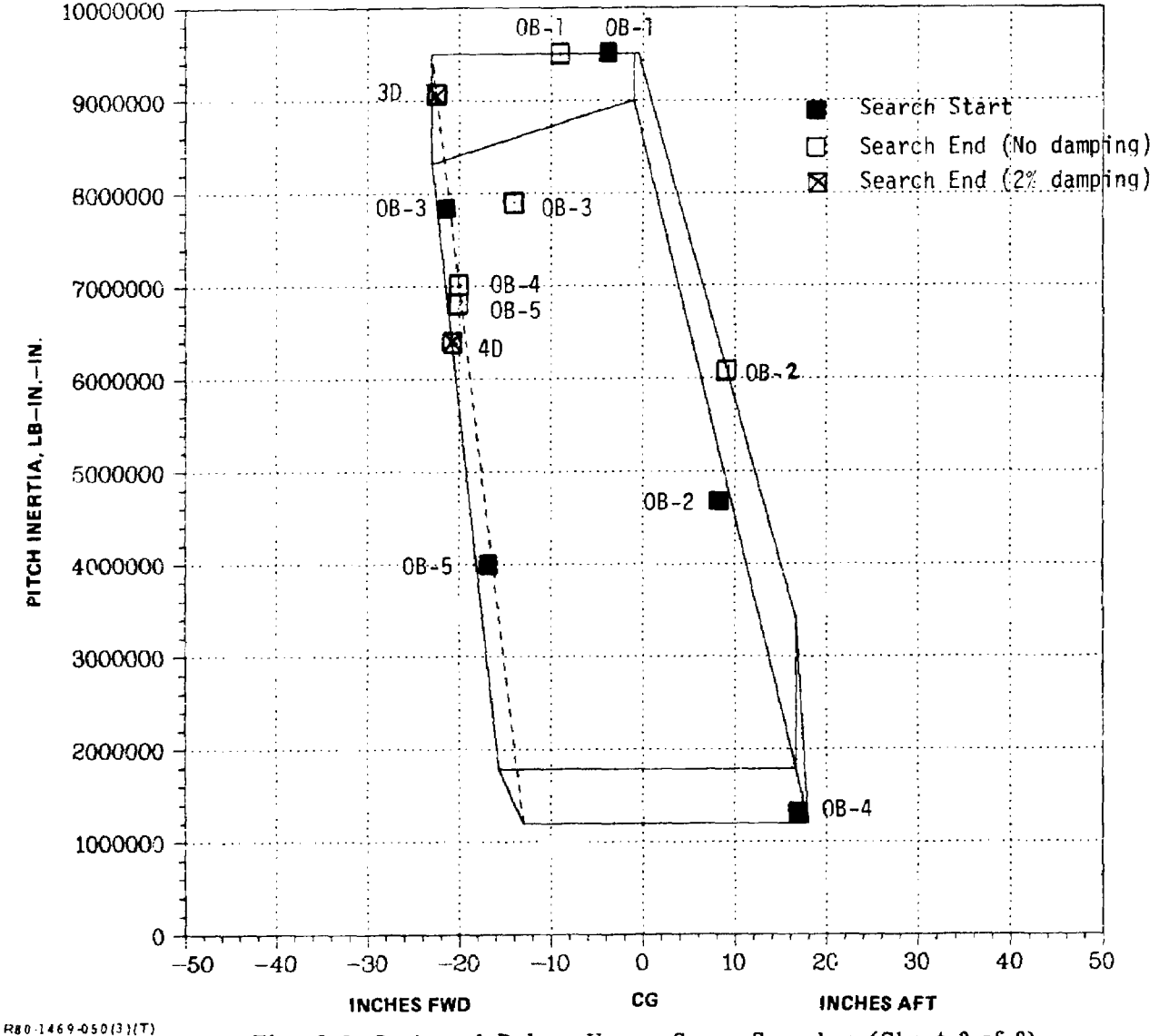

R80-1469-050(3)(T)

Fig. 8-3 Outboard-Pylon, Upper-Space Searches (Sheet 3 of 3)

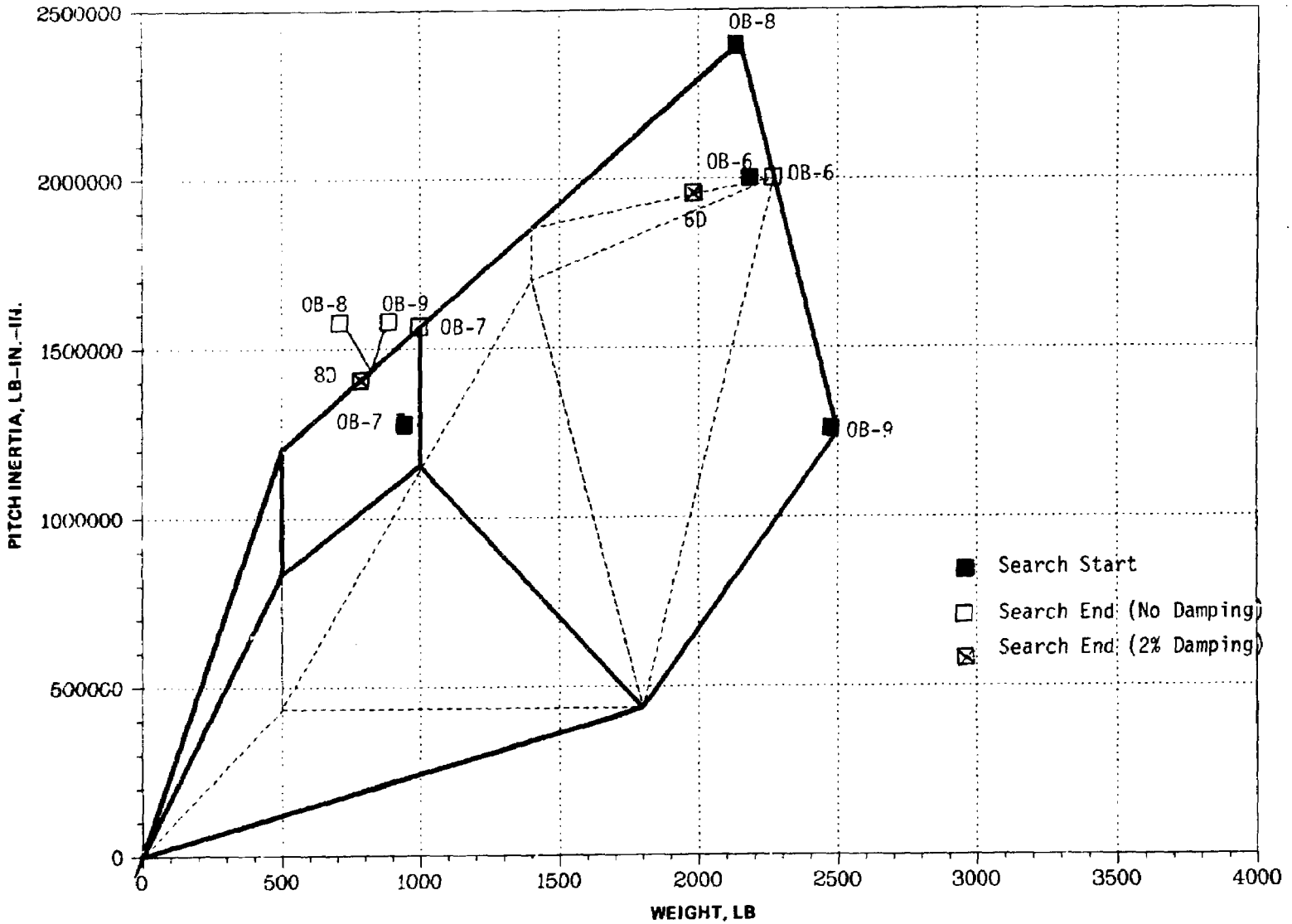

R80-1469-051(1)(T)

Fig. 8-4 Outboard-Pylon, Lower-Space Searches (Sheet 1 of 3)

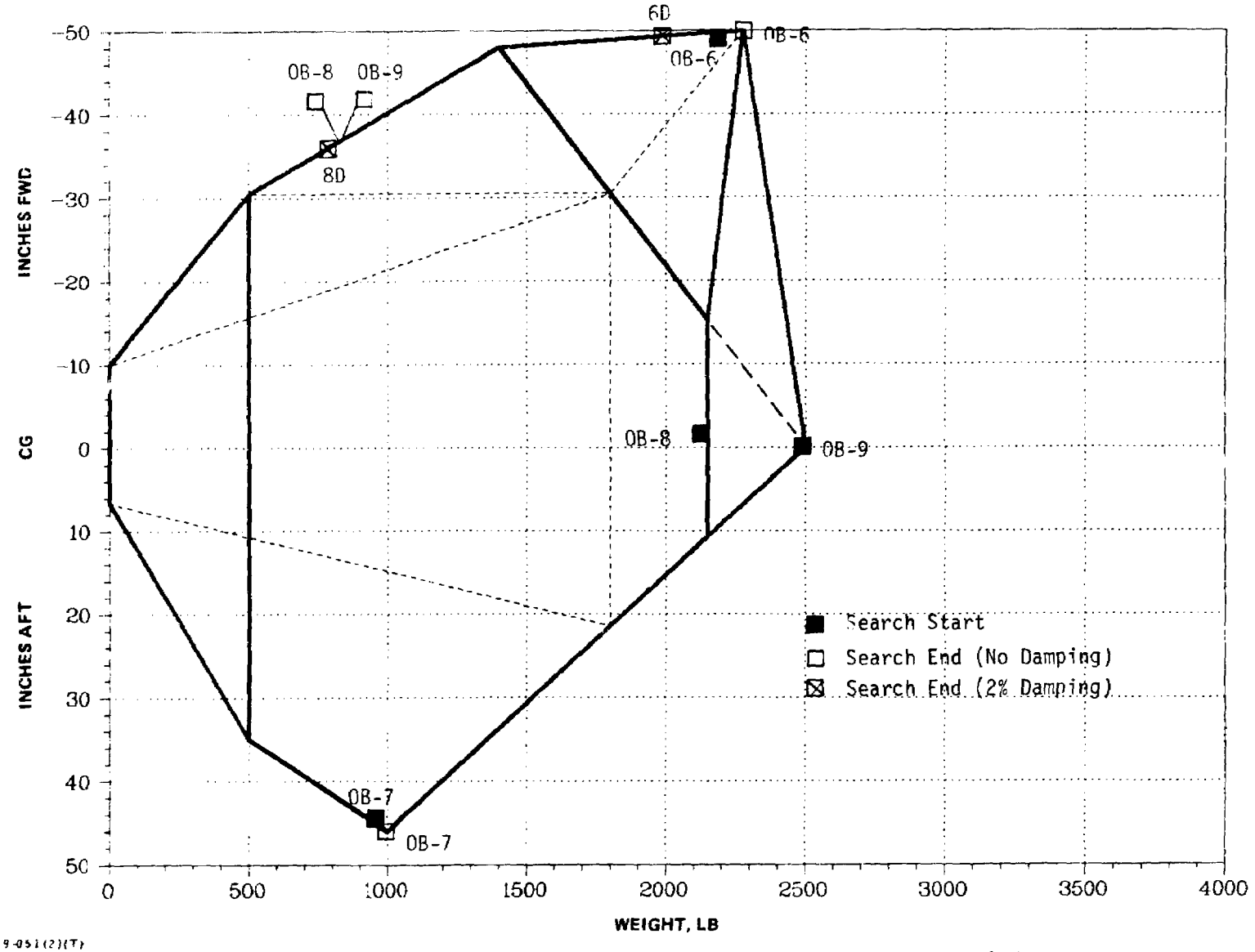

RB0-1469-051(2)(T)

Fig. 8-4 Outboard-Pylon, Lower-Space Searches (Sheet 2 of 3)

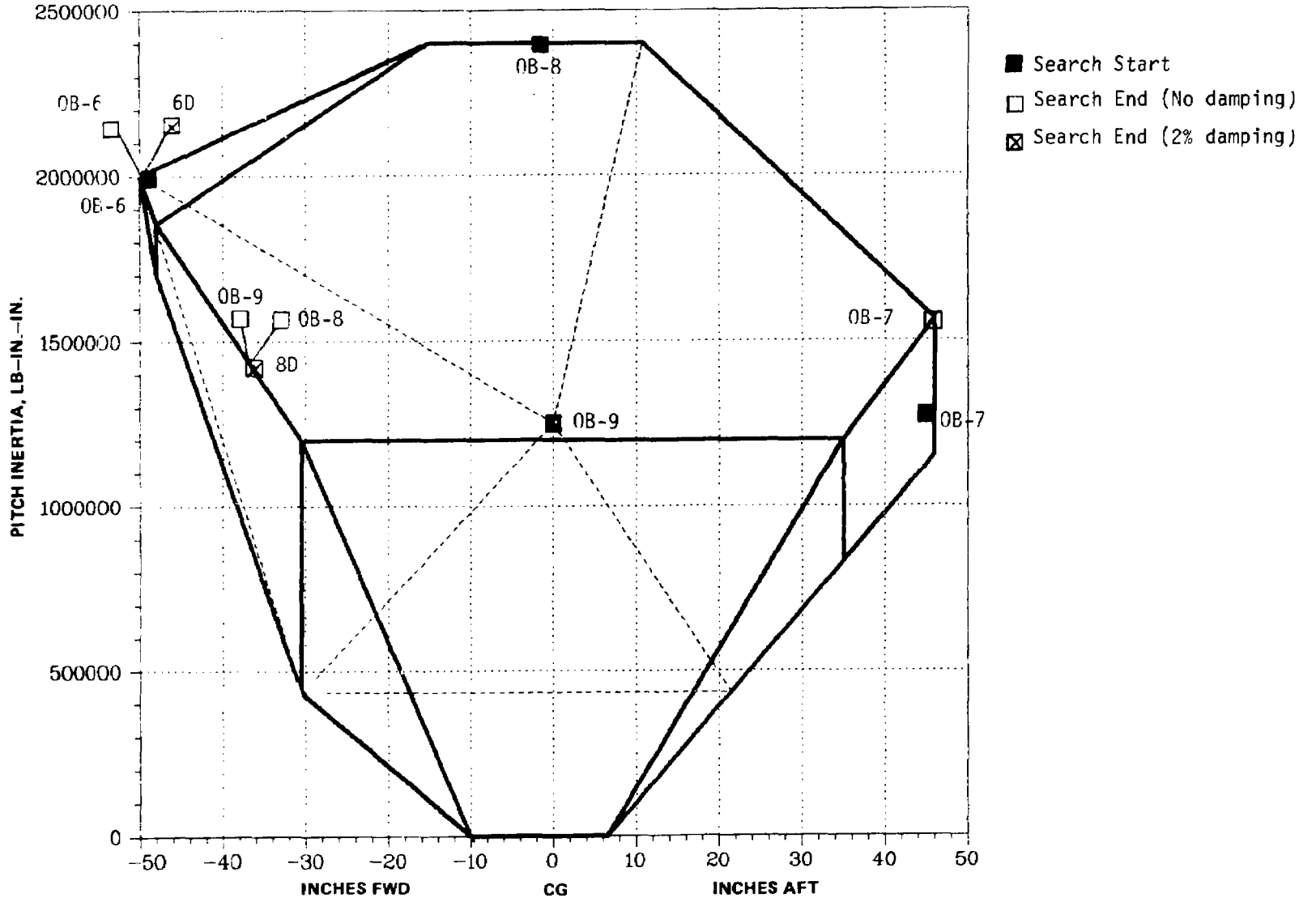

R80-1469-051(3)(T)

Fig. 8-4 Outboard-Pylon, Lower-Space Searches (Sheet 3 of 3)

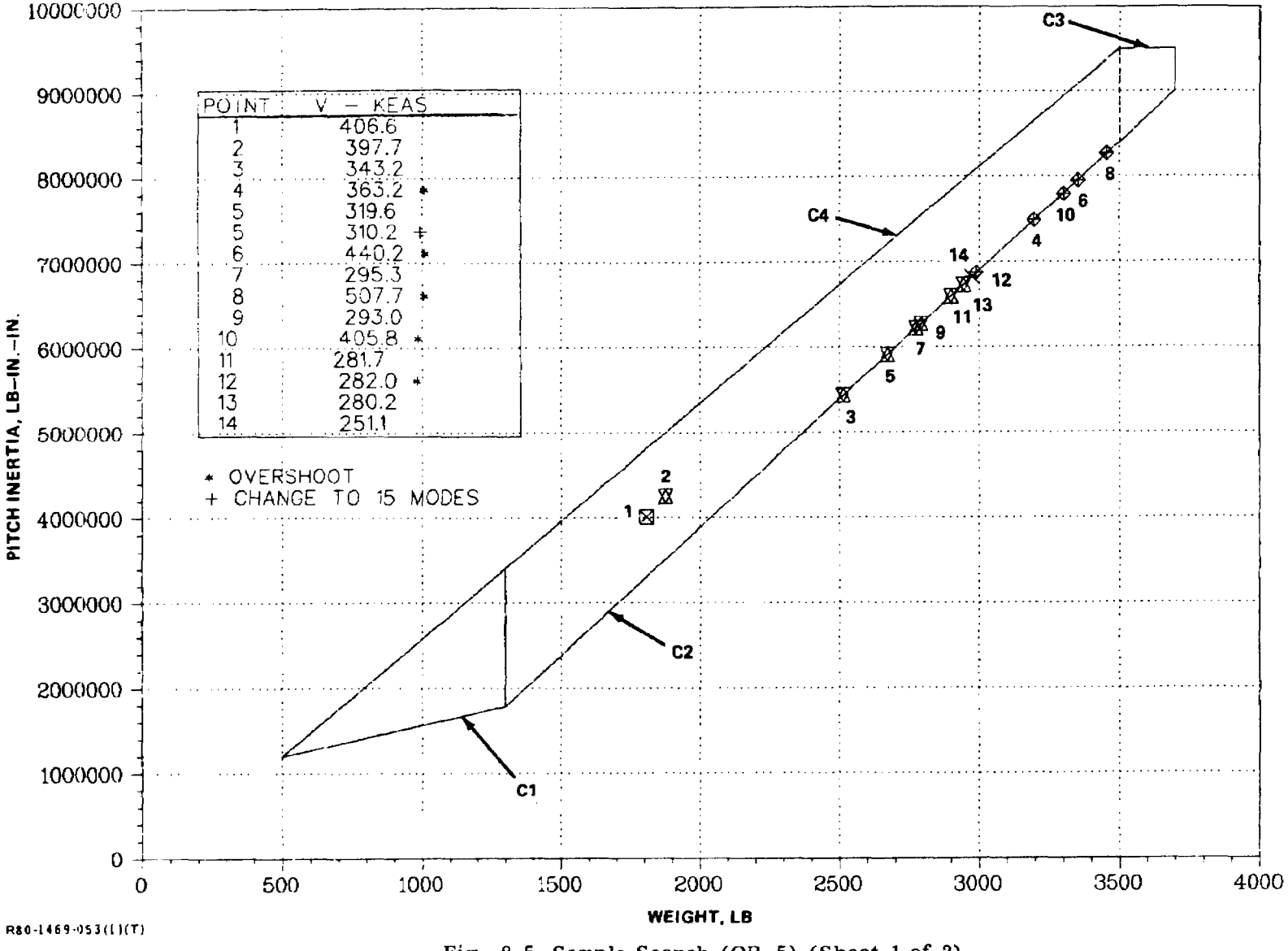

Fig. 8-5 Sample Search (OB-5) (Sheet 1 of 2)

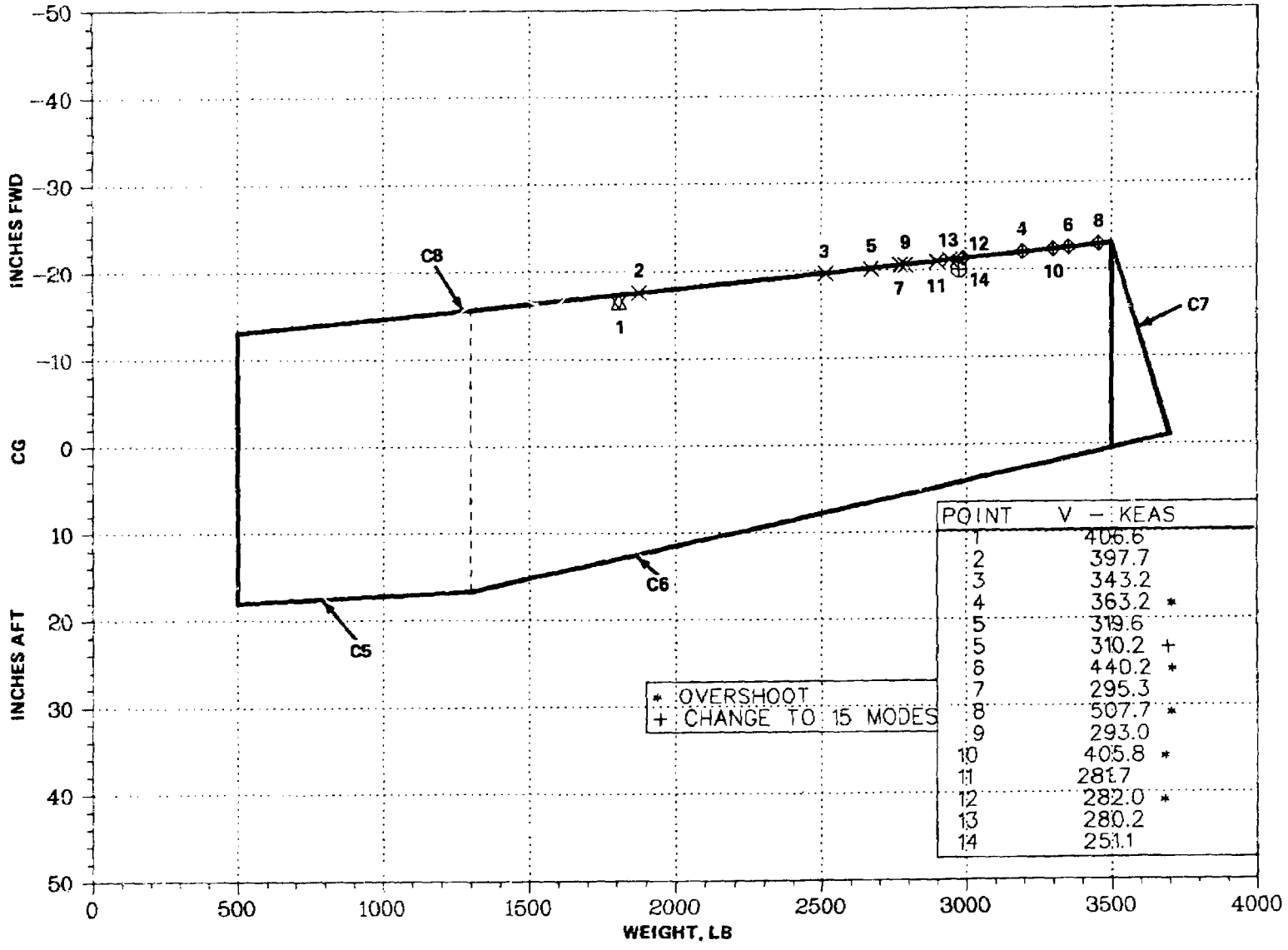

R80-1469-053(2)(T)

Fig. 8-5 Sample Search (OB-5) (Sheet 2 of 2)

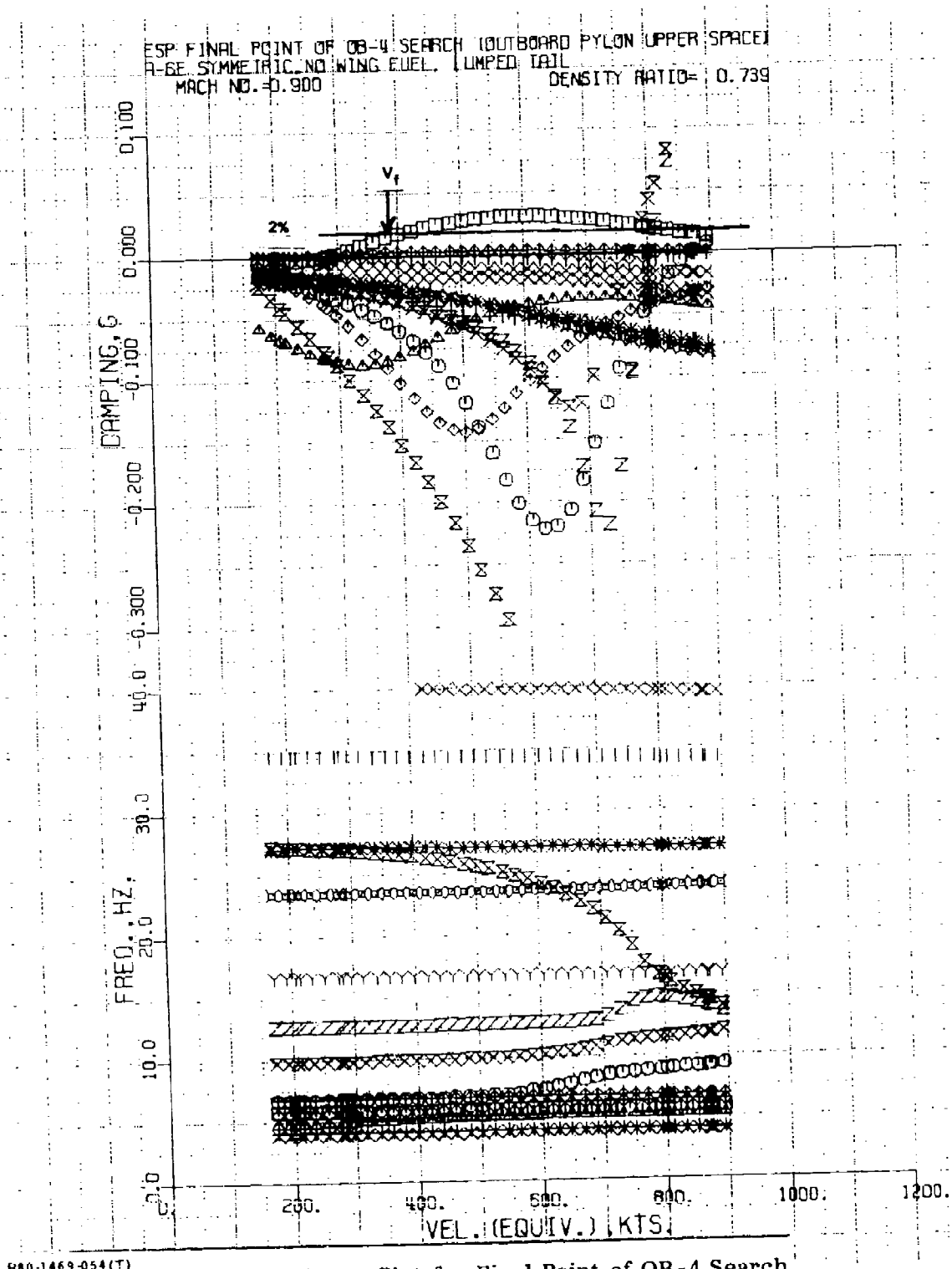

Fig. 8-6 V-g-ω Plot for Final Point of OB-4 Search

8.4 INBOARD SEARCHES

Table 8-VI specifies the starting points for these searches. Searches IS1 - IS4 were run with the outboard store fixed at point 4D; searches IS5 - IS9 were run with it fixed at point 6D. The (inboard) starting points are shown in Fig. 8-7 and 8-8. The results are marked on these figures and recorded in Table 8-VII. Searches IS1 - IS3 converge to the same point; IS4 reaches a non-critical local minimum. Searches IS5 and IS7 converge to the same point (very close to IS1 - IS3); IS6 and IS9 reach separate non-critical points. Consequently, two combined critical configurations have emerged. Denoted CR1 and CR2, these points are given in Table 8-VIII.

TABLE 8-VI STARTS FOR INITIAL INBOARD SEARCHES

	FIXED OUTBOARD STORE			VARIABLE INBOARD STORE		
NO.	WEIGHT, LB	MOMENT-OF-INERTIA, LB–IN.^{2} X 10^{-6}	CG, IN. (+AFT)	WEIGHT, LB	MOMENT-OF-INERTIA, LB–IN.^{2} X 10^{-6}	CG, IN. (+AFT)
IS1	2823	6.373	-20.7	3385	8.320	11.1
IS2				2494	6.000	-15.2
IS3				2594	6.770	7.7
IS4				1271	1.420	-42.0
IS5	1982	1.952	-49.3	3385	8.320	11.1
IS6				2494	6.000	-15.2
IS7				2594	6.770	7.7
IS8				1271	1.420	-42.0
IS9				2328	1.830	39.3

R80-1469-056(T)

TABLE 8-VII RESULTS OF INITIAL INBOARD SEARCHES

NO.	FLUTTER SPEED, KEAS	WEIGHT, LB	MOMENT-OF-INERTIA, LB–IN.^{2} X 10^{-6}	CG, IN. (+AFT)
IS1	376.2	3500	9.500	6.89
IS2	380.8	3500	9.500	6.56
IS3	376.2	3500	9.500	6.98
IS4	797.9	1144	1.660	-43.00
IS5	379.6	3500	9.090	8.83
IS6	759.5	2011	5.380	-18.03
IS7	380.8	3500	9.500	6.00
IS8	740.4	1667	0.860	-36.35
IS9	770.4	2328	1.830	39.3

R80-1469-059(T)

TABLE 8-VIII STARTS FOR INBOARD/OUTBOARD SEARCHES

NO.	OUTBOARD PYLON			INBOARD PYLON		
	WEIGHT, LB	MOMENT-OF-INERTIA, LB–IN.^{2} X 10^{-6}	CG, IN. (+AFT)	WEIGHT, LB	MOMENT-OF-INERTIA, LB–IN.^{2} X 10^{-6}	CG, IN. (+AFT)
CR1	2823	6.373	-20.70	3500	9.500	6.89
CR2	1982	1.952	-49.30	3500	9.090	8.83

R80-1469-060(T)

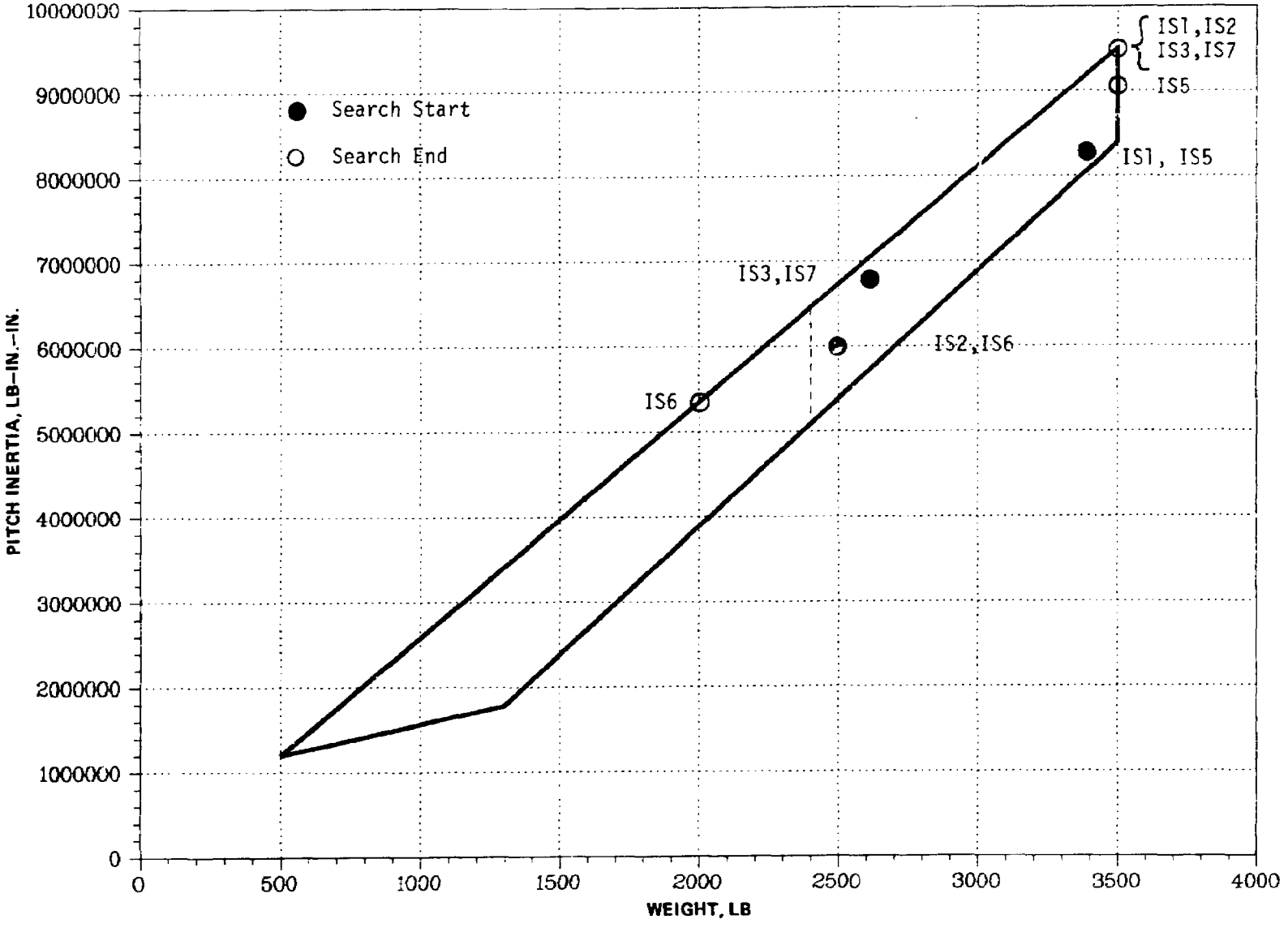

R80-1469-057(1)(T)

Fig. 8-7 Inboard-Pylon, Upper-Space Searches (Sheet 1 of 3)

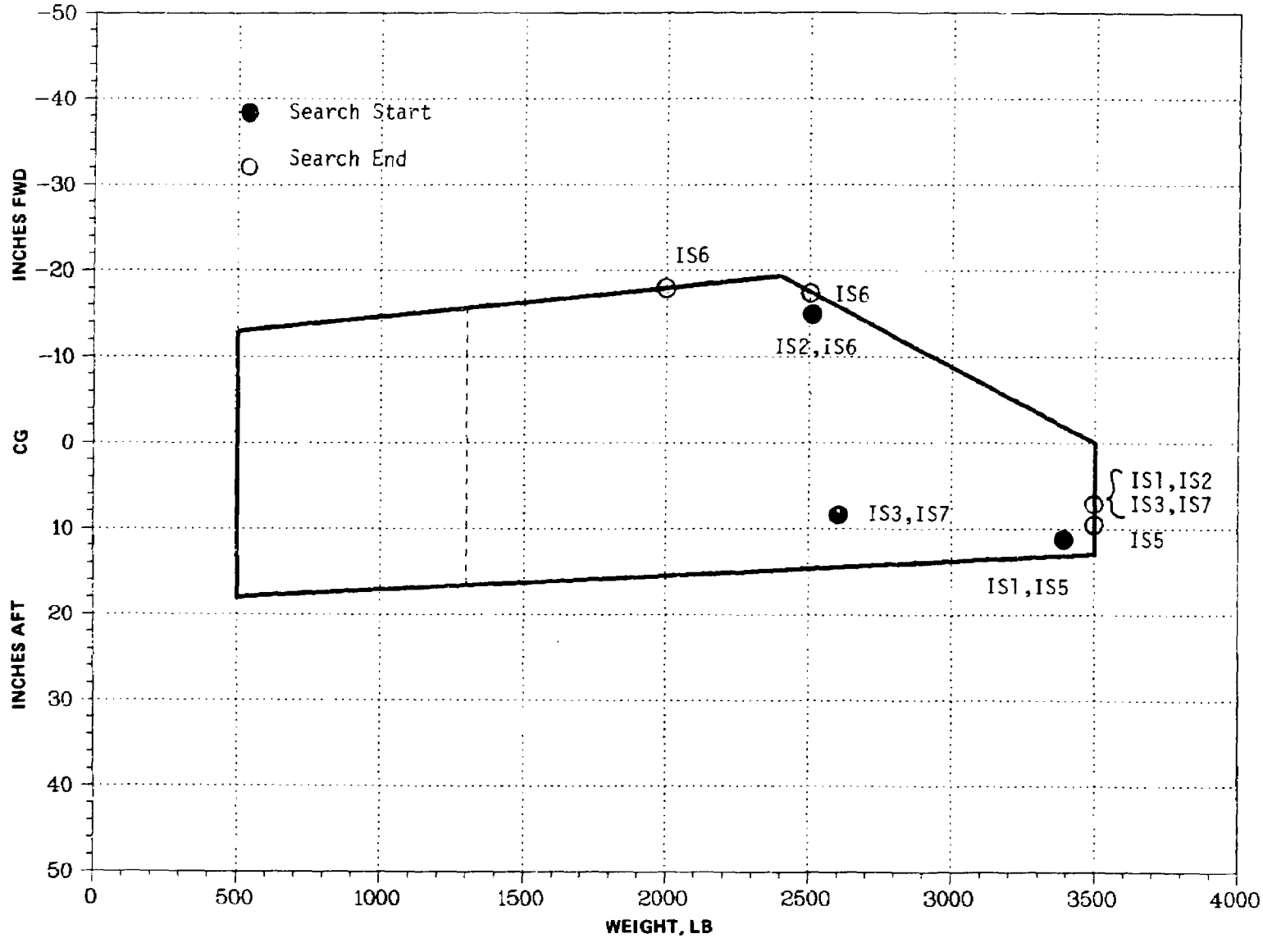

R80-1469-057(2)(T)

Fig. 8-7 Inboard-Pylon, Upper-Space Searches (Sheet 2 of 3)

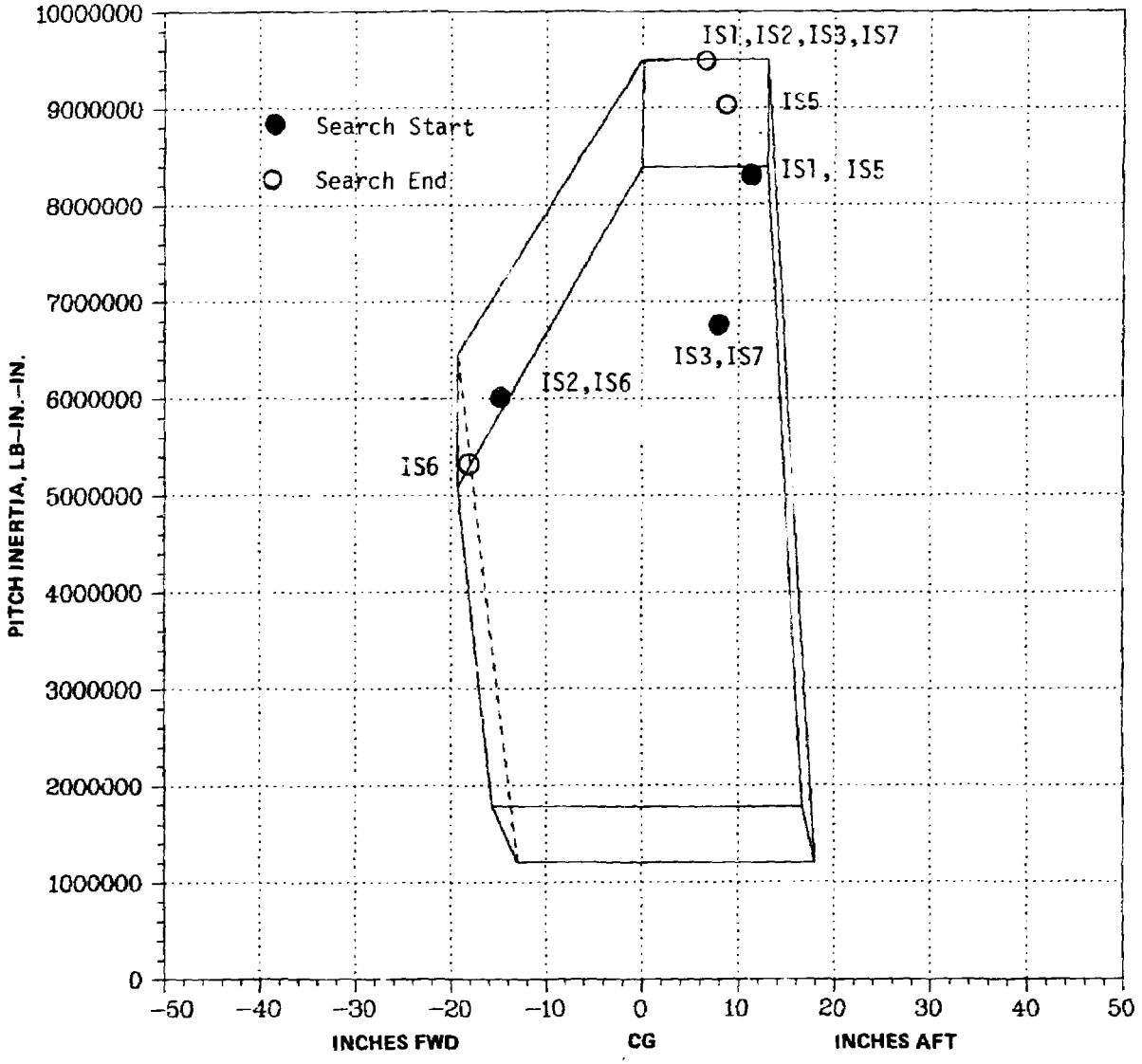

R80-1469-057(3)(T)

Fig. 8-7 Inboard-Pylon, Upper-Space Searches (Sheet 3 of 3)

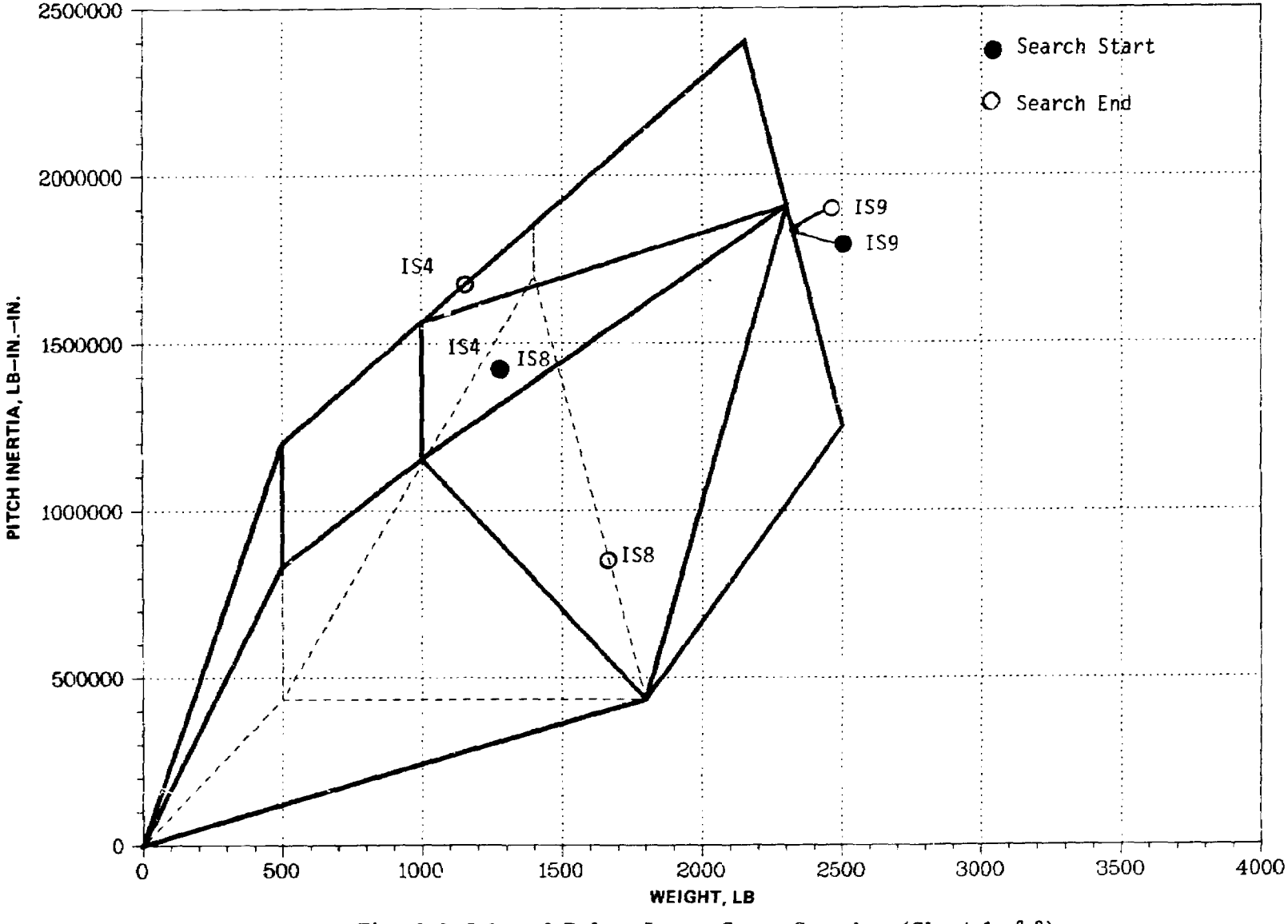

R80-1469-058(1)(T)

Fig. 8-8 Inboard-Pylon, Lower-Space Searches (Sheet 1 of 3)

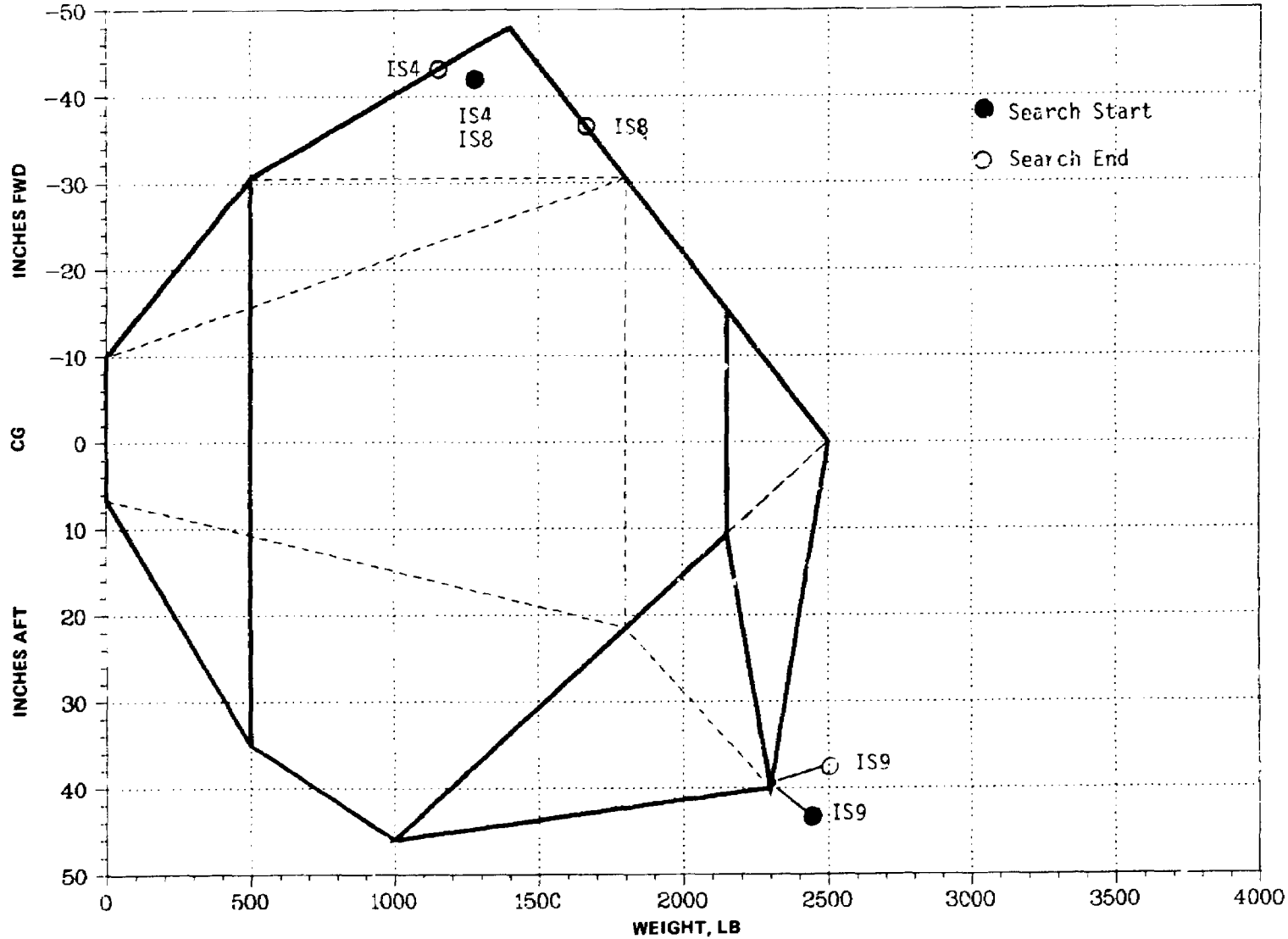

R80-1469-058(2)(T)

Fig. 8-8 Inboard-Pylon, Lower-Space Searches (Sheet 2 of 3)

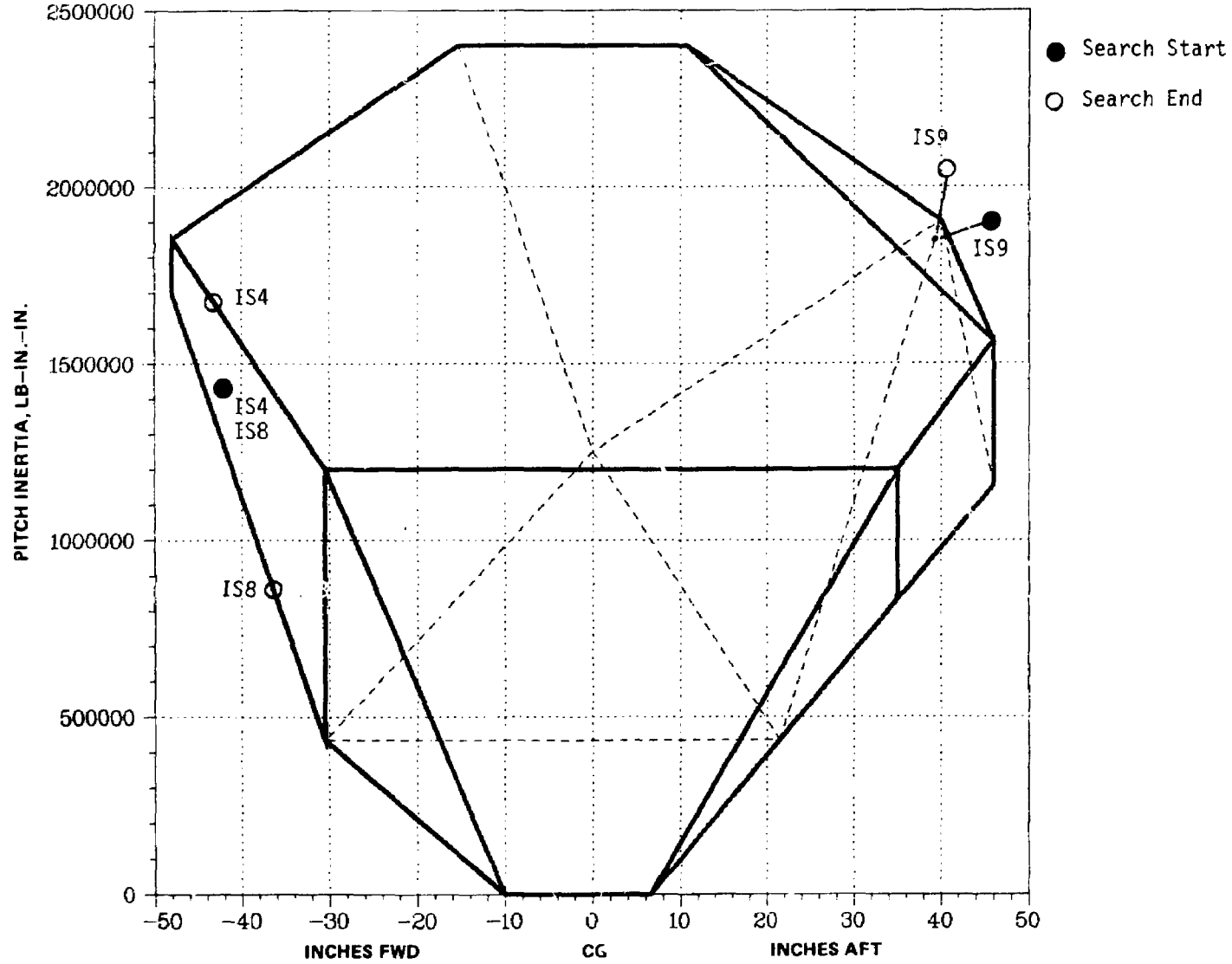

Fig. 8-8 Inboard-Pylon, Lower-Space Searches (Sheet 3 of 3)

8.5 COMBINED SEARCHES

Starting from CR1 and CR2, combined searches of inboard and outboard parameters simultaneously were made for the two tentative critical configurations. The results (denoted by CR1* and CR2*) are given in Table 8-IX and shown in Fig. 8-9 through 8-11. In the case of CR1, the final search did change the critical outboard-pylon store mass and moment-of-inertia parameters somewhat, while only the center of gravity of the inboard pylon store was altered. For CR2, there were essentially no changes in any of the parameters at either pylon.

By comparing the critical parameters with actual stores in the inventory (marked on Fig. 8-9 through 8-11), the identities of candidate critical store combinations were determined. These combinations, circled in the figures and summarized (as N1 and N2) in Table 8-IX, are quite close to CR1 and CR2. Flutter analyses of these configurations were performed; the resultant flutter speeds, also given in Table 8-IX, are only 31 and 16 knots higher than the corresponding speeds of CR1* and CR2*.

Figures 8-12 and 8-13 are V-g-ω plots for N1 and N2, respectively. The crossovers with 2% structural damping are marked on these plots. As can be seen, the instabilities are gradual. These figures also show that an additional 1% damping would eliminate these store instabilities altogether. In practice, the amount of damping present is variable - subject, among other things, to pylon/store installation procedures - but no more than 2% is normally assumed in flutter clearance analyses. Consequently, if these instabilities were uncovered during aircraft design and were within the flight envelope, a precautionary fix (structural or mass balance) might be employed or, more likely, the configurations would be marked for flight test evaluation.

From inspection of the eigenvectors (not shown) associated with the flutter points CR1* and CR2*, it was found that the instabilities involve coupling between mode 3 (first wing bending), mode 4 (first wing torsion), and mode 5 (inboard/outboard store pitch, in phase). The mode shapes for CR1* are given in Fig. 8-14 through 8-23.

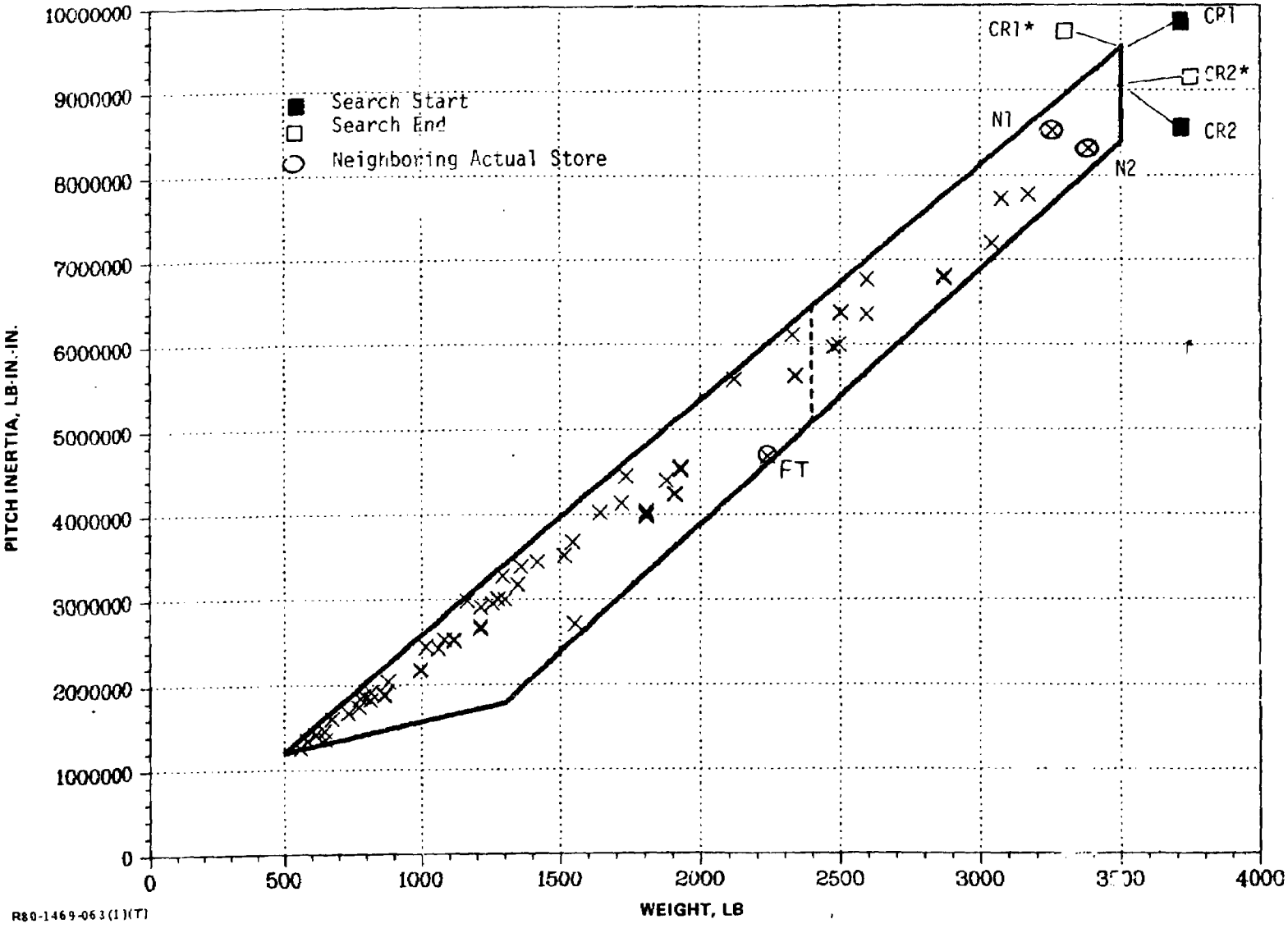

Fig. 8-9 Locations of Critical Configurations: Upper Space, Inboard Pylon (Sheet 1 of 3)

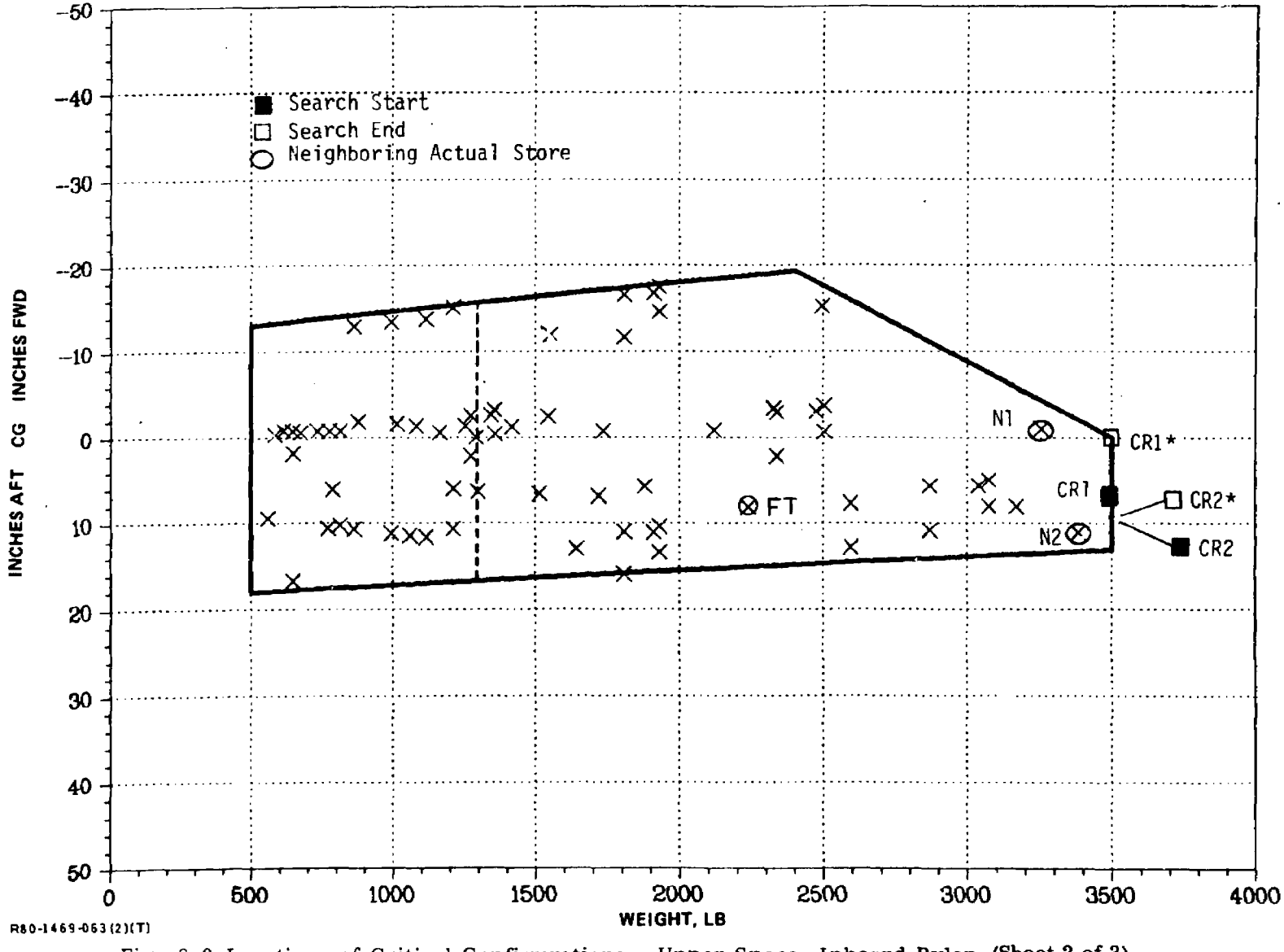

Fig. 8-9 Locations of Critical Configurations: Upper Space, Inboard Pylon (Sheet 2 of 3)

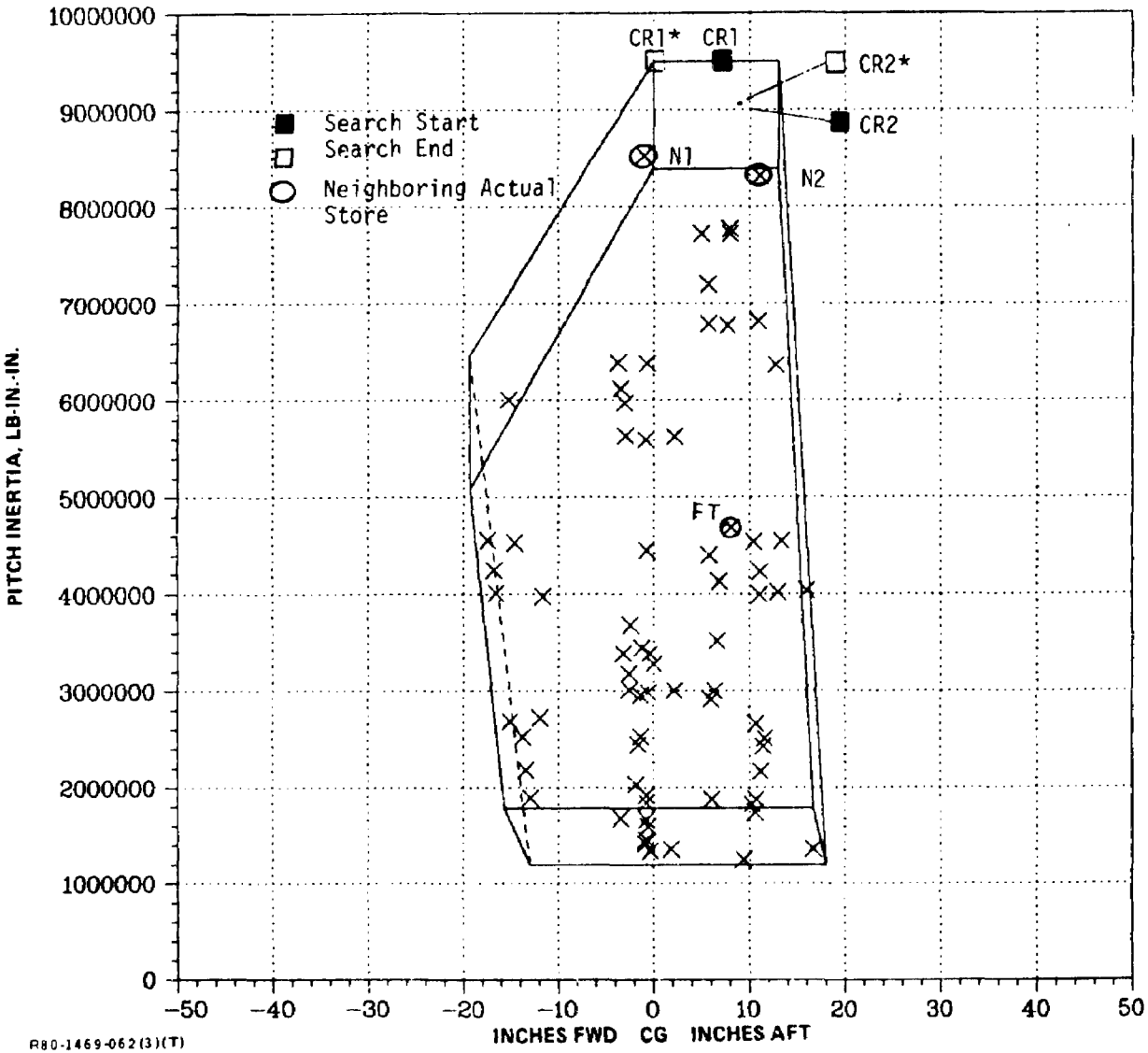

Fig. 8-9 Locations of Critical Configurations: Upper Space, Inboard Pylon (Sheet 3 of 3)

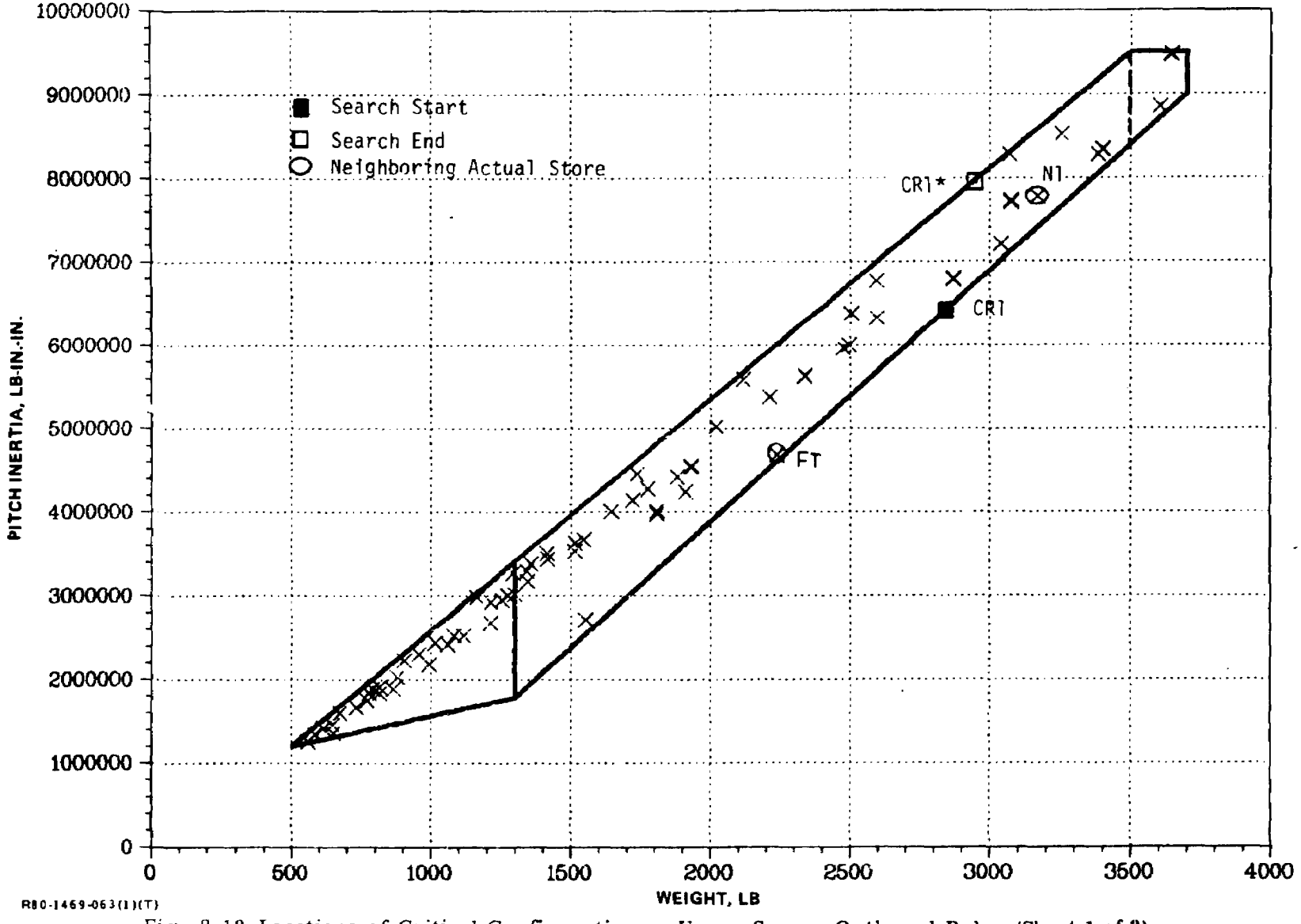

Fig. 8-10 Locations of Critical Configurations: Upper Space, Outboard Pylon (Sheet 1 of 3)

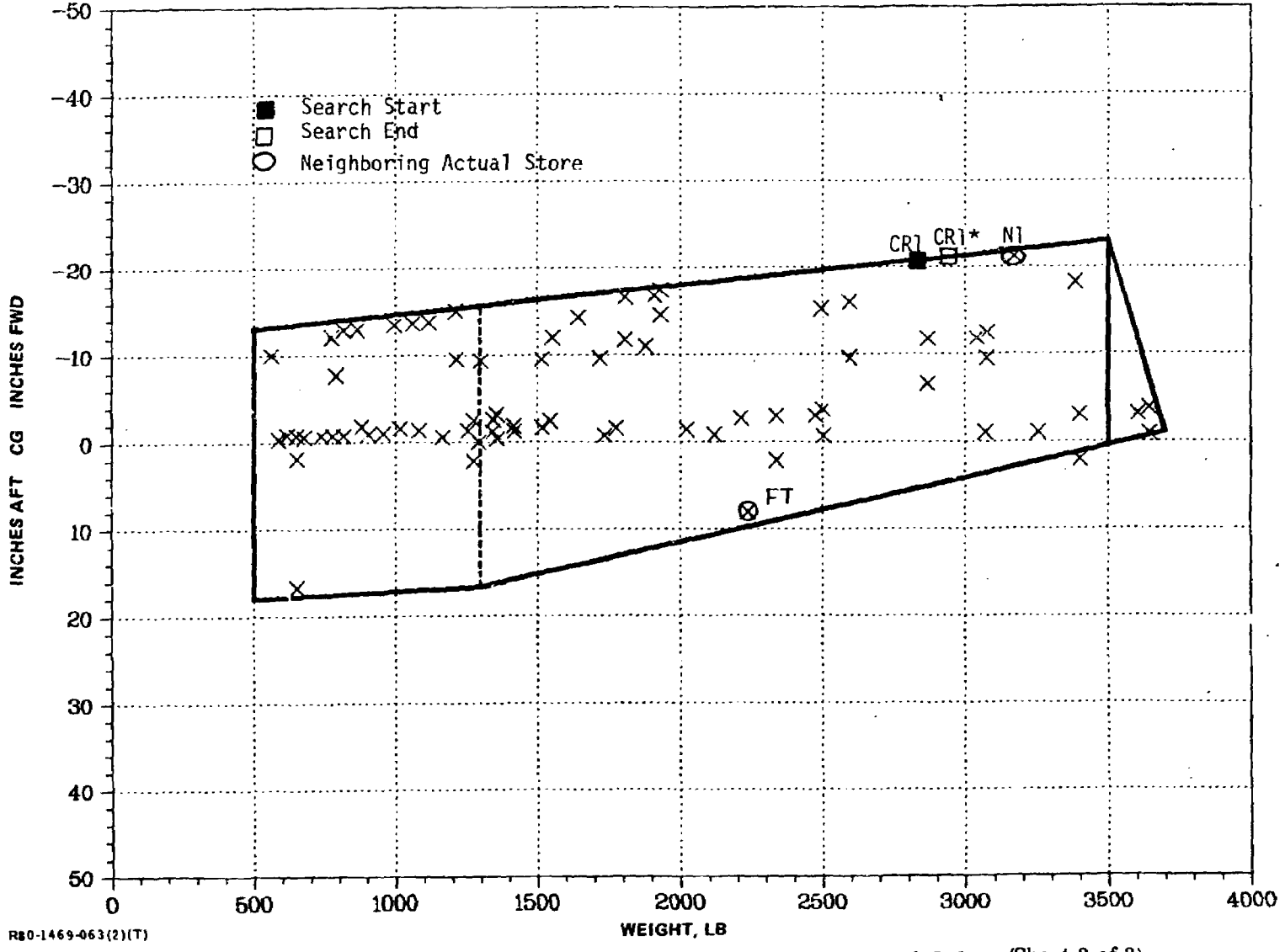

Fig. 8-10 Locations of Critical Configurations: Upper Space, Outboard Pylon (Sheet 2 of 3)

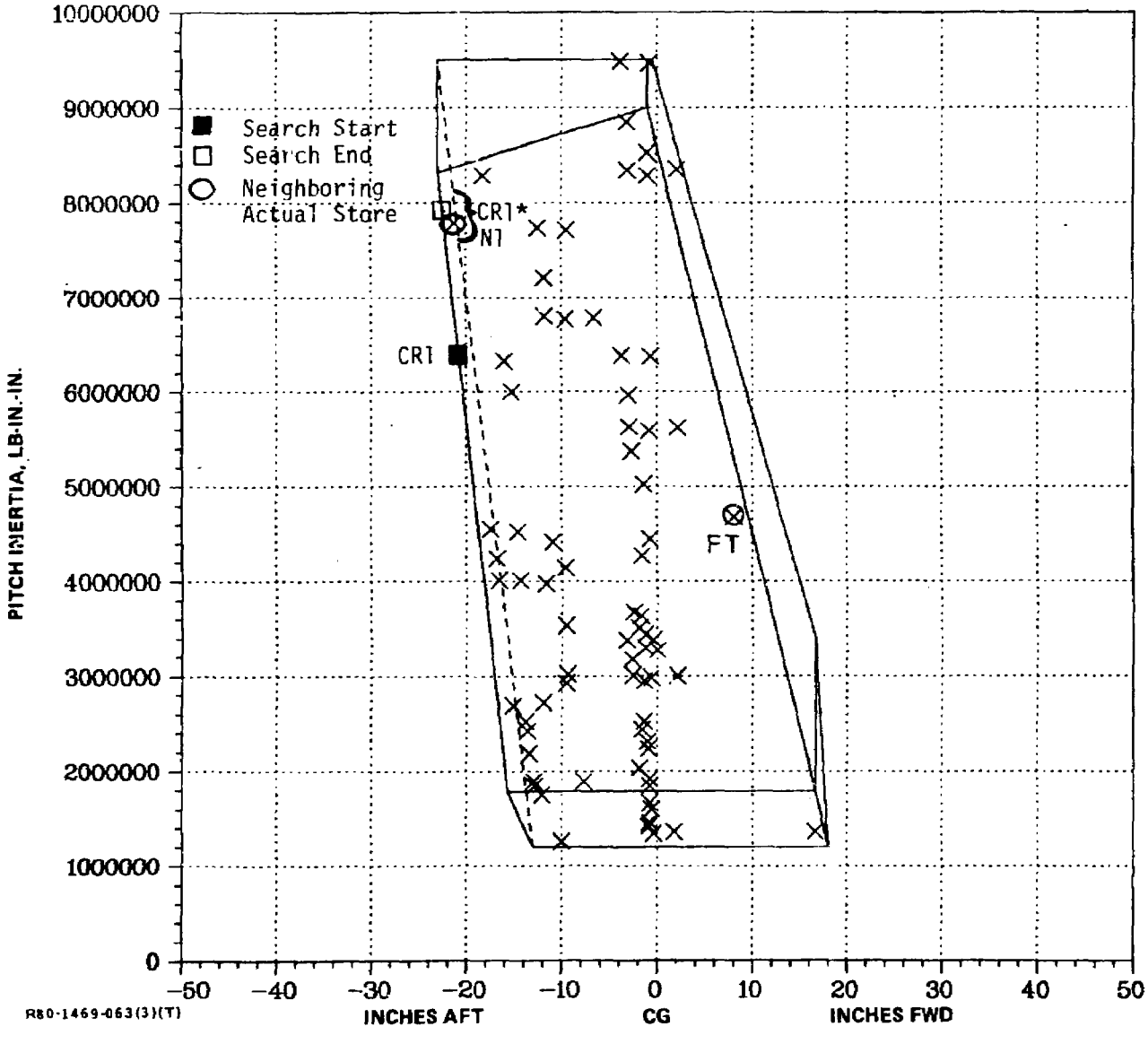

Fig. 8-10 Locations of Critical Configurations: Upper Space, Outboard Pylon (Sheet 3 of 3)

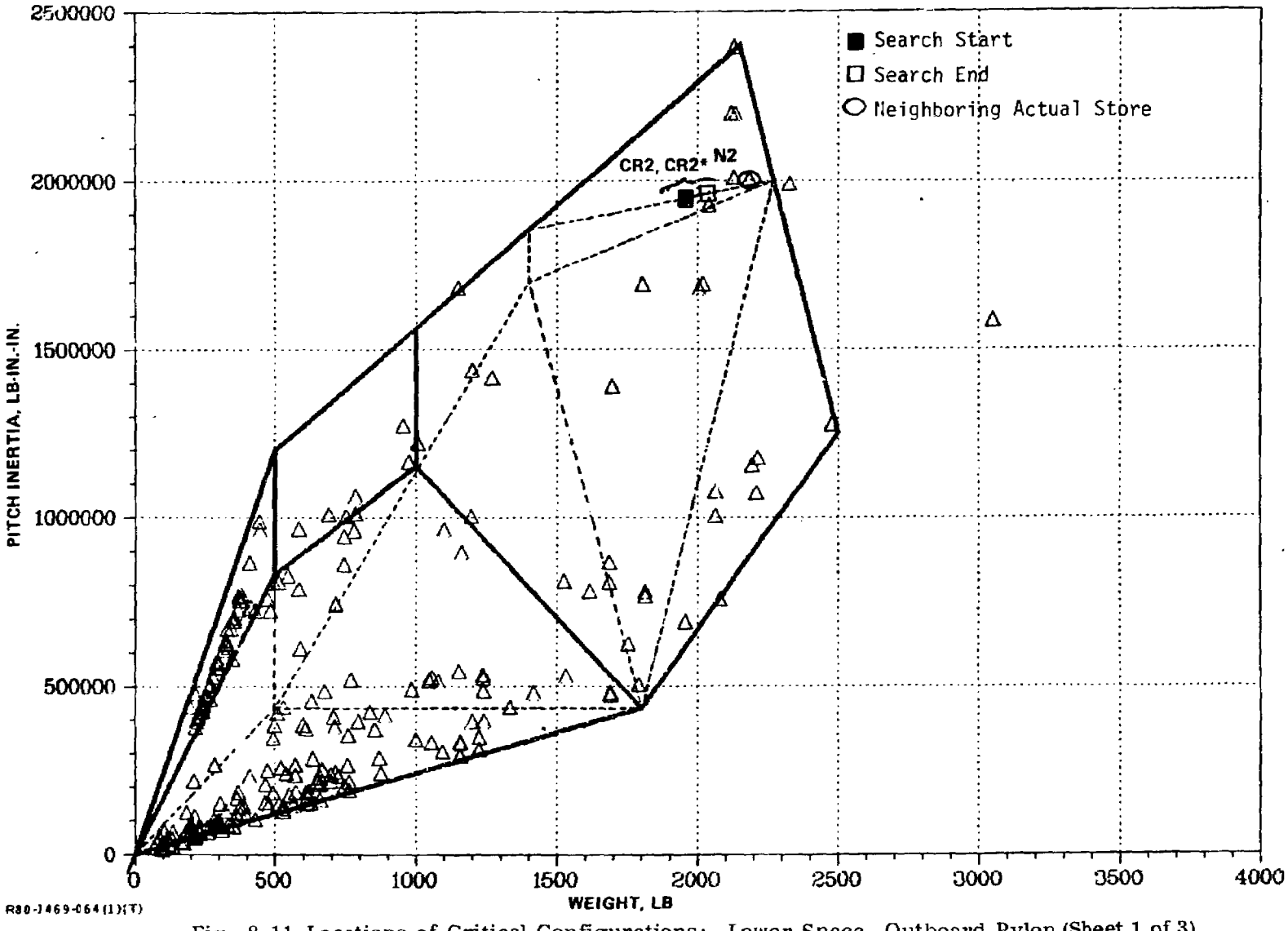

Fig. 8-11 Locations of Critical Configurations: Lower Space, Outboard Pylon (Sheet 1 of 3)

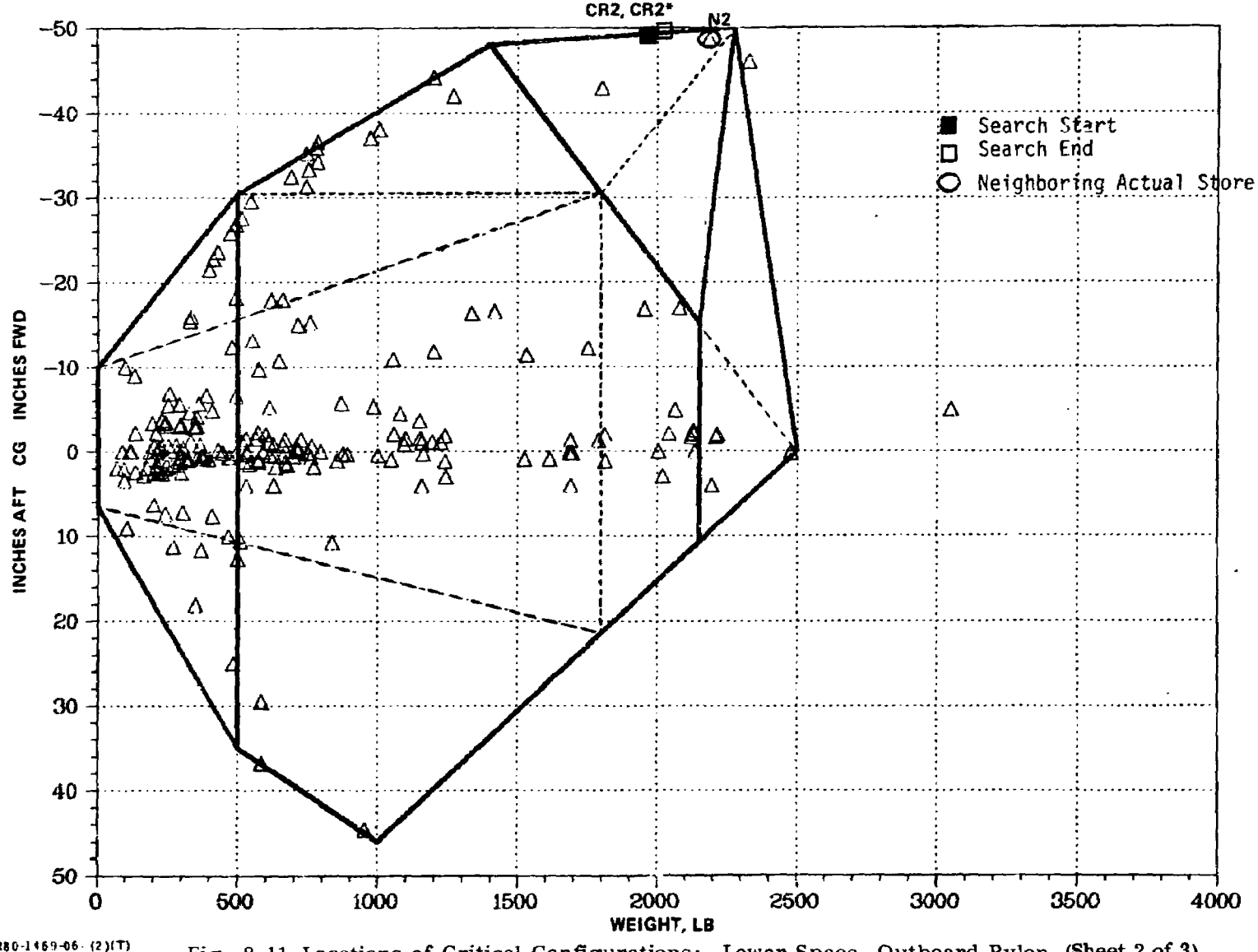

R80-1469-06-(2)(T)

Fig. 8-11 Locations of Critical Configurations: Lower Space, Outboard Pylon (Sheet 2 of 3)

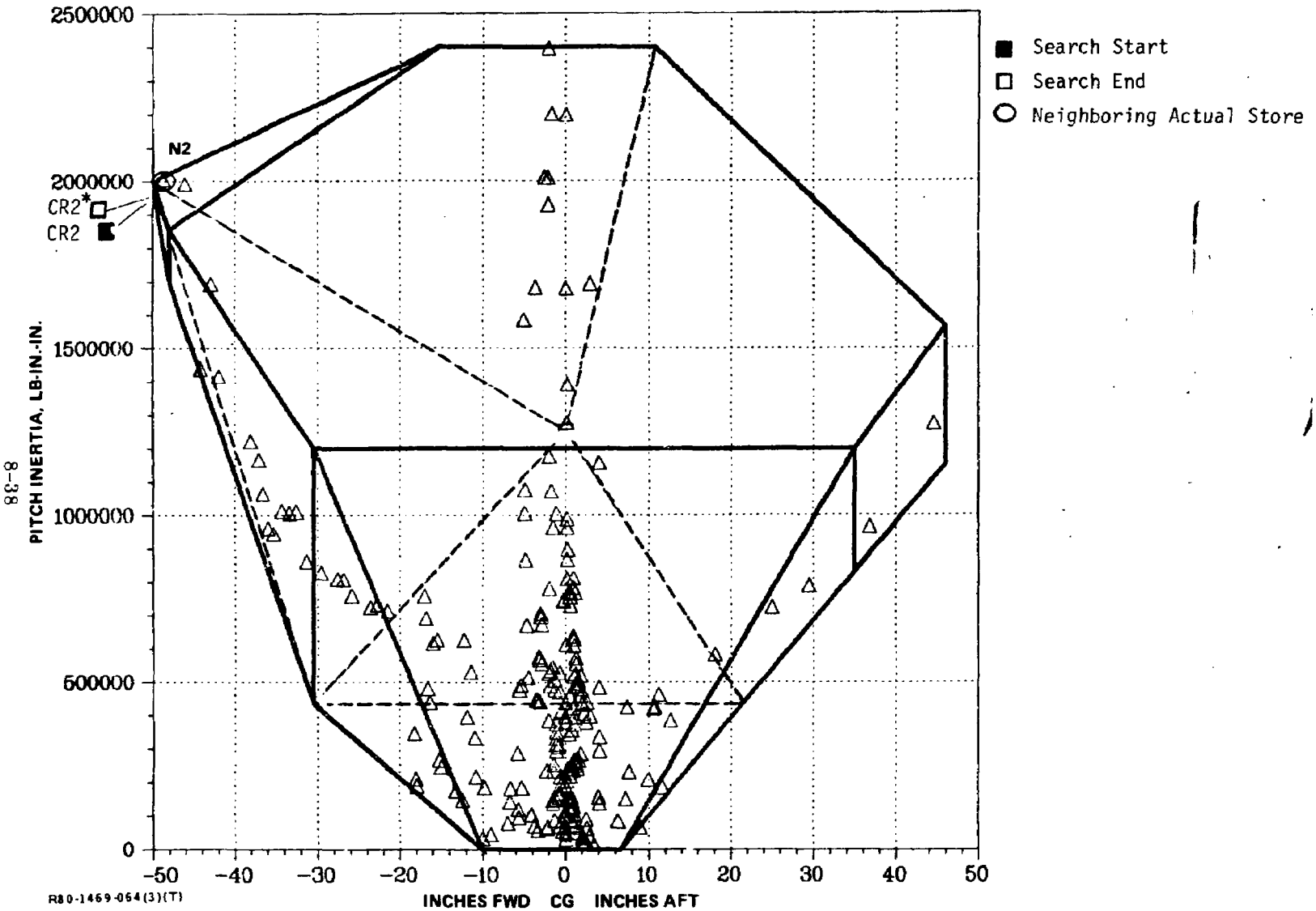

Fig. 8-11 Locations of Critical Configurations: Lower Space, Outboard Pylon (Sheet 3 of 3)

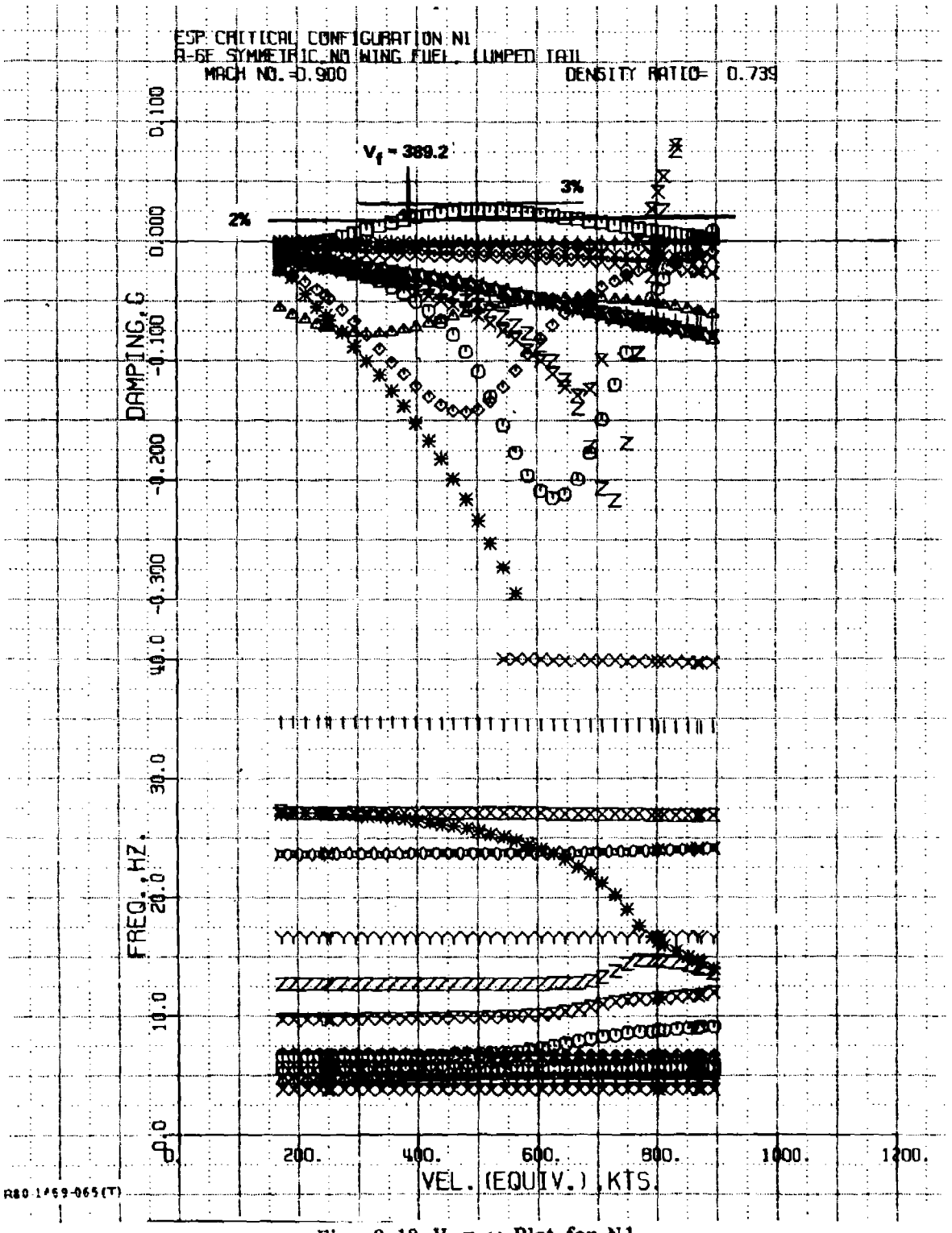

Fig. 8-12 V-g-ω Plot for N1

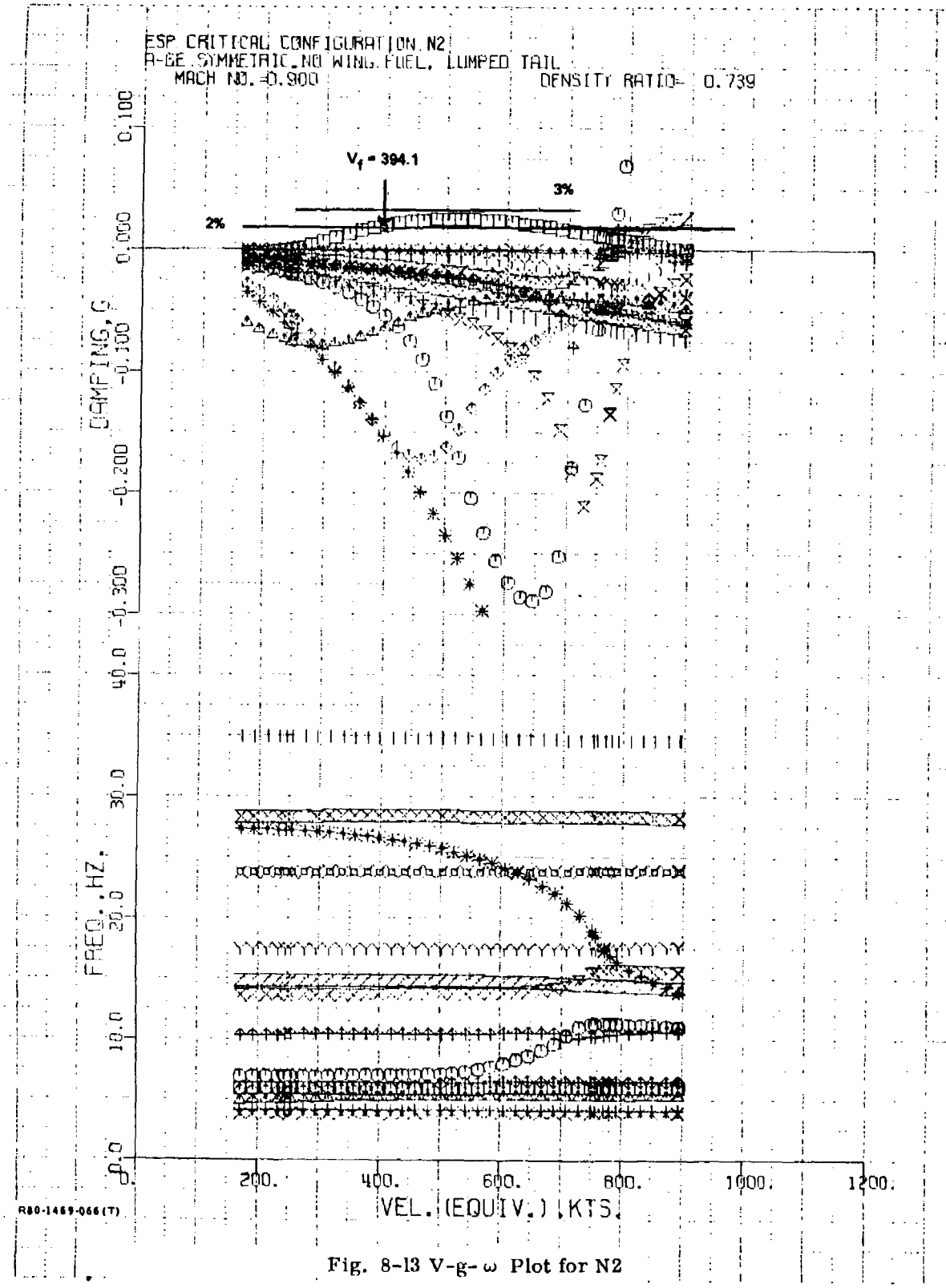

Fig. 8-13 V-g-ω Plot for N2

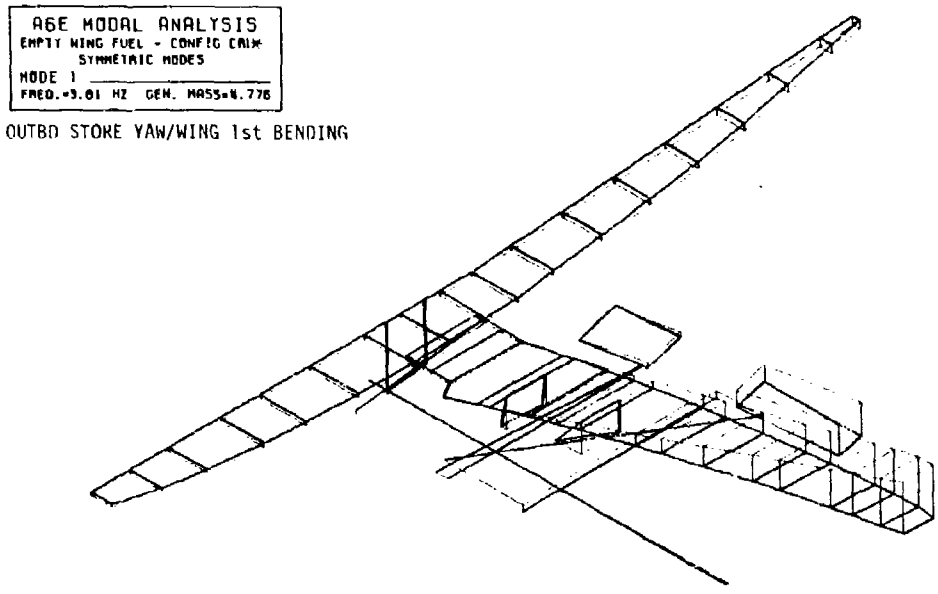

A80-1469-067(T)

Fig. 8-14 A-6E with Critical Stores: Mode 1

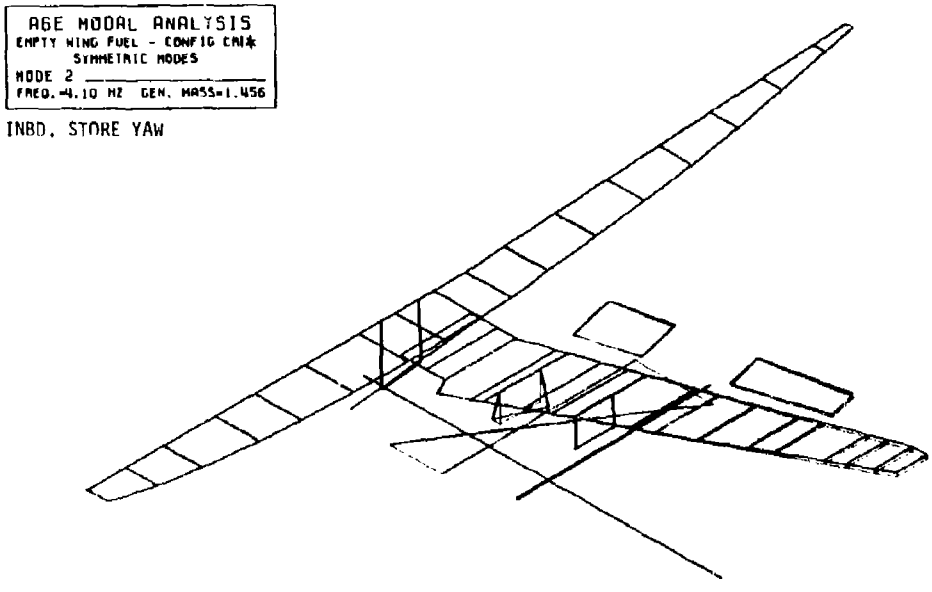

A80-1469-065(T) Fig. 8-15 A-6E with Critical Stores: Mode 2

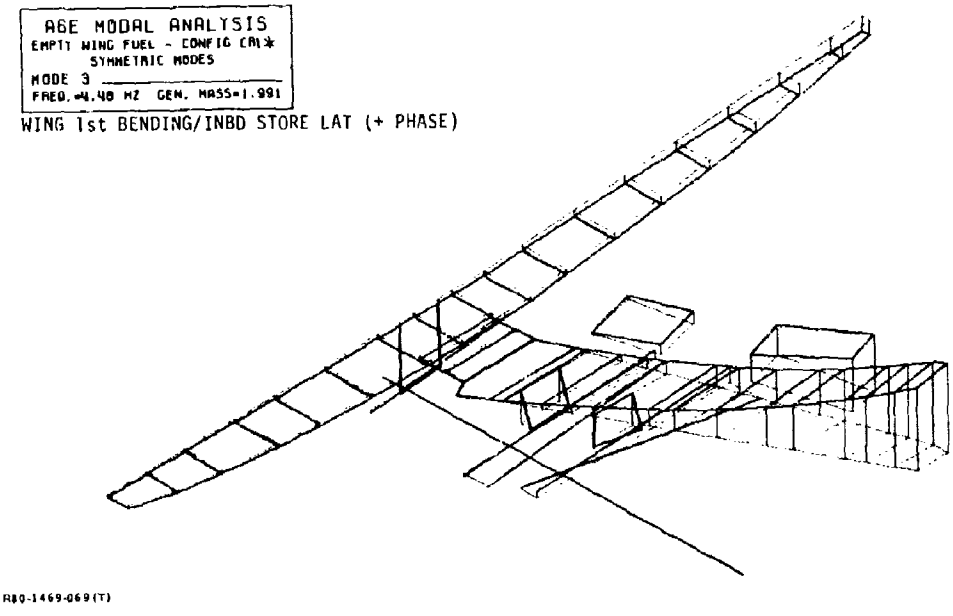

Fig. 8-16 A-6E with Critical Stores: Mode 3

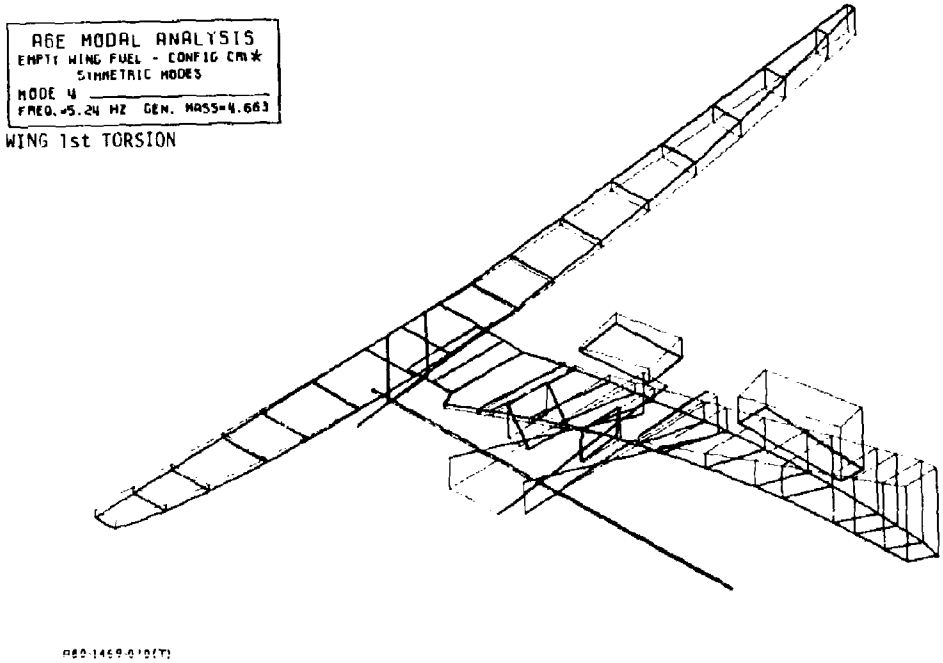

Fig. 8-17 A-6E with Critical Stores: Mode 4

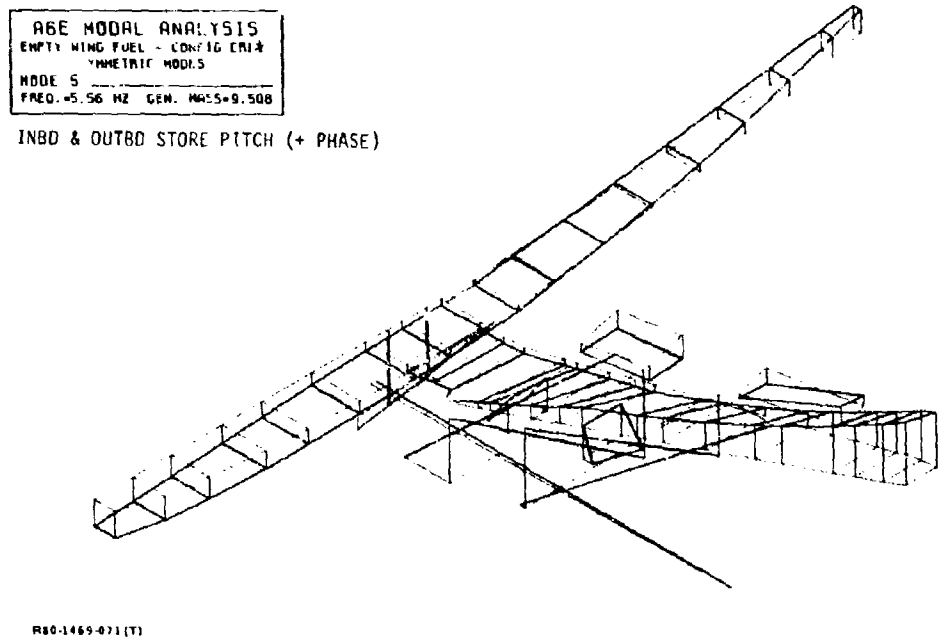

Fig. 8-18 A-6E with Critical Stores: Mode 5

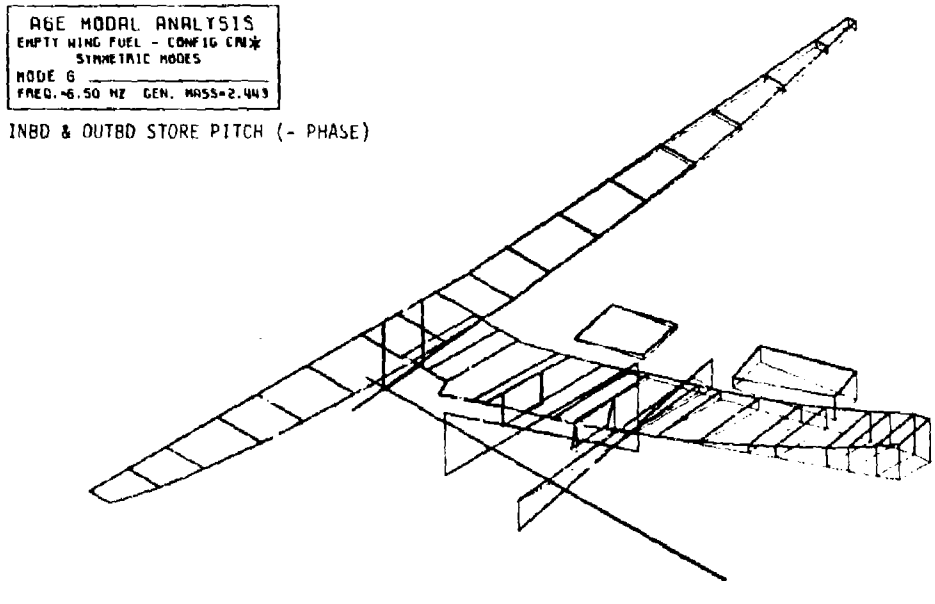

Fig. 8-19 A-6E with Critical Stores: Mode 6

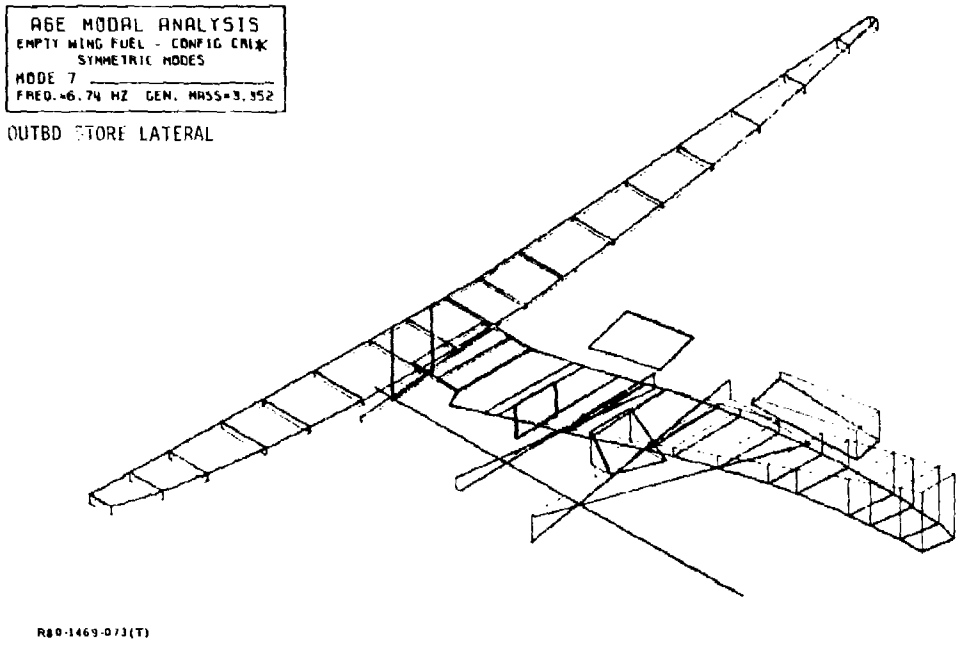

Fig. 8-20 A-6E with Critical Stores: Mode 7

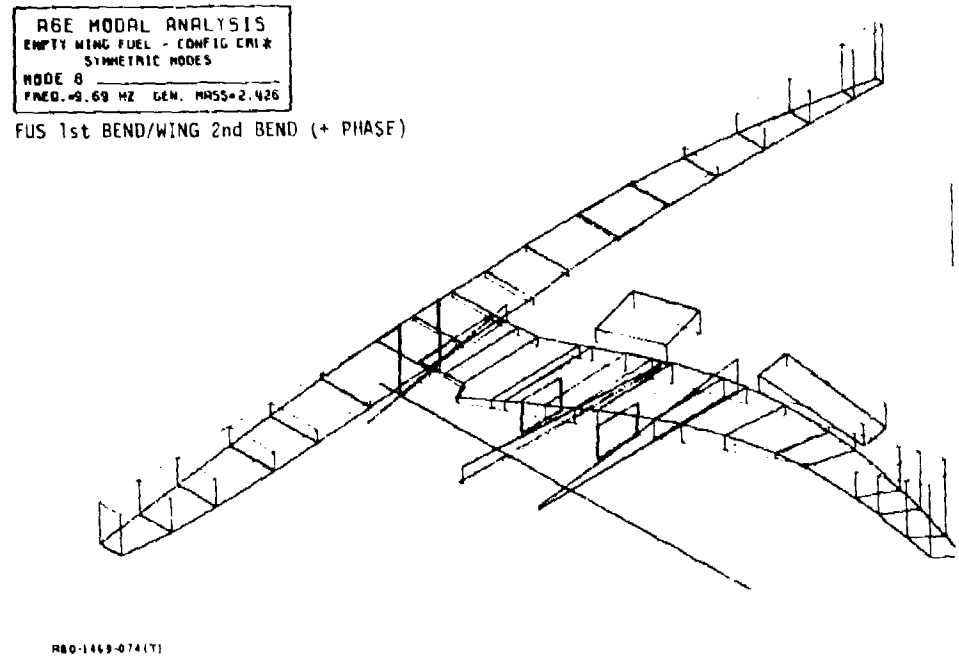

Fig. 8-21 A-6E with Critical Stores: Mode 8

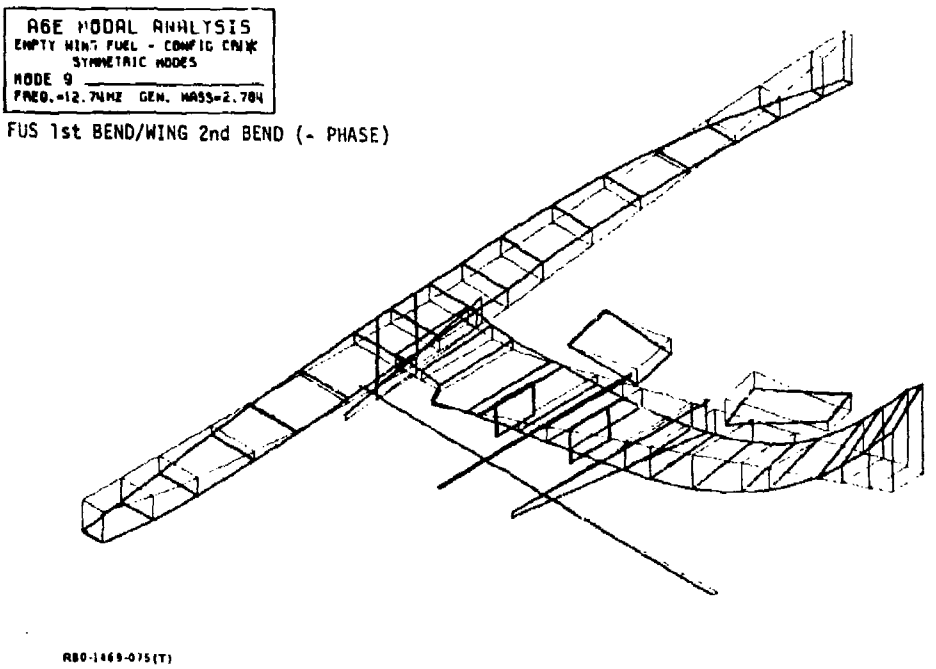

Fig. 8-22 A-6E with Critical Stores: Mode 9

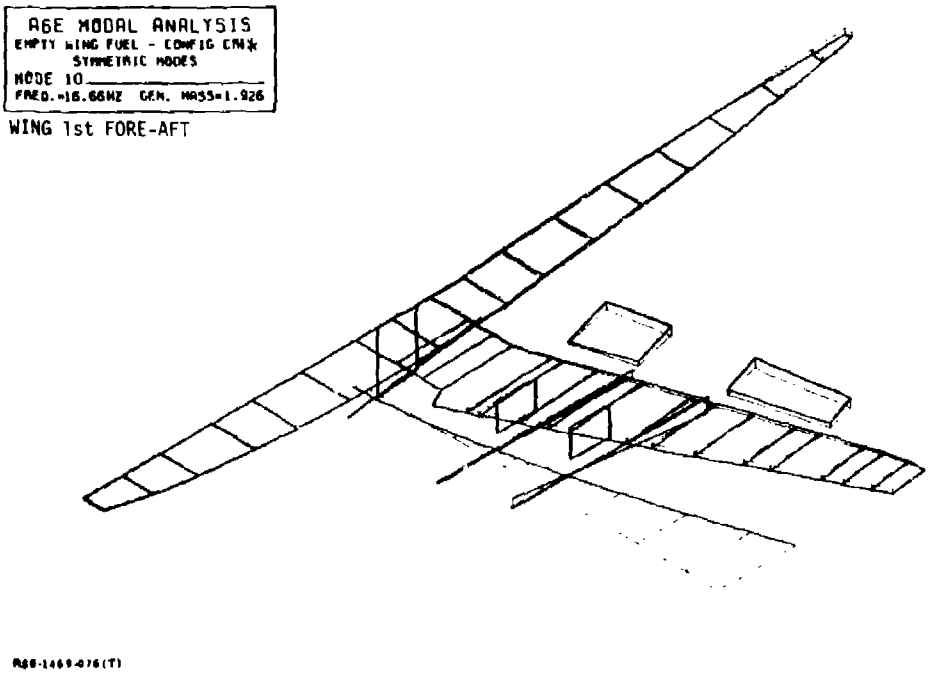

Fig. 8-23 A-6E with Critical Stores: Mode 10

TABLE 8-IX RESULTS OF INBOARD/OUTBOARD SEARCHES WITH NEIGHBORING ACTUAL STORES

NO.	FLUTTER SPEED, KEAS	OUTBOARD PYLON			INBOARD PYLON		
		WEIGHT, LB	MOMENT-OF-INERTIA, LB–IN.^{2} X 10^{-6}	CG, IN. (+AFT)	WEIGHT, LB	MOMENT-OF-INERTIA, LB–IN.^{2} X 10^{-6}	CG, IN. (+AFT)
CR1*	358.3	2935	7.930	-21.08	3500	9.500	0.46
CR2*	379.5	2018	1.956	-49.40	3500	9.170	8.50
N1	389.2	3169	7.790	-21.25	3254	8.520	-0.99
N2	394.1	2184	2.007	-48.70	3385	8.320	11.10
ACTUAL STORE CONFIGURATION	N1	3 MK 83 LDGP ON MER 2 FWD, 1 AFT			4 CBU-59/B APAM ON MER 2 FWD, 2 AFT		
	N2	2 MK 83 LDGP ON MER 2 FWD			3 MK 40 DST ON MER 1 FWD, 2 AFT		

R80-1469-061(T)

8.6 PYLON SEARCHES

To demonstrate the capability of treating pylon flexibility as a design variable, searches in this parameter were conducted using the previously determined critical configurations CR1* and CR2* as the search starting points. In these searches, all inertial variables were held fixed while the pitch flexibility, f_{yy}, of the outboard pylon was allowed to vary by ± 50% of its nominal value. Although ESP allows for variation of flexibility in all six degrees of freedom, inspection of the eigenvectors for the flutter points of CR1* and CR2* indicated that a variation of f_{yy} should have the most significant effect on flutter speed. (In both cases, the mechanism causing the instability was the coupling of modes 3 (wing first bending), 4 (wing first torsion), and 5 (inboard and outboard pylons pitching in phase).) Surprisingly, however, both searches failed to achieve any significant decrease in the previously determined flutter speeds. These results indicated that configuration CR1* and CR2* were already at a minima with respect to f_{yy}. Due to the unexpected nature of these results, a further investigation was deemed necessary. To determine the sensitivity of flutter speed to pylon flexibility, several single-point analyses were performed using the CR1* inertial parameters (M, I, S_x) in combination with various values of f_{yy} for the outboard pylon. The results of this investigation are presented in

Fig. 8-24 and 8-25, which show the effect of f_{yy} on modal frequencies and flutter speed, respectively. Several observations can be made from these plots. Configuration CR1* (f_{yy}/(nominal f_{yy}) = 1.0) is a minimum, characterized by a certain relative spacing or tuning of the natural frequencies of modes 3, 4, and 5. Since this tuning was arrived at during the original CR1 search, in which M, I, and center of gravity were varied, variations of f_{yy} serve only to detune the system and, consequently, increase the flutter speed. In fact (as seen in Fig. 8-25), if f_{yy} is increased beyond 1.2 of its nominal value, the instability involving the store mode vanishes and the mechanism with the lowest flutter speed is that associated with wing modes having little relative store motion.

In view of this behavior, it was conjectured that, once all parameters were roughly tuned so that the critical mechanism was operative, the minimum flutter speed could be reached in a number of distinctly different ways. For example, if a different variable (other than f_{yy} was held fixed, it was hypothesized that the same minimum could be reached by tuning the other variables. To substantiate this, an additional search was run starting from the CR1 (start) configuration. In this test, I_{yy} of the outboard pylon was held fixed at its CR1 value of 6.373×10^6 lb-in.^{2} and f_{yy} of the outboard pylon was allowed to vary, together with the other inertial parameters of both pylons. As indicated (Test 1) in Table 8-X, this search achieved nearly the same minimum flutter speed as CR1* but did so through a different combination of parameters. A second search (Test 2) was then initiated in the previously fixed I_{yy} parameter alone using the final Test 1 values of the other parameters. As shown in Table 8-X, this search failed to significantly decrease the flutter speed below the Test 1/CR1* minimum value. (This case is analogous to the previous unsuccessful attempt to appreciably decrease the flutter speed from the CR1* minimum by varying f_{yy}.)

Finally, as a demonstration of the fact that pylon flexibility would effect significant changes in flutter speed for a configuration not already tuned to a minimum, a search in f_{yy} alone (Test 3) was conducted beginning at CR1 (start). As noted in the table, a significant reduction in flutter speed was achieved although the minimum could not be obtained through this one parameter alone.

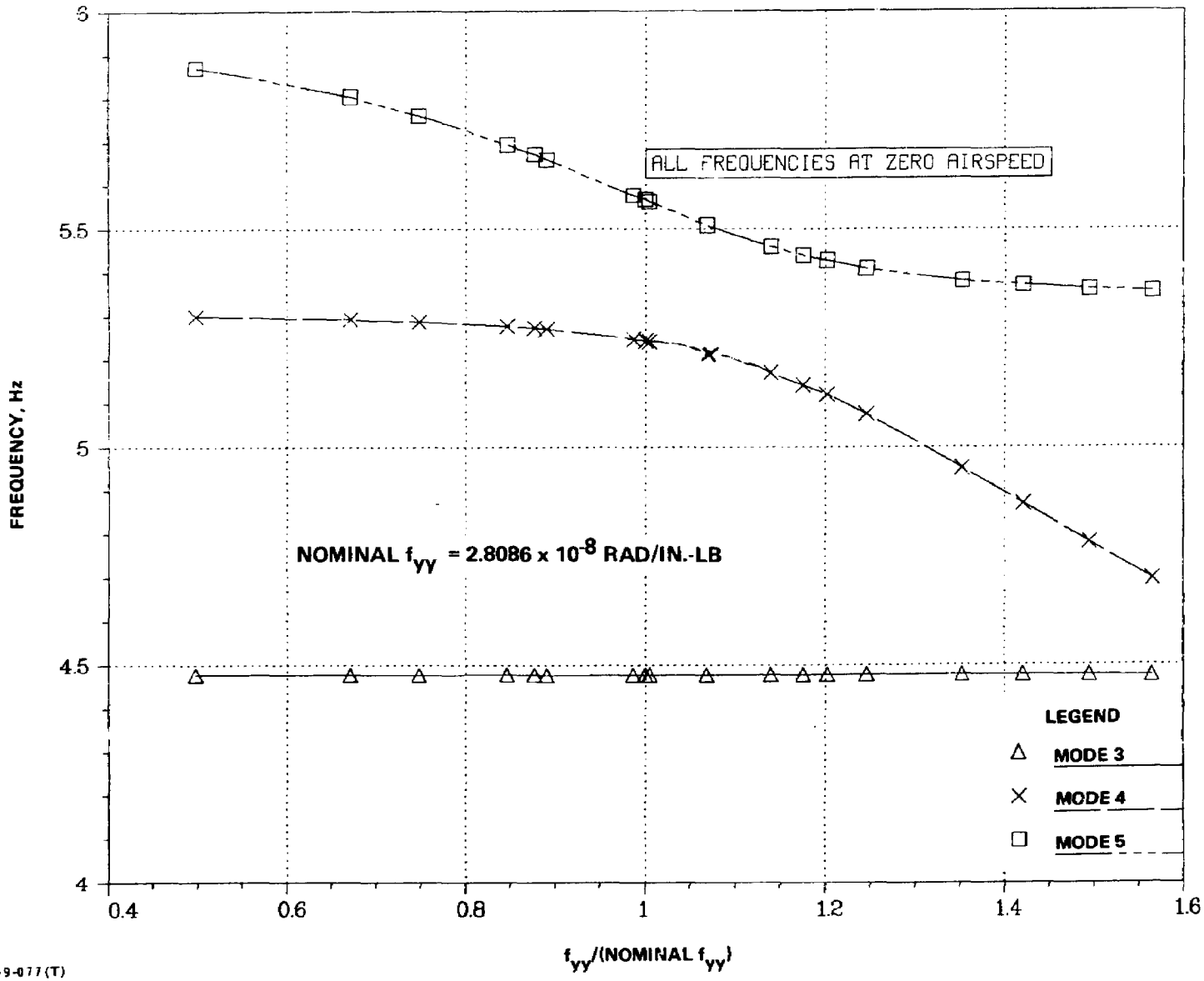

Fig. 8-24 Effect of Pylon Flexibility on Modal Frequencies

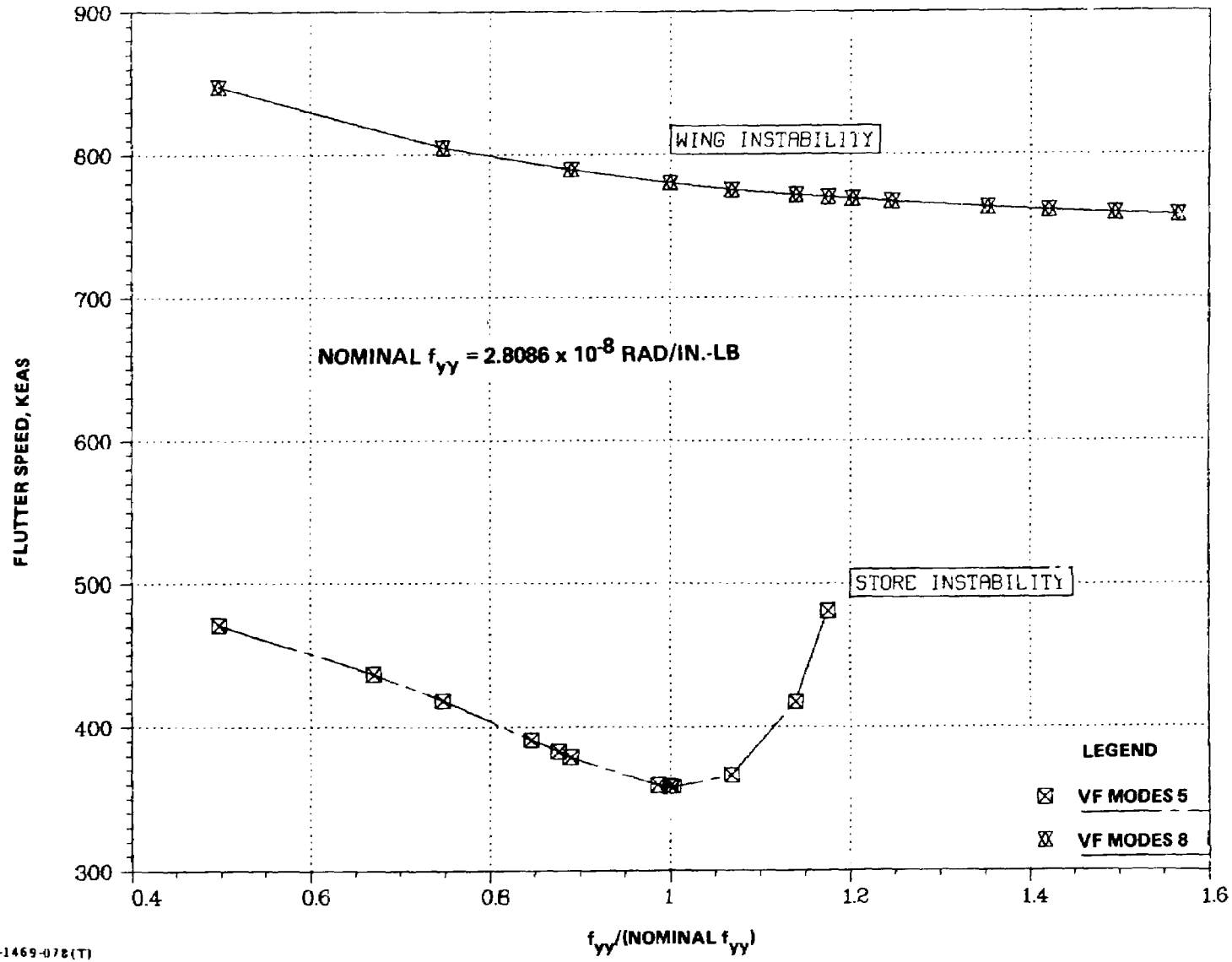

Fig. 8-25 Effect of Pylon Flexibility on Flutter Speed

TABLE 8-X RESULTS OF SUPPLEMENTARY SEARCHES TO INVESTIGATE PYLON-FLEXIBILITY ANOMALY

CASE	FLUTTER SPEED, KEAS	PARAMETERS						
		OUTBOARD PYLON				INBOARD PYLON		
		W, LB	$I_{yy} \times 10^{-6}$, LB-IN.^{2}	CG, IN.	$f_{yy} \times 10^{-8}$, RAD/IN.-LB	W, LB	$I_{yy} \times 10^{-6}$, LB-IN.^{2}	CG, IN.
CR1*	358.3	2935	7.930	-21.08	2.809**	3500	9.500	0.46
TEST 1	358.7	2861	6.373**	-20.89	3.263	3500	9.500	0.46
TEST 2	358.2	2861**	6.474	-20.89**	3.263**	3500**	9.500**	0.46**
TEST 3	366.4	2823**	6.373**	-20.70**	3.153	3500**	9.500**	6.89**
CR1 (START)	376.2	2823	6.373	-20.70	2.809	3500	9.500	6.89

TEST 1 AND 3 BEGIN AT CR1 (START). TEST 2 BEGINS AT THE END POINT OF TEST 1. FOR REFERENCE, CR1 (START) AND CR1* ARE GIVEN.

** INDICATES A PARAMETER FIXED FOR THE SEARCH.

R80-1469-079(T)

In conclusion, it has been shown that the search capability for pylon flexibility does function properly but that, due to the characteristics of the particular flutter mechanism involved, this variable (or any other, for that matter) can occassionally be redundant in a particular search.

8.7 DISCUSSION OF RESULTS

Upon inspection of the located critical combinations, the following observations can be made:

- The identities of the critical inboard-pylon stores are not surprising; they are the stores with the highest masses and pitch moments of inertia.
- The identities of the critical ~~inboard~~ outboard-pylon stores do come as a surprise. CR1* (N1), although massive, is by no means the heaviest allowable store

configuration. CR2* (N2) is not nearly as massive and exhibits a pronounced forward center of gravity. (Normally, an aft center of gravity is regarded as more detrimental to flutter stability.) "Rules of thumb" and "engineering experiences" would not have singled out these configurations

- The critical flutter speeds are well within the flight envelope (approximately 30% lower in velocity than the limit value at 10,000 ft). This is not cause for alarm since the A-6 airplane has been flight-flutter-tested for numerous configurations and has flown in service with the full inventory for over a decade. Various factors can be mentioned to explain this anomaly. First and foremost is the previously aforementioned sensitivity of flutter speed to structural damping. As discussed, an additional 1% damping (total of 3%) would eliminate the critical instabilities altogether. Secondly, it should be noted that the present word does not use a matched-point analysis. Thirdly, store roll moment of inertia was neglected and a fixed representative vertical-center-of-gravity location was used for the analyses

- In Ref. 8, it is stated that the combination of full 300-gallon fuel tanks at both inboard and outboard pylons has been predicted by past analyses to be the most flutter-critical of all approved A-6 store configurations. Market as FT in Fig. 8-9 through 8-11, this combination is far removed from both CR1* and CR2*. The factors mentioned above may also partly explain this disparity. To explore this issue further, an analysis of the tank-inboard/tank-outboard configuration was made. Figure 8-26 presents the appropriate V-g-ω plot. As can be seen for this case, flutter speed increases with damping but the instability is still present with even as much as 10% damping

- Finally, however, one must admit that the configurations determined as critical in the present work, if uncovered during design, would have been flagged for flight test. Thus, it appears that previous analysts, not possessing ESP, did miss potentially critical configurations and that, fortunately, this omission has not proved disastrous.

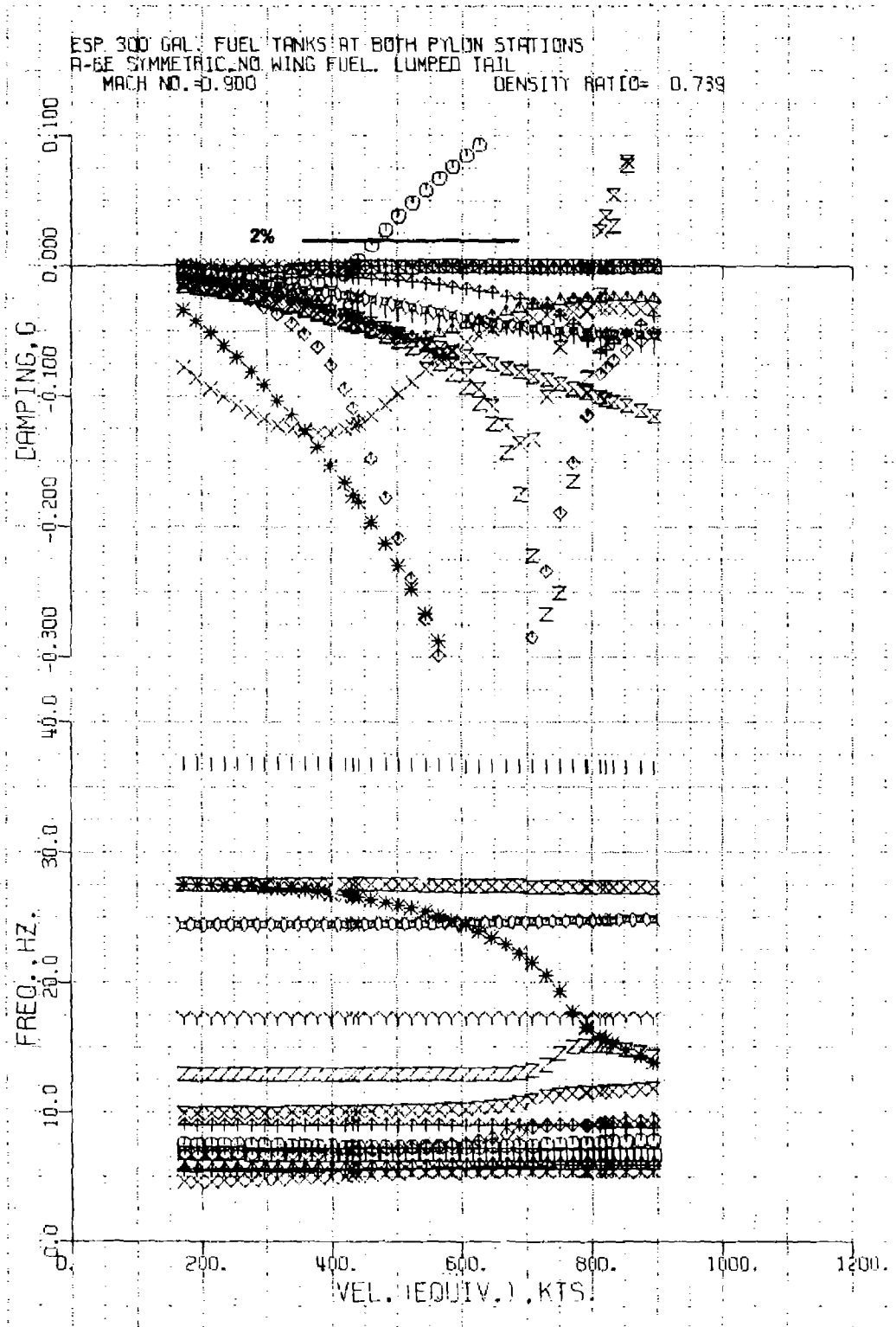

R80-1469-080(T)

Fig. 8-26 V-g-ω Plot for 300-Gallon-Tank Configuration

9 - CONCLUSIONS AND RECOMMENDATIONS

The demonstration points out the possibility (likelihood) of current practices missing potentially flutter-critical store configurations. It also shows ESP to be more reliable in this respect. Experience with the new method during the course of the demonstration proved it to be extremely efficient (in terms of calendar time) relative to current procedures; furthermore, by its very nature, the approach tended to systematize the investigation of the store inventory and quickly identified potentially critical families of store configurations.

Based on these highly promising results, the following additional work is recommended:

- The pilot code should be revised to produce a well-documented and structured production code to be made available to industry and government agencies
- The method should be used on an ongoing in-design aircraft project to resolve any store-flutter problems and to determine the method's true payoff.

10 - REFERENCES

1. Chipman, R.R. and Malone, J. B., "Study of a Method for Determining Critical Store Configurations for Wing-Store Flutter," Report No. ADCR-76-1, Grumman Aerospace Corporation (for Naval Air Systems Command), Sept. 1976.

2. Chipman, R. R. and Malone, J. B., "Application of Optimization Technology to Wing/Store Flutter Prediction," Journal of Aircraft, Vol. 15, No. 11, Nov. 1978, pp. 786-793.

3. Murtagh, B. A. and Sargent, R. W. H., "Computational Experience with Quadratically Convergent Minimization Methods," Computer Journal, Vol. 13, May 1970, pp. 185-194.

4. Murtagh, B. A. and Sargent, R. W. H., "A Constrained Minimization Method with Quadratic Convergence," Optimization Symposium of the Institute of Mathematics and its Applications, U. of Keele, England, 1968.

5. Rosen, J. B., "The Gradient Projection Method for Nonlinear Programming, Part I. Linear Constraints," Journal SIAM, Vol. 8, March 1960, pp. 181-217.

6. Rudisill, C. S. and Bhatia, K. G., "Optimization of Complex Structures to Satisfy Flutter Requirements," AIAA Journal, Vol. 9, Aug. 1971, pp. 1487-1491.

7. Wilkinson, K., et al. "An Automated Procedure for Flutter and Strength Analysis and Optimization of Aerospace Vehicles," AFFDL-TR-75-137, Vols. I and II, Dec. 1975.

8. Pasyanos, E., and Squires C. E., "Flutter Analysis of the A-6E Aircraft with Harpoon Missiles," LD 128-183-1, Grumman Aerospace Corporation, Feb. 1980.

9. A-6 Tactical Manual (U), NWP55-3-A6, Vol. 1, NAVAIR 01-85ADA-1T, Dept. of the Navy, Office of the Chief of Naval Operations.

10. Steeper, et al., "Aircraft Stores Interface Manual, JTCG/MD, WP-12-2.

11. Escalante, L., "Mass Property Data for Military Aircraft Stores (U)", WT-9972-121, Grumman Aerospace Corporation, March 1970.

12. Sulton, A., "Airborne Weapon Characteristic Data Bank, User Manual for Program J3", EG/RAVES-UM-215-75, Grumman Aerospace Corporation, Aug. 1975.

13. Aoki, M., Introduction to Optimization Techniques, Macmillan Company, N.Y., N.Y. 1971.

APPENDIX A

DERIVATION OF REVISED STIFFNESS MATRIX

Assume we desire variations in the pylon flexibilities associated with degrees of freedom p. Let us partition the original flexibility and stiffness matrices as

$$[C_D] = \begin{bmatrix} A & B \\ B^T & C_{pp} \end{bmatrix}, \quad [K_D] = \begin{bmatrix} E & F \\ F^T & K_{pp} \end{bmatrix} \tag{A-1}$$

where, for convenience, the matrices have been rearranged so that the p-p elements appear in the lower right portion of the matrices. The revised matrices are then written as

$$[C_D] = \begin{bmatrix} A & B \\ B^T & C_{pp} + \Delta \end{bmatrix}, \quad [K_D] = \begin{bmatrix} \overline{E} & \overline{F} \\ \overline{F}^T & \overline{K}_{pp} \end{bmatrix} \tag{A-2}$$

The following identities can thus be constructed:

$$\begin{bmatrix} A & B \\ B^T & C_{pp} \end{bmatrix} \cdot \begin{bmatrix} E & F \\ F^T & K_{pp} \end{bmatrix} = [I], \tag{A-3}$$

$$\begin{bmatrix} A & B \\ B^T & C_{pp} + \Delta \end{bmatrix} \cdot \begin{bmatrix} \overline{E} & \overline{F} \\ \overline{F}^T & \overline{K}_{pp} \end{bmatrix} = [I]. \tag{A-4}$$

Expanding the top-right equations of (A-3) and (A-4) yields

$$[A] \cdot [F] + [B] \cdot [K_{pp}] = [O] \tag{A-5}$$

$$[A] \cdot [\overline{F}] + [B] \cdot [\overline{K}_{pp}] = [O] \tag{A-6}$$

Inspecting these equations, we conclude

$$[\overline{F}] \cdot [\overline{K}_{pp}]^{-1} = [F] \cdot [K_{pp}]^{-1} \tag{A-7}$$

Expansion of the lower-right equations of (A-3) and (A-4) yields

$$[B^T] \cdot [F] + [C_{pp}] \cdot [K_{pp}] = [\bar{I}] \tag{A-8}$$

$$[B^T] \cdot [\bar{F}] + ([C_{pp}] + [\Delta])[\bar{K}_{pp}] = [\bar{I}] \tag{A-9}$$

Using (A-7), (A-9) becomes

$$([B^T] \cdot [F] \cdot [K_{pp}]^{-1} + [C_{pp}] + [\Delta])[\bar{K}_{pp}] = [\bar{I}] \tag{A-10}$$

Using (A-8), this becomes

$$([K_{pp}]^{-1} - [C_{pp}] + [C_{pp}] + [\Delta])[\bar{K}_{pp}] = [\bar{I}] \tag{A-11}$$

Hence,

$$[\bar{K}_{pp}] = ([K_{pp}]^{-1} + [\Delta])^{-1} \tag{A-12}$$

$$[\bar{K}_{pp}] = [K_{pp}]([\bar{I}] + [\Delta][K_{pp}])^{-1}. \tag{A-13}$$

Then using (A-7)

$$[\bar{F}] = [F]([\bar{I}] + [\Delta][K_{pp}])^{-1}. \tag{A-14}$$

Together, (A-14) and (A-13) give the desired p-columns of the revised stiffness matrix:

$$[\bar{K}_p] \equiv \begin{bmatrix} \bar{F} \\ \bar{K}_{pp} \end{bmatrix} = \begin{bmatrix} F \\ K_{pp} \end{bmatrix} \cdot ([\bar{I}] + [\Delta][K_{pp}])^{-1} = [K_p][R] \tag{A-15}$$

where $[R] = ([I] + [\Delta][K_{pp}])^{-1}$. Notice that an inversion of a matrix of the dimension of the submatrix $[K_{pp}]$ is required. Since $[K_{pp}]$ is at most a 6-by-6, this is not overly time-consuming for the computer.

If only one flexibility, Δ_l, is chosen as a store variable, (A-15) simplifies considerably:

$$[\bar{K}_p] = \left\{\bar{K}_i\right\} \equiv \begin{Bmatrix} \bar{F}_i \\ \bar{k}_{ll} \end{Bmatrix} = \begin{Bmatrix} F_i \\ k_{ll} \end{Bmatrix} \cdot r = \left\{K_i\right\} \cdot r, \tag{A-16}$$

where $\left\{\bar{K}_i\right\}$ is the i-th column of $[\bar{K}_D]$ and

$$r = \frac{1}{1 + \Delta_l k_{ll}} \tag{A-17}$$